Faculté des Bioingénieurs

Characterization and modeling of water infiltration in a swelling soil in the Palo Verde National Park, Costa Rica

Présenté par Nicolas Stipo

Promoteur(s) : Prof. Marnik Vanclooster PhD (UCL/ELI/ELIE)

Lecteurs : Prof. Rafael Muñoz-Carpena PhD (UF/IFAS)
Prof. Charles Bielders PhD (UCL/ELI/ELIE)
Prof. Pierre Delmelle PhD (UCL/ELI/ELIE)
Alice Alonso ABE Graduate Student (UF/IFAS)

Mémoire de fin d'études présenté en vue de l'obtention
du diplôme de Bioingénieur : **sciences et technologies de l'environnement**

Année académique 2014-2015

Contents

Acknowledgement 12

1 Introduction and context **15**

1.1 Project background 15

1.1.1 Historical background 15

1.1.2 Description of the Tempisque Basin 16

1.1.3 Effect of irrigation on the Palo Verde wetlands 17

1.2 Project significance 19

1.3 Objectives of the master thesis 20

2 Assessing and modeling water transport in shrinking swelling soils: a literature review **21**

2.1 Vertisols: Properties, typology and behavior 21

2.2 Shrinking-swelling characteristics of Vertisols and consequences 22

2.3 Methods for quantifying shrinkage-swelling properties 24

2.3.1 Coefficient of Linear Extensibility 24

2.3.2 Soil Shrinkage Characteristic Curve 25

2.4 Characterization of SSCC 28

2.4.1 Laboratory methods 28

2.4.2 In-situ methods 35

2.5 Hydraulic characterization 39

2.5.1 Laboratory methods 39

2.5.2 In-situ methods 41

2.6 Model selection and description 43

2.6.1 Model selection 43

2.6.2 General model description 44

2.6.3 Water flow 45

2.6.4 Upper boundary conditions 46

2.6.5 Runoff, interflow and drainage 46

2.6.6 Surface water management 47

2.6.7 Macropore flow 47

2.7 Inverse problem and well posedness 55

2.7.1 Inverse problem 55

2.7.2 Well-posedness of the inverse problem . . . 56
2.7.3 Methods for assessing the well-posedness of the inverse problem . . . 56

3 Materials and methods 59
3.1 Experimental design . . . 59
3.1.1 Sampling protocol . . . 59
3.1.2 Physico-chemical characterization . . . 61
3.1.3 Characterization of SSCC . . . 61
3.1.4 Hydrological characterization (WRC, CC) . . . 63
3.1.5 Macroporosity distribution and flow . . . 66
3.2 Model setup . . . 67
3.3 Inverse problem . . . 68
3.3.1 Numerical experiments . . . 68
3.3.2 Model parameterization . . . 69
3.3.3 Description of the inversion problem . . . 71
3.4 Direct modeling scenario . . . 72

4 Results and Discussions 75
4.1 Experimental results . . . 75
4.1.1 Physico-chemical results . . . 75
4.1.2 SSCC results . . . 82
4.1.3 Infiltration results . . . 84
4.1.4 Tempisque . . . 86
4.2 Numerical experiment results . . . 89
4.2.1 General sensitivity . . . 89
4.2.2 Identifiability, uniqueness, and sensitivity . . . 91
4.2.3 Optimization algorithm robustness . . . 92
4.2.4 Model validity . . . 93
4.3 Inversion results . . . 94
4.4 Forward modeling scenario . . . 97
4.4.1 Swelling soil with inverse parameters . . . 98
4.4.2 Rigid, homogeneous soil with inverse parameters . . . 100
4.4.3 Rigid, homogeneous soil with Rosetta parameters . . . 100
4.4.4 Rigid, homogeneous soil with simulated groundwater level . . . 103

5 Conclusion 105
5.1 General conclusion . . . 105
5.2 Recommendations . . . 106
5.2.1 Characterization of shrinkage properties . . . 106
5.2.2 Characterization of hydraulic properties . . . 107
5.2.3 Characteriation of macropore distribution . . . 107
5.3 Future applications . . . 108

Bibliography **109**

Appendices **115**

Appendix A Figures **115**

Appendix B Tables **125**

List of Figures

1.1 Map Maps of land cover evolution in 1975, 1987, and 2000 (Daniels, 2004) 17
1.2 Map situating the Palo Verde National Park in Costa Rica (Jiménez, 2001) . . . 18

2.1 Variation of bulk density with water content according to soil type (Taboada, 2003) 23
2.2 Diagram of clay sheet dispersion (Taboada, 2003) 23
2.3 Diagram of swelling geometry (Taboada, 2003) 24
2.4 Diagram describing primary, secondary, tertiary cracks. (Dexter, 1988) 24
2.5 Initial graph for plotting a shrinkage curve (Taboada, 2003) 26
2.6 Soil shrinkage curve of a non-structured soil (Cornelis et al., 2006b) 27
2.7 Demonstration of volume determination via Archimedes principle (Taboada, 2003) 30
2.8 Glue mass fraction calibration curve (Tadza, 2011) 30
2.9 (a) Results of tensile tests; (b) Theoretical revolution of the restraining pressure exerted by the coating as a function of volumetric deformation; (c) Experimental evolution of vollumetric deformation versus water content; (d) Unconfined axial stress-strain relationships (Liu and Buzzi, 2014) 32
2.10 Schematic of the experimental setup for simultaneous determination of SSCC, WRC and CC (Garnier et al., 1997) 33
2.11 Experimental soil shrinkage curves determined with the core method, the balloon method and the paraffin method. B3 refers to the horizon. Adapted from Cornelis et al. (2006b) 33
2.12 The residuals e_r associated with the core method and the balloon method (Tariq and Durnford, 1993a) 34
2.13 Experimental setup for the rubber balloon method (Tariq and Durnford (1993a), adapted from Cornelis et al. (2006b)) 35
2.14 Disks for measuring changes in layer thickness, viewed from above (Bronswijk, 1988) 36
2.15 Schematic of the THERESA soil layer thickness transducer. 1. Central cylindrical PVC rod joined to the bottom of the layer by the thread 4. 2. Peripheral PVC pipe joined to the top of the layer by the thread 5. 3. PVC pipe. e is the actual thickness of the layer. (Cabidoche and Ozier-Lafontaine, 1995) 37
2.16 Schematic of the 3:1 shrinkage gauge used by Favre et al. (1997) 39

2.17 Diagram for the computation of $\theta(h)$ and $k(h)$ relationships in Kim's proposed method (Kim et al., 1992c) 41
2.18 SWAP model domain and transport processes (Kroes et al., 2008) 45
2.19 A: Schematic representation of the two domains; B: Mathematical representation of the two domains. (Kroes et al., 2008) 49
2.20 Schematic representation of the effect of a variation of m on macropore distribution with depth (Kroes et al., 2008) 49
2.21 Schematic representation of water flow and balance with the macroporosity and divided over the MB and IC domains. (Kroes et al., 2008) 53

3.1 Map of the location of groundwater dataloggers and thus of our experimental sites. 1. Palo Verde Laguna, 2. Tempisque, 3. Chamorro, 4. Posaverde, 5. Varillal, 6. La Bocana 60
3.2 Image of HSP used and the spraying setup 62
3.3 Graph of the effect of smoothing on the evaporative flow of a soil core (Ruy and Cabidoche, 1998) 64
3.4 Photos of rainfall simulator components. Upper left: pump; Upper right: threaded coupling for easy assembly; Bottom left: pressure regulator; Bottom right: 50WSQ nozzle 65
3.5 Photo of rain simulator setup 66

4.1 Laguna profile 76
4.2 Chamorro profile 77
4.3 Posaverde profile 79
4.4 Varillal profile 80
4.5 La Bocana profile 81
4.6 Tempisque profile 82
4.7 Shrinkage curves: (a) Laguna; (b) Chamorro; (c) Posaverde; (d) Varillal; (e) La Bocana; (f) Tempisque 83
4.8 Infiltration curves: (a) Laguna; (b) Chamorro; (c) Posaverde; (d) Varillal; (e) La Bocana; (f) Tempisque 88
4.9 Graph of total sensitivity calculated from modeled soil water content. 1. Van Genuchten - Mualem parameter; 2. Shrinkage parameters; 3. Macropore distribution parameters 89
4.10 Graph of total sensitivity calculated from the variation rate of modeled soil water content 91
4.11 Results of the inverse parameter estimation for the Varillal site 95
4.12 Results of the inverse parameter estimation for La Bocana site 95
4.13 Graphs of model response for manually estimated parameters (solid lines: model) 96
4.14 Precipitation and evapotranspiration data for 1st Feb. 2002 - 31st January 2003 98

4.15 Graph of soil water content at depths of 10, 20 and 45 cm for swelling soil with inverse parameters 98
4.16 Graph of bottom flux variation during the simulation period for a swelling soi with inverse parameters 100
4.17 Graph of soil water content at depths of 10, 20 and 45 cm for a rigid, homogeneous soil 102
4.18 Graph of bottom flux variation during the simulation period for a rigid, homogeneous soil 102
4.19 Graph of soil water content at depths of 10, 20 and 45 cm for a rigid, homogeneous soil with simulated GWL 103
4.20 GWL relative to the soil surface 103

A1 Method used in SWAP to derive actual transpiration and soil evaporation of partly covered soils from basic input data 115
A2 Hydraulic digger used for digging the soil profiles (Posaverde site) 116
A3 Shrinkage curves: (a) Laguna; (b) Chamorro; (c) Posaverde; (d) Varillal; (e) La Bocana; (f) Tempisque 117
A4 Graph of the results of model inversion or testing robustness with K_{sat} and α. The first line represents water content and the second line represents the variation of moisture content. 118
A5 Graph of the results of model inversion or testing robustness with K_{sat}, α, Z_{IC}, m, and $P_{IC,0}$. The first line represents water content and the second line represents the variation of moisture content. 118
A6 Graph of the results of model inversion or testing robustness with K_{sat}, α, Z_{IC}, m, $P_{IC,0}$ and $V_{st,0}$. The first line represents water content and the second line represents the variation of moisture content. 119
A7 Graphs of model response to parameter variation 120
A8 Graphs of model response to parameter variation 121
A9 Response surface for parameters K_{sat} and α 122
A11 Graph of the results of the X-ray diffraction for La Bocana site at -100 cm 122
A10 Response surfaces for macropore parameters, Z_{IC}, m, $P_{IC,0}$, $V_{st,0}$, and $FacParl$. 123

List of Tables

1.1 Climate of the TRB (Source: Instituto Meteorológico Nacional) 17

2.1 Table of COLE values, adapted from Taboada (2003) 25
2.2 Table of soil parameters as they relate to COLE values, adapted from Parker (1982) 25

3.1 Coordinates of the sampling sites (WGS84) 59
3.2 Sampling depths for each site 60
3.3 List of SWAP parameters that must be defined 70
3.4 Table of approximate parameter values used for numerical experiments 71
3.5 Parameter ranges for model inversion and response surfaces 72
3.6 Table of estimated parameters for the Tempisque site using Rosetta pedotransfer functions built in to HYDRUS-1D 73

4.1 Table of physico-chemical data for the Laguna site 76
4.2 Table of physico-chemical data for the Chamorro site 77
4.3 Table of physico-chemical data for the Posaverde site 78
4.4 Table of physico-chemical data for the Varillal site 79
4.5 Table of physico-chemical data for La Bocana site 81
4.6 Table of physico-chemical data for the Tempisque site 82
4.7 Saturated moisture content measured from soil aggregates 82
4.8 Inversely estimated parameters and their sensitivities for the six sites considered 84
4.9 Table of parameter sensitivities relative to water content and water content variation 90
4.10 Summary of effects of separate parameter variation on the model output 92
4.11 Table of estimated parameters and their confidence intervals derived from robustness tests 93
4.12 94
4.13 Overview of soil water balance for a swelling soil with inverse parameters 99
4.14 Overview of macropore water balance 99
4.15 Overview of soil water balance for a rigid soil with inverse parameters 100
4.16 Overview of soil water balance for a rigid soil with pedotransfer parameters . . . 101

B1 pH and exchangeable bases 125

ACKNOWLEDGMENTS

When this Master's thesis started, the thesis subject was far from being defined. Needless to say that to get from that point to now, I needed the help of many people. Most of all, I would like to thank Alice Alonso who really helped me to organize my thoughts, ideas and research, especially in the beginning. The brainstorming sessions with her and/or M. Vanclooster were extremely helpful.

I would also like to mention Frédéric and Sébastien whose experience and know-how as invaluable when it came to translating concepts and methods into practical experimental protocols. Their creativity was extremely helpful. Staying in the GERU research unit, I don't think any master's student could write their acknowledgments without mentioning all the PhD students who give there time without hesitating. Especially Félicien, Albéric, J-B, and Laurence.

Thanks you to the University of Florida and Rafael Muñoz-Carpena for graciously providing me with the rain simulator and soil moisture probes.

Moving to Costa Rica, I of course have to thank OTS for their support, both financial and logistical. I would like to thank Barbara Lewis especially and the OTS fellowship team for rewarding my budding work with a grant. I would also like to thank Carolina Murcia for our few discussions that were of great help to me.

All of the work that was done in the field would have been impossible (and much less interesting) without the help of Juan Serrano. He has been of great help to the UF project in general and his work ethic is amazing. Of course I would still be trying to figure out a way to assemble my rain simulator if it wasn't for the help of the Palo Verde team, especially Salomon and Pajarin as well as Papucho. When I arrived, much of the practical aspects of my protocol still had to be established, and they helped me greatly in doing so. Also, I would like to mention the rest of the Palo Verde team, especially Davinia, Sergio, and Roberto as well as the other researchers for their help and welcome distractions.

And last but not least, I would like to thank Sandrine, without whom I would have eaten nothing but frozen pizza during the last month of my thesis and would surely have had a nervous breakdown by now. I'm a lucky guy!

Nomenclature

CEC Cation Exchange Capacity

ECEC Effective Cation Exchange Capacity

ET evapotranspiration

GMCS Global Multilevel Coordinate Search

GWL Groundwater level

HSP Hand-spray Plaster

MEK Methyl Ethyl Ketone

MEL Methyl Ethyl Ketone

OTS Organization for Tropical Studies

PVAc PolyVinyl Acetate

PVNP Palo Verde National Park

SSCC Soil Shrinkage Characteristic Curve

THERESA Transfert Hydriques Évalués par le REtrait des Sols Argileux

TRB Tempisque-Bebedero Basin

See Tab. 3.3 for a definition of all model parameters.

1

Introduction and context

1.1 PROJECT BACKGROUND

1.1.1 HISTORICAL BACKGROUND

Although the main area of focus for this study is the Palo Verde National Park, more notably the wetlands, it is important to put this area into its more general context. The Palo Verde National Park (PVNP) is situated in the lower part of the Tempisque-Bebedero watershed, situated in NW Costa Rica (Fig. 1.2) in the province of Guanacaste. This river basin is an extremely dynamic watershed and contains an impressive diversity of environments that range from cloud forest on the summits of volcanoes to marsh lands in the lowlands.

The Tempisque River Basin has been subject to many changes over the years. It started as tropical dry forest with itinerant agriculture during the pre-Columbian era, then extensive cattle ranching during colonial times, and finally intensive agriculture with widespread irrigation. It was during the colonial times that the *hacienda* landscape gradually started to replace the natural tropical dry forest, as Spaniards started introducing cattle, horses, asses, pigs, goats, and chickens (Jiménez, 2001). During this period, the region became a large exporter of beef, lard, leather and cheese to neighbouring countries. This system prevailed for several centuries as it required very low capital investments and and was not subject to problems caused by seasonal flooding, which complicates the transport of produce.

From the 1950s and onwards, there occurred a series of major land-use changes. These changes were driven by three main factors (Jiménez, 2001): development of transportation routes, modifications in state economic policies and changes in international markets. These changes first led to a modernisation and intensification of the hacienda cattle grazing system. This boosted beef production and allowed the country to become a main exporter to North America. However, the dependency on Northern American market fluctuations led to heavy financial losses in the cattle sector. The land owners turned to alternative means of revenue, such as agriculture.

Although farming had traditionally been practiced in the region (mainly rice, sugarcane and cotton), this agriculture was mainly smallholder agriculture oriented to local markets. Many

factors jeopardized the real development of intensive modern agriculture. These factors include: the need for subsidies from the state, climate variability of the region (especially precipitation), unavailability of water during parts of the year, and unstable international markets.

Over the last few decades however, the upper Tempisque watershed has been facing drastic changes in the hydrological and socio-economical landscape of the area. This change was boosted by the water transfer from the Lake Arenal for hydropower production. In the 1970s and 1980s, the government of Costa Rica proposed a large scale irrigation project, utilizing the waters from this hydro-electric system (Arenal-Tempisque Irrigation Project (PRAT)). The PRAT was conceived and implemented by the National Service of Subterranean Waters, Irrigation and Drainage between 1975 and 1978 (SENARA). The waters are pumped from the Arenal Lake and then passed through a cascade of hydroelectric power plants: the Arenal, Corobici, and Sandillal plants. Once the waters pass through the plants, they enter the irrigation network. This network is made up of two main canals, the southern canal and the western canal, irrigating between 40,000 and 44,000 ha. This irrigation, in conjunction with water pumped from aquifers and the Tempisque itself permitted the development of large scale, intensive agriculture in the seasonally water scarce region. The system allowed cropping two crops per year with the main crops being rice and sugarcane, representing respectively 50 and 40 % of the total cultivated area. The water from irrigation canals also benefits around 155 ha of tilapia farms (Hazell et al., 2001).

1.1.2 DESCRIPTION OF THE TEMPISQUE BASIN

Geography

The Tempisque-Bebedero watershed is situated in northwest Costa Rica, in the province of Guanacaste and is the largest river basin in the country with an area of 5404.5 km^2 (Jiménez, 2001). The Tempisque's source is in the volcanic sierra of Guanacaste.

Hydrology

Together, the Tempisque and Bebedero rivers drain most of the water of the Province of Guanacaste. Both of these rivers present marked seasonal changes in water levels. The Tempisque, for example, has been known to periodically run dry during periods of extremely low precipitation. Both rivers are subject to pollution pressure of agricultural origin (Jiménez, 2001).

There are two main aquifers in the Tempsique-Bebedero Basin (TRB): the Bagaces Formation aquifer and the colluvial, alluvial aquifer of the right bank of the Tempisque river. These aquifers produce between 5 to 25 l/s and 25 to 50 l/s respectively.

Climate

The climate of the TRB is a typical tropical dry climate and thus presents a strong dual behaviour with a rainy season from May to November and an extremely dry season from November to April (Fig. 1.1). However, the region is described as iso-thermal with a mean temperature of 27.4°C

Table 1.1: Climate of the TRB (Source: Instituto Meteorológico Nacional)

Month	J	F	M	A	M	J	J	A	S	O	N	D
$T_{max.}$ (°C)	33.4	34.4	35.4	35.9	33.9	32.0	32.1	32.1	31.3	30.9	31.6	32.5
T_{min} (°C)	20.7	21.2	21.6	22.7	23.4	23.2	22.8	22.6	22.4	22.3	21.5	21.0
P (mm)	1.3	1.7	4.2	24.7	198.4	247.4	157.3	210.9	360.5	327.1	102.4	10.9

As can be expected, such seasonal extremes produce severe droughts in the dry season and widespread flooding in the wet season, both of which create problems for the management of the area. Droughts render agriculture very difficult logistically, while floods regularly destroy crops and property. Structural solutions have been put into effect, such as the SENARA canal, meant to drain the wetland during periods of floods. However, in more recent years, floods have been becoming more severe, which suggests that non-structural solutions should be implemented in order to resolve the issue in a more sustainable way.

1.1.3 EFFECT OF IRRIGATION ON THE PALO VERDE WETLANDS

The new irrigation network put into place with PRAT, as well as the land-use changes that it induced, have long been a point of environmental concern. Water that originally flowed to the Caribbean sea, now flows to the Gulf of Nicoya, on the Pacific side, potentially disturbing the hydroperiods in the TRB. Also, the quality of water resources has decreased due to sedimentation problems and polluion from pesticides that have affected fish and bird populations in the TRB (Jiménez, 2001). The change of land-use over the past few decades can be observed in Fig. 1.1

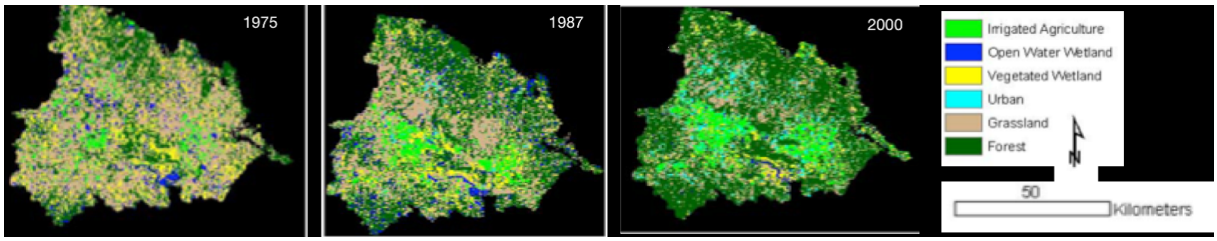

Figure 1.1: Map Maps of land cover evolution in 1975, 1987, and 2000 (Daniels, 2004)

More surprisingly, the switch in the agricultural system from extensive cattle to intensive irrigation agriculture entailed a significant *increase* in water withdrawal in the Tempisque river, regardless of the increased irrigation coming from the Arenal reservoir. This caused a significant decrease in the Tempisque river discharge. It further highlights that the water demand is increasingly higher than the supply offered by precipitation and irrigation canals.

The effects of these changes on hydrological dynamics and land-use are felt all over the TRB, but are more acutely felt in the lower basin, especially in the Palo Verde (PV) wetlands (Fig. 1.2).

The Palo Verde National Park encompasses 20,000 ha of Costa Rican tropical dry forest and wetlands. The PV marsh is a seasonal marsh whose existence depends on season rainfall and

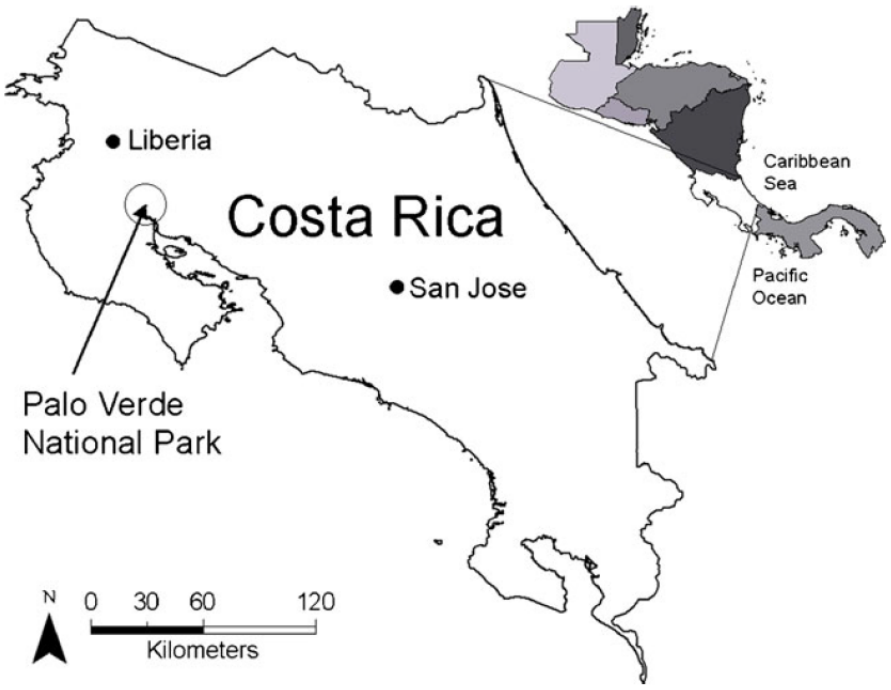

Figure 1.2: Map situating the Palo Verde National Park in Costa Rica (Jiménez, 2001)

runoff from the surrounding hills and drying by evaporation (Trama et al., 2009). It is not yet known whether water levels in the marsh are at all affected by ground water levels. Our study contributes to answering this question. The wetlands cover approximately 1,207 ha and are considered one of the most important nesting and feeding sites for native and migrant birds in Costa Rica (60+ species, Trama et al., 2009), the park has been protected since the mid-1970s and its wetland has been designated a Wetland of International Importance under the RAMSAR wetland Convention (Jiménez, 2001).

In the 1980s, the wetland's ecosystem underwent a massive regime shift and was subject to invasion from cattails (Typha domigensis). This shift in regime resulted in decreased plant diversity as well as reduced avian habitat and a recorded decrease of 50% in bird species (Trama et al., 2009; Jiménez, 2001). As a result, the Palo Verde wetland was included in the Montreux Record in 1993, calling for action to restore the previous conditions of the wetland (Guzman, 2007). Some of the phenomenon that have been advocated as being the cause of cattail invasion are the reduction of cattle grazing, Typha hybrization, reduced salinity, increased nutrient inputs from intensification of agriculture in the upper watershed, hydrological and land-use changes and altered fire regimes (Osland et al., 2011a).

Several strategies have been deployed to restore the Palo Verde wetland (Osland et al., 2011b). Examples are controlled fire or the flattening of cattails using farm tractors equipped with special paddle wheels. While these mitigation techniques led to successful short term results, as demonstrated by an increase in diversity and number of birds (Trama et al., 2009), they lack effectiveness on the long term. For instance, because of the rhizomatous nature of Typha spp., the tractor-crushing strategy has to be repeated quite regularly with potential destructive side-effects to biodiversity. Hence, sustainable restoration strategies that target the

causes of the cattail development problem should be enacted.

Several studies have shown that changes in hydroperiod can trigger the development of cattail (Wilcox et al., 2008; Lishawa et al., 2010; Newman et al., 1998). This might be especially true in wetlands in such tropical-dry climates, that are flooded during the wet season (typically fill to a depth of about 1.5m in PVNP) and subsequently exposed to drought-like conditions in the dry seasons (Loaiciga and Robinson, 1995)(Fig. 2). These cyclical fluctuations in water and oxygen availability influence the ecological balance of the ecosystem (Osland et al., 2011a). Small hydrological fluctuations can therefore have impacts on the plant population dynamics (Wilcox et al., 2008).

Understanding the spatio-temporal dynamic of water coming into and out of the wetland and the hydrological connections with the surrounding catchment is therefore crucial to quantifying the changes caused by the aforementioned transformations, establishing potential causal relationships with the cattail invasion, and eventually establishing sound management strategies. The establishment of such a "water budget" involves the necessity of quantifying the different components influencing it, namely precipitation, evapo-transpiration, surface water inflow and outflow, groundwater inflow and outflow.

The first four components of the water budget have been measured and characterized by previous studies and a study currently lead by Dr. Muñoz-Carpena and his PhD student Alice Alonso from the University of Florida. However, the mechanisms of interaction between groundwater and surface waters, and hence the groundwater inflow and outflow components of the water budget, remain still poorly understood. Soils in the PVNP are comprised mostly of Vertisols (Loaiciga and Robinson, 1995) which are subject to shrinking and swelling during the dry and wet seasons. Because of this, hydrodynamic behavior of those soils change drastically from one season to another, which might have a significant impact on the flooding dynamic of the wetland.

Characterizing the hydrodynamic behavior of those soils is therefore a necessity to fully approach the system. This characterization would allow the parameterization of a hydrodynamic model enabling us to quantify the amount of groundwater inflow and outflow to eventually integrate them into the water budget of the wetland.

1.2 PROJECT SIGNIFICANCE

This study is part of a larger study of water sustainability in the Tempisque Basin, Costa Rica, led by Dr. Muñoz-Carpena and his PhD. student Alice Alonso from the University of Florida as well as others such as Carolina Murcia from the Organization for Tropical Studies (OTS)[1]. Their study aims to understand the hydrological dynamics of the wetland by fully integrating the hydrological interactions with the upper part of the Tempisque watershed. The final objective is to construct a spatially distributed model to evaluate how alternative water management and allocation strategies in the catchment impact the water behavior of the wetland. By using

[1]Water Sustainability in the Tempisque Basin, Costa Rica, `http://abe.ufl.edu/carpena/research/Integrated_Modeling_Tempisque.shtml`, accessed on 13-08-2015

sophisticated data diagnostic tools applied on historical time series of hydrological and meteorological variables and of land cover and use, they aim to detect and understand the changes that happened during the last decades, including cattail invasion in the PVNP, while characterizing the responsible drivers.

The input of our study would greatly inform this larger study by filling the gap linked with the understanding of soil hydraulic properties and the dynamic of interactions between the groundwater and surface water stores in the wetland. This will enable them to incorporate it in their model and hence reduce the uncertainty that would otherwise have been introduced by making gross estimations of those variables.

Furthermore, the characterization of hydrodynamic and physico-chemical properties on soils sampled in various locations of the park will constitute valuable information for the database of OTS since this information has only been poorly described so far. This will undoubtedly serve future studies focusing on this precious ecosystem.

1.3 OBJECTIVES OF THE MASTER THESIS

Global objective

The global objective of this study is to improve understanding of the dynamics of the hydrological system in the Palo Verde wetland.

Specific objectives

The soil of the PVNP has a strong control on the hydrological regime of the PVNP, as it determines infiltration and recharge of the aquifer, and hence the interaction between surface and groundwater. The modeling of the soil hydrological behaviour in the PVNP is however very complicated due to the presence of Vertisols, which are characterized by important transient hydraulic properties and soil swelling-shrinking behaviour. The specific objectives of the project focus therefore on the soil hydraulic functions of the PVNP. The specific objectives of the study are (i) to characterize the physico-chemical and hydraulic properties of the soils of the PVNP, in order (ii) to model the soil hydraulic behaviour of the PVNP wetland soils, which will lead to a better understanding of the relationship between the surface water and groundwater.

2

Assessing and modeling water transport in shrinking swelling soils: a literature review

2.1 VERTISOLS: PROPERTIES, TYPOLOGY AND BEHAVIOR

Soil hydrodynamic models are excellent tools to support soil and water management and engineering. However, most soil hydrodynamical models that have been developed are based on the assumption that soils are rigid and homogeneous. Since as early as the 1950s (i.e. Stirk (1954)), this assumption has been challenged.

The soils found in the Palo Verde National Park belong to the class of soil known as vertic soils, or Vertisols. These soils are easily recognized by their dark colors and their very characteristic properties due to their clayey texture.

Because of their unique properties, Vertisols are easily recognized in the landscape. The transition from another soil type is usually easily noticeable, making it easy to delineate them on a soil map. Vertisols are alluvial or colluvial soils and are usually found in basin and lower landscape positions.

The main mineral that is responsible for Vertisols properties is montmorillonite, which belongs to the smectite family. Montmorillonite is capable of adsorbing large amounts of water, making it subject to shrinking and swelling. For this reason, the presence of shrinking/swelling is the main identifying characteristic of Vertisols.

According to *Soil Taxonomy*, the definition of a Vertisol is as follows:

- Do not have a lithic or paralithic contact, petrocalcic horizon, or duripan within 50 cm of the surface.
- Have 30 % or more clay in all sub-horizons to a depth of 50 cm or more after the soil has been mixed to a depth of 18 cm
- Have, at some time in most years unless irrigated or cultivated, open cracks at a depth of

50 cm that are at least 1 cm wide and extend upward to the surface or to the base of a plough layer or surface crust; and

- Have one or more of the following: a gilgai; slickensides close enough to intersect, at a depth between 25 cm and 1 m; wedge-shaped natural structural aggregates that have their long axis tilted 10-60°from horizontal, at a depth of 25 cm to 1 m.

The Vertisol group is comprised of four sub-groups: Xererts, Torrerts, Uderts, and Usterts. Xererts are soils that have a mean annual temperature of less than 22°C and a mean summer-winter temperature difference of less than 5°C. These are Vertisols of the mediterranean areas, making up 0.01% of the world's land surface. Torrerts are desert Vertisols that have cracks that very rarely close. These occupy about 0.001% of the world's land surface. Uderts are cracks that appear in humid areas and remain open less than 90 cumulative days in a year. They occupy about 0.03% of the world's land surface. Finally, Uderts are Vertisols of the semi-arid regions or the monsoonal climates and occupy the largest territory, 1.8% of the world's land surface (FAO, 2005).

Each of these sub-groups is divided into 'great groups' which are classed by the color of the upper 30 cm of soil. The *chrom* great groups, called this was way because of their color, have a chrome of >1.5 and the *pelf* great groups have a chrome of <1.5.

2.2 SHRINKING-SWELLING CHARACTERISTICS OF VERTISOLS AND CONSEQUENCES

Soil physics for traditional soils are based on the assumption that these soils are rigid. That is, that the ratio of solid phase to pore space in a soil remains constant, while only the volumes of air and water phases vary. When a rigid soil dries, air enters the pore space, replacing the water. Because of this, these soils have constant specific volumes and bulk densities. Completely rigid soils however, tend to be poor soils with low aggregate stability and a low resilience after damage.

Within an expansive soil such as a Vertisol however, the ratio of solids to pore space is not constant, meaning that the soil's bulk density varies with its humidity (Fig. 2.1). The extent of this will be determined by the amount of clay in the soil, and the proportion of this clay that is made up of montmorillonite. Indeed, montmorillonite has a very high surface charge and a low Zero Point of Net Charge (ZPNC), meaning that at normal field pH (6.0-7.5) and in the presence of water, the clays will be dispersed. This dispersion is caused by intercalation of water molecules between the negatively charged montmorillonite sheets (Fig. 2.2). The presence of these water molecules causes an increase in plane spacing, resulting in swelling. Upon drying, the sheets of montmorillonite shrink against each other, increasing the bulk density from about 1.33 g cm^{-3} in a wet state to more than 1.8 g cm^{-3} in a dry state.

The vertical and horizontal swelling and shrinking of Vertisols are directly visible in the field as soil subsidence and cracking, respectively. When the soil wets, swelling is at first three-dimensional as the presence of cracks permit it. As soon as desiccation cracks close, swelling

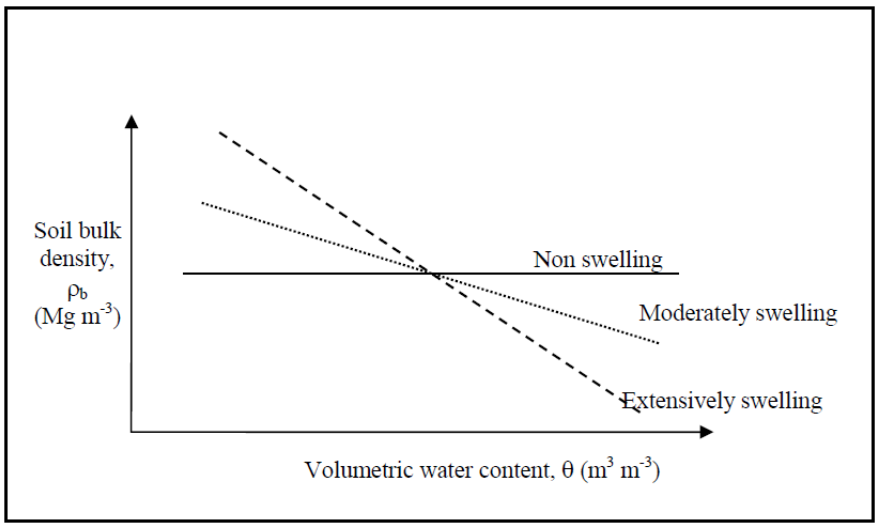

Figure 2.1: Variation of bulk density with water content according to soil type (Taboada, 2003)

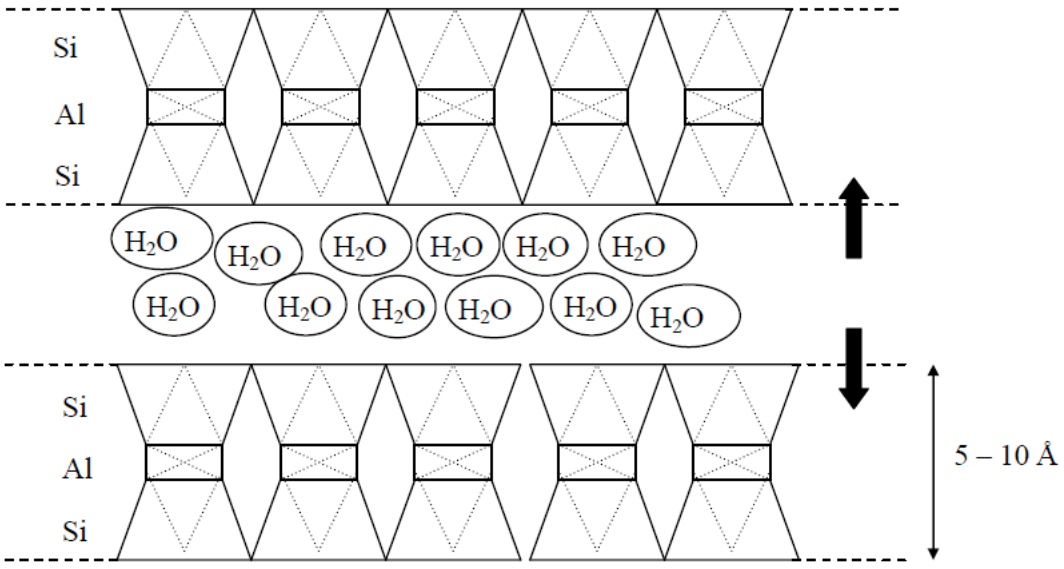

Figure 2.2: Diagram of clay sheet dispersion (Taboada, 2003)

becomes one dimensional (Fig. 2.4).

The inherent properties of Vertisols makes them difficult soils to manage. These soils tend to be very hard when dry and extremely plastic, even liquid when wet. This has an affect on root growth since few roots can penetrate a soil with a bulk density higher than 1.6 g cm^{-3}, meaning that upon shrinking, many roots are simply crushed. Other unfavorable effects are the destruction of buildings, roads and pipelines. Also, the presence of cracks can facilitate the leaching of pesticides and fertilizers below the root zone. Horizontal cracks can break the capillary flux of water.

On the other hand, swelling soils can be used to create an impermeable layer in landfills to prevent the downward migration of contaminants. Shrinking and swelling cycles are also associated with improved soil structure, notably for previously compacted soils. Cracks improve water drainage and soil aeration and decrease surface runoff. Management can generally be

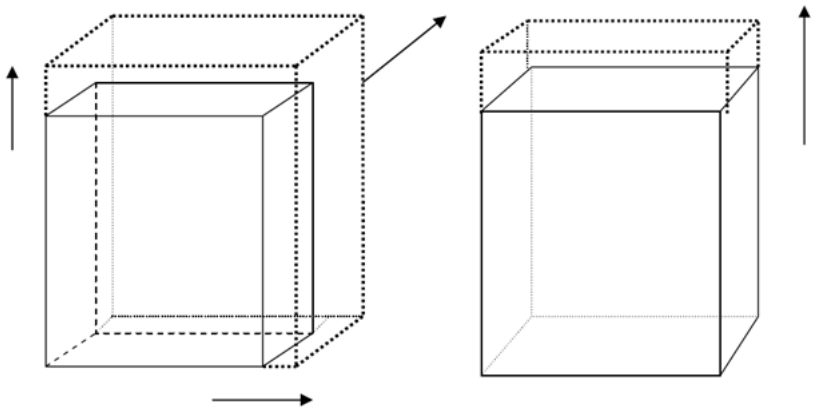

Figure 2.3: Diagram of swelling geometry (Taboada, 2003)

facilitated by taking into account the self-mulching properties of Vertisols (Taboada, 2003,FAO, 2005). This makes Vertisols good candidates for continuous zero-tillage (Dexter, 1988).

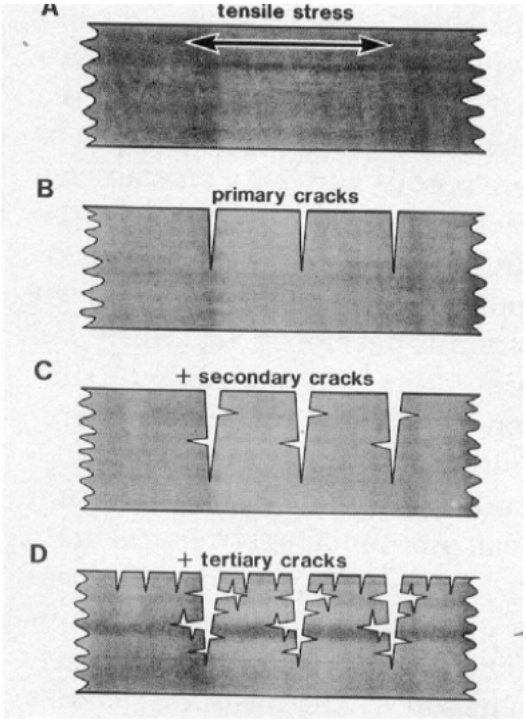

Figure 2.4: Diagram describing primary, secondary, tertiary cracks. (Dexter, 1988)

2.3 METHODS FOR QUANTIFYING SHRINKAGE-SWELLING PROPERTIES

2.3.1 COEFFICIENT OF LINEAR EXTENSIBILITY

The coefficient of linear extensibility, or COLE, characterizes the variation of length of a soil sample from 1/3 atm of suction (-33 kPa) to oven-dry conditions (Eq. 2.1).

$$COLE = (\frac{z_w}{z_d}) - 1 \tag{2.1}$$

Table 2.1: Table of COLE values, adapted from Taboada (2003)

Shrink-swell potential	COLE
Low	< 0.03
Moderate	0.03 - 0.06
High	0.06 - 0.09
Very high	> 0.09

Table 2.2: Table of soil parameters as they relate to COLE values, adapted from Parker (1982)

Variables	R^2
Clay $< 2\ \mu m$	0.87
Clay 2-0.2 μm	0.41
Clay $< 0.2\ \mu m$	0.43
Smectites $< 0.2\ \mu m$	0.61
Interstratified swelling clay $< 0.2\ \mu m$	0.2
Swelling clay $< 0.2\ \mu m$	0.91
Porosity	0.33
Organic C	0.08
Sodium Absorption Ration	0.01

where z_w is the length of a soil sample equilibrated at -33 kPa and z_d is the soil volume at oven-dry conditions. According to the value of the COLE, the shrink-swell potential of a given soil can be qualified (Tab. 2.1).

The COLE index can be very useful as it has been proven to to be closely correlated to certain soil parameters, such as clay content or swelling clay content (Tab. 2.2). In this table, we see that the COLE index is highly correlated with total clay content and swelling clay content. This is promising because it increases the chances of being able to construct pedo-transfer equations for soil hydrological properties from these physico-chemical properties.

2.3.2 SOIL SHRINKAGE CHARACTERISTIC CURVE

Every soil has a characteristic water retention curve (WRC) which relates water content to the energy at which the water is retained by the soil matrix (soil matric potential). Likewise, every soil also has a a characteristic conductivity curve (CC) which relates soil conductivity (as a unit of length/height over time) to soil matric potential. In most soils, which do not present swelling properties, these two characteristic curves are sufficient for describing water flow within the soil. Swelling soils, however, require an additional curve for modeling water flow, the soil shrinkage characteristic curve (SSCC).

The SSCC relates the variation of pore volume to soil water content. Because the total volume of a swelling soil sample is not constant, the pore and moisture volumes must be expressed

over the volume of soil solids rather than the total soil volume. Thus, the variation of pore volume is expressed as specific volume or void ratio e (Eq. 2.2), while the water content is expressed as the moisture ratio ϑ (Eq. 2.3).

$$e = \frac{V_p}{V_{sol}} \tag{2.2}$$

$$\vartheta = \frac{V_w}{V_{sol}} \tag{2.3}$$

where, V_p is the total pore volume, V_w is the total volume of water, and V_{sol} is the total volume of soil solids.

The moisture ratio can be linked to the volumetric moisture content as follows:

$$\vartheta = \frac{\theta}{1 + \theta_s} \tag{2.4a}$$

$$\vartheta = \theta \frac{\rho_s}{\rho_b} \tag{2.4b}$$

While the void ratio is given by:

$$e = \frac{\rho_s}{\rho_b} - 1 \tag{2.5}$$

The soil characteristic curve expresses the void ratio as a function of the moisture ratio. The exact shape of this shrinkage curve depends mostly on texture, especially swelling clay content, and on organic matter content (Tab. 2.2). On the shrinkage curve graphic, two theoretical lines can be plotted: the solid phase line, representing the lowest possible void ratio of a soil having zero pore space; and the 1:1 saturation line that represents soil swelling with zero air within the pore space (Fig. 2.5).

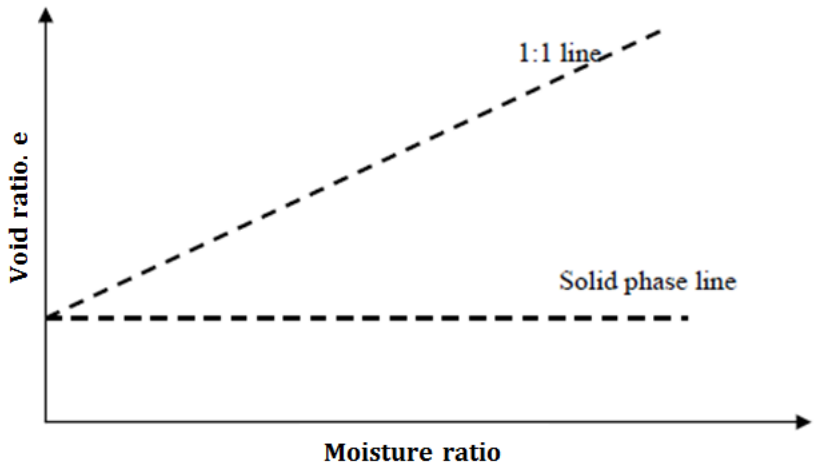

Figure 2.5: Initial graph for plotting a shrinkage curve (Taboada, 2003)

When a shrinking soil dries out, four shrinkage stages can be distinguished (Bronswijk, 1988): (i) structural shrinkage, (ii) normal shrinkage, (iii) residual shrinkage, (iv) zero shrinkage. In the first stage, inter-aggregate macropores are emptied without much, if any, change in bulk volume. This stage only occurs in well structured soils with high biological activity. In the

second stage, the decrease in water content results in an equal decrease of water content and bulk volume, meaning that the soil matrix remains saturated at all times. In the case of a structureless clay paste, the slope of this stage is equal to one. In the third stage, air begins to enter the matric porosity, meaning that the decrease in water content is greater than the decrease in bulk volume. The point where this begins to happen is the air-entry point, not to be confused with the air-entry point of a WRC. Finally, in the fourth stage, the soil matrix is at its densest and bulk volume decrease is null. The matric porosity continues to empty but without any further shrinkage. See Fig. 2.6.

Regarding, structural shrinkage, most models that take into account macropore flow do so separately using information on initial macropore geometry combined with a shrinkage curve limited to normal and residual shrinkage. For each time-step, based on shrinkage, the volume of macroporosity is calculated. Thus, when characterizing the shrinkage curve, the structural shrinkage stage can be disregarded. This is important because it means that the shrinkage curve can be measured on small volumes of soils, or even on de-structured soils, despite the fact that they don't contain structural macroporosity.

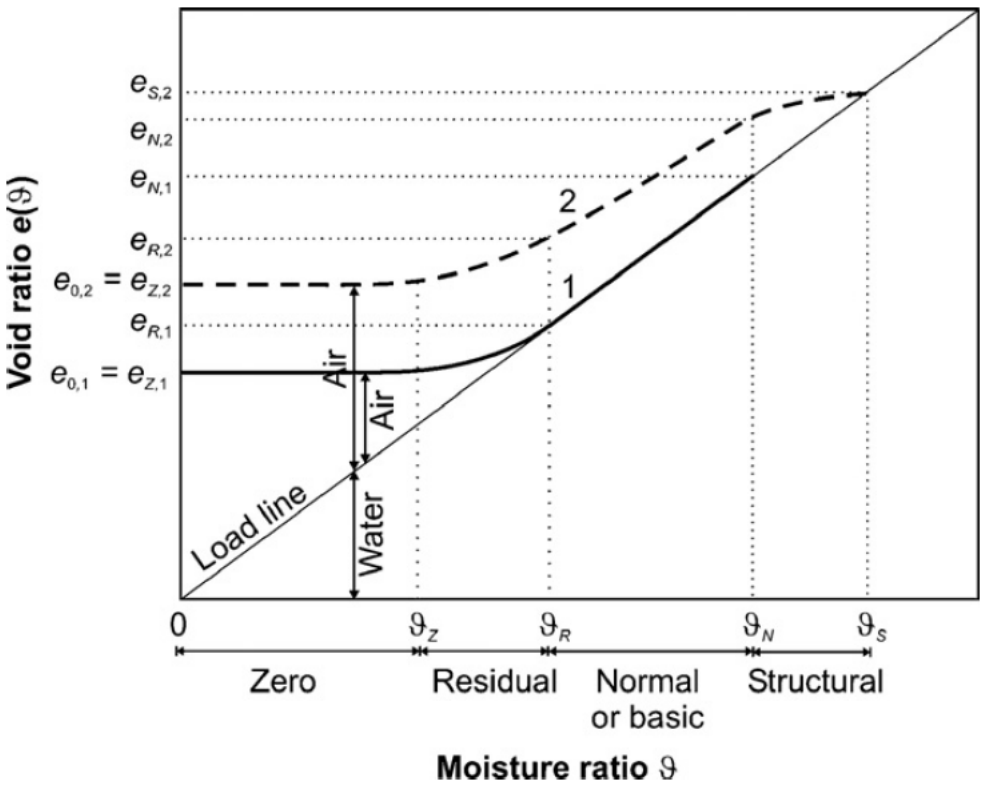

Figure 2.6: Soil shrinkage curve of a non-structured soil (Cornelis et al., 2006b)

As illustrated in Fig. 2.6, when neglecting structural macoporosity, normal shrinkage becomes equal to the saturation or load line. Thus, when observing the shrinkage curve, it might seem difficult to define the saturated water content. Indeed, it is impossible to identify a unique saturated water content as all water contents between the beginning of normal shrinkage and the air-entry point are saturated. For the purposes of this thesis and in order to clarify definitions,

we will define saturated water content as the water content when the void ratio is at its highest value, represented by ϑ_s in Fig. 2.6.

In order to model water and solute transport in a swelling soil, a continuous shrinkage curve is needed, rather than a discrete one. In order to obtain this, a model must be fitted to the data. Many models have been created to link the void ration to the moisture ratio (Cornelis et al., 2006b). Cornelis et al. (2006b) describe the more prominent of these models. These include polynomial models (Giraldez et al., 1983, Giraldez and Sposito, 1983), linear models constructed of straight lines for each shrinkage phase (McGarry and Malafant, 1987), logistic models (McGarry and Malafant, 1987), and sigmoid models (Groenevelt and Grant, 2001,Groenevelt and Grant, 2002, Cornelis et al., 2006a). Some models propose combining exponential or polynomial models with linear ones (Kim et al., 1992b, Tariq and Durnford, 1993b, Bradeau et al., 1999).

Shrinking geometry

A model describing the variation of volume according to moisture content is not sufficient in and of itself for modeling soil shrinkage. In addition to the SSCC, the geometry of the shrinking/swelling process is of equal importance. The shrinking geometry uses the notion a of geometry factor and was expressed by Bronswijk (1988) (Eq. 2.6).

$$1 - \frac{\Delta V}{V} = \left(1 - \frac{\Delta z}{z}\right)^{r_s} \tag{2.6}$$

where, V is the original soil volume, ΔV is the volume change during shrinkage, z is the original height, Δz is the surface subsidence, and r_s is the geometry factor. For three-dimensional shrinkage, r_s is equal to 3. When $r_s > 3$, horizontal shrinkage dominates vertical shrinkage, and in the case of subsidence only, $r_s = 1$ (Cornelis et al., 2006b).

2.4 CHARACTERIZATION OF SSCC

To accurately model shrinkage, the shrinkage curve of the specific site or layer must be recreated precisely. A review of the literature shows that there are several different methods for characterizing the soil shrinkage curve. These can be sorted into the following categories: laboratory methods (aggregate methods, core methods, destructive methods) and in-situ methods (transducer methods, gauge methods).

Determination of the SSCC requires simultaneous measurement of the pore volume and the volume of water in a known volume of soil (i.e. the void ratio and the moisture ratio) and over the entire range of water contents, from saturation to oven dryness (Cornelis et al., 2006a).

2.4.1 LABORATORY METHODS

Aggregate methods

Most of the earliest proposed methods consisted in saturating a small soil clod and measuring its bulk density by fluid displacement with fluids such as kerosene or petroleum (McIntyre and

Stirk, 1954), mercury or toluene (Sibley and Williams, 1989). Alternatively, the aggregates can first be coated with a coat of parrafin (Lauritzen and Stewart, 1941) or a semi-permeable coating, such as saran resin dissolved in methyl ethyl ketone (MEK) and then weighed hydrostatically in water or another fluid (Brasher et al., 1966). The volume is derived from this measurement using Archimedes' principle.

The goal with all of these methods is to completely saturate the aggregates and let them dry (air dry at first, followed by drying in a desiccator and then a 105°C oven) while taking total mass and volume measurements. The exception to this is the paraffin method where, because of the impermeable nature of the coating, several clods must be equilibrated at varying pFs before being coated and weighed both in air and in fluid. This method also requires a WRC in order to link pFs to water content. None of this is needed with the semi-permeable coatings because they can continue drying, despite the presence of the barrier.

There are different coatings available for measuring bulk density. Traditionally, saran F-310 resin has been often used for its good permeability to water vapor and its ease of use (Agriculture Canada, Research Branch, 1984). Different solvents can be used, but most often, the solvent used is methyl ethyl ketone (MEK), which is a known irritant for to the human respiratory track[1]. The clods are dipped successively in MEK solution of 1:4 and 1:8 saran to solvent ratio (Agriculture Canada, Research Branch, 1984). Then, using a saw, a surface of the clod is exposed so that it can be saturated on a tension table at 5-10 cm of tension. Once, the coating is white and the clod is at equilibrium (no more mass variation), the clod is removed and a final coat of saran is applied. Afterwards, the clod is weighed repeatedly in air and in fluid (Fig. 2.7) during drying, first at atmospheric conditions, then in a dessicator and finally in an oven.

Kim et al. (1992c) described a method to simultaneously determine the SSCC and the WRC on disturbed, unripe clay. In his experimental setup, he uses the clod method using saran F-310 resin, described by Bronswijk (1988) which is in turn based on Brasher et al. (1966).

However, due to the toxic and hazardous nature of MEK, Krosley et al. (2003) tested alternative types of coating materials. Their study showed that typical polyvinyl acetate (PVAc) craft glue is more adapted than the commonly used saran/MEK solution. Indeed, PVAc glue is non-hazardous, low-cost, widely available, and enables fast testing time due to the glue's high permeability to water vapor. It also has higher liquid water repellent properties. For several different expansive soils, nearly identical volumetric strain-water content curves were obtained for PVAc glue as for the tradition saran resin. To improve workability, a ratio of 10:1 water to glue ratio can be considered (Tadza, 2011). One disadvantage of the PVAc is that it's mass varies with time as it dries. This requires determining a calibration curve in order to ensure accurate mass measurements. Also, the glue was only tested along the drying path (Fig. 2.8). It is unsure how it would behave during swelling.

Liu and Buzzi (2014) tested spray-on band-aids[2], what they refer to as "hand-spray plaster" or HSP, as a replacement for other coatings such as saran or PVAc glue. There are several

[1]Methyl Ethyl Ketone (2-Butanone), EPA, `http://www.epa.gov/ttnatw01/hlthef/methylet.html`, `accessedonthe01/08/2015`

[2]In french: Pansement en spray

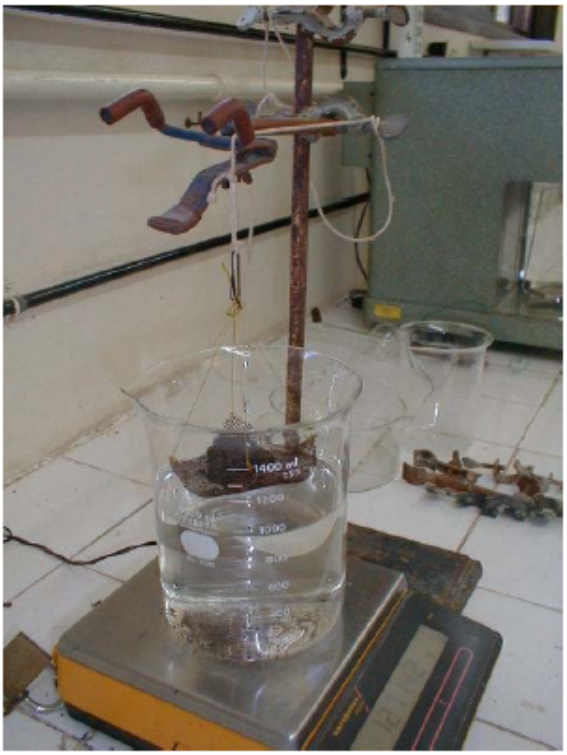

Figure 2.7: Demonstration of volume determination via Archimedes principle (Taboada, 2003)

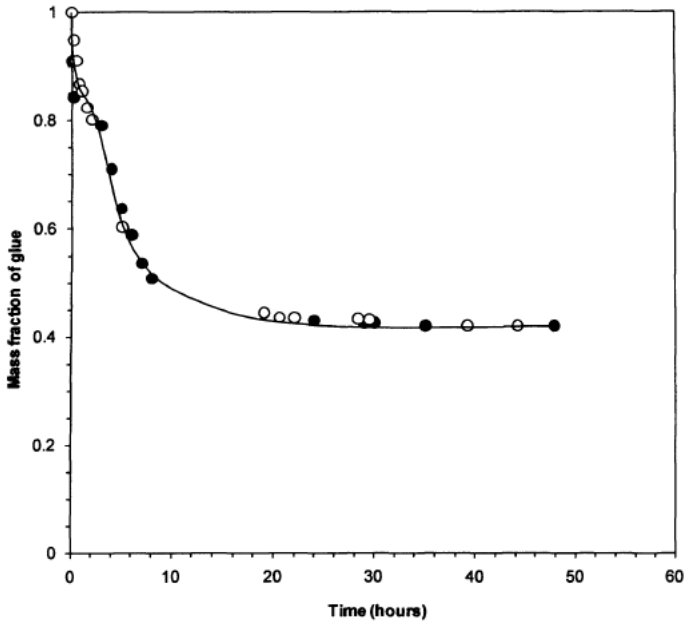

Figure 2.8: Glue mass fraction calibration curve (Tadza, 2011)

advantages of the HSP over other coatings: it is easy to apply, stretchable, non toxic, relatively long lasting, inexpensive, and available from most pharmacists. Just like other methods, clod volume was derived from fluid displacement methods. In this case they used silicon oil as a displacement fluid. The HSP method was validated by comparison to the wax and plastic bag methods (see disturbed methods) and displayed a reduced data scatter.

The HSP is made of a mix of acrylic copolymers and polyurethane polymers in water and dimethylether. Testing shows that the coating can last up to three weeks under air-drying conditions and more than a month in case of swelling in a fog room. Volume changes induced by layers of HSP is assessed from mass measurements and a measured density of 0.77 g/cm^3. Effect of the HSP on volumetric deformation was also assessed by (1) conducting a series of tensile tests on the coating, (2) by computing the restraining pressure exerted by the coating for different volumetric deformations, (3) by comparing the evolutions of volumetric deformation upon swelling of a coated and uncoated specimen, and by (4) comparing the unconfined compressive strength of coated and uncoated specimens. The results of these tests, shown in Fig. 2.9, demonstrate that there is no significant restraining effect of the coating on the soil clods upon swelling.

One other method that uses a coating, or protective barrier is the "plastic bag" method developed by Boivin et al. (1991). For this method, a clod is saturated and then placed in the plastic bag. A vacuum is applied to the bag so that it is airtight around the clod. The clod's volume is then measured by fluid displacement. In theory, the plastic bag method could be used with only one aggregate for the entire curve. However, in practice, the handling of the specimen in and out of the bag is not practical and can damage the specimen, especially if the specimen is saturated. For this reason, several clods must be prepared at different water contents before being measured. Additionally, the pressure applied to the clod by the plastic under vacuum could deform it.

Another method, which is non-destructive, was developed by Stewart et al. (2012) and is low-cost and utilizes free open-source software. The method uses a digital camera in order to image a rotating clod, which allows for the reconstruction of its three dimensional surface and subsequent calculation of its volume. The method was validated against the standard saran-displacement method and displayed an acceptable error rate of 0.4-1.6%. To determine clod volumes, Stewart et al. (2012) placed the samples on a rotating imaging stand which contains a calibration object with a known volume, brightly painted with highly contrasting features. The clod and calibration object are then photographed with a fixed focal length lens while rotating the imaging stand, photographing the clod from all 360°. The photos are then joined using the free web-based program *Photosynth®*. Next the *Photosynth®* files are converted into polygon .ply format and manipulated in *Meshlab®* to calculate clod volume.

For resin coated samples, it has been observed that the coating can inhibit the swelling of the sample, particularly near saturation (Tunny, 1970). Furthermore, the resin loses mass during oven drying and thus without proper correction can cause over prediction of the water content. In addition, it is effectively a destructive process since the aggregate cannot be used for other

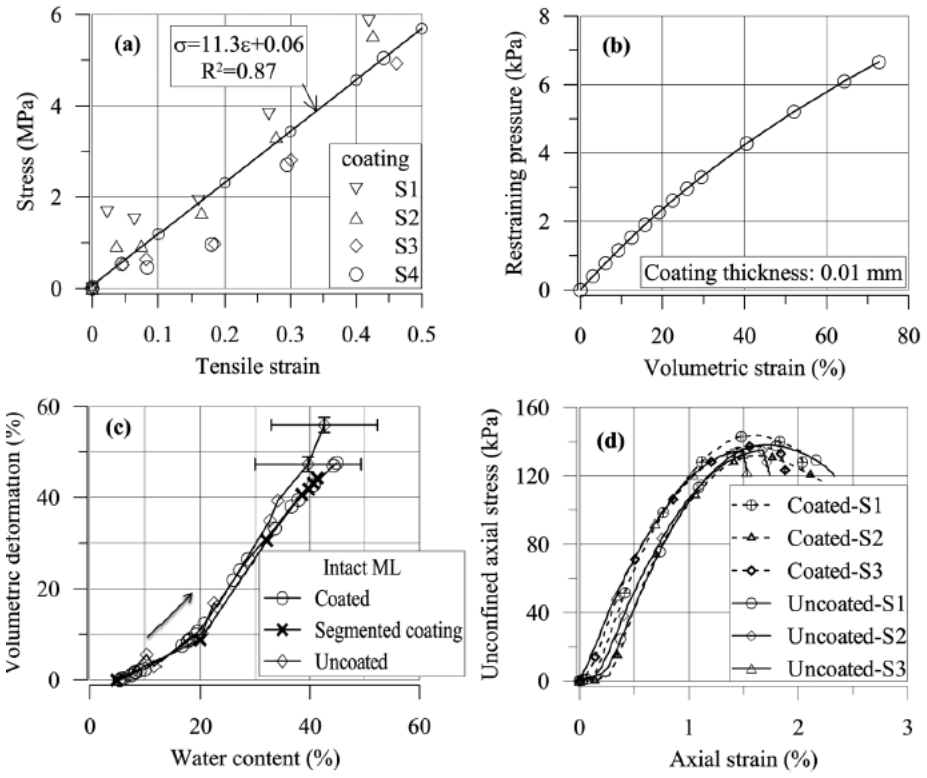

Figure 2.9: (a) Results of tensile tests; (b) Theoretical revolution of the restraining pressure exerted by the coating as a function of volumetric deformation; (c) Experimental evolution of vollumetric deformation versus water content; (d) Unconfined axial stress-strain relationships (Liu and Buzzi, 2014)

purposes afterwards. Schafer and Singer (1976) showed that the clods coated at saturation became compacted due to handling and subsequently had lower measured volumes. They also showed that the resin can slightly penetrate into the pores, which causes the clod to retain less water in subsequent water content measurements. The resin does not always coat all the larger and deeper pores, leading eventually to water penetration into the clod. All of these things point towards an underestimation of the clod volume by clod coating methods.

Core methods

Another type of method for determining bulk soil volume is via direct measurement of soil core dimensions. This can be done simply via rulers, tape measurers, calipers or strain gauges (Berndt and Coughlan, 1976), or more advanced methods. For example, Braudeau (1987) proposed using a retractometer, which was later modified to a laser setup in order to track core deformation in all directions.

The Berndt and Coughlan (1976) method takes 100 cm^3 core samples using metal kopecki rings. The cores are saturated by capillary rise and then air-dried at 60% relative humidity. The mass, height and diameter of the cylindrical samples are measured daily using an electronic balance and a vernier caliper.

Garnier et al. (1997) described a method to simultaneously determine the SSCC, the WRC

and the CC. In this method, shrinkage is determined using a laser sensor setup, while the WRC and CC are determined by small-cup tensiometers and gravimetric measurements during an evaporation experiment. The laser sensors used were a laser spot (LB-72, Keyence Corp., Nanterre, France) and laser barriers (LX2-12, Keyence Corp.)(Fig. 2.10). However, the equipment and software needed for the laser sensors are relatively expensive. The void ratio is given by Eq. 2.7.

$$e(t) = \frac{\rho_s}{\rho_{d_0}} \left[\frac{D(t)^2 L(t)}{D_0^2 L_0} \right] - 1 \tag{2.7}$$

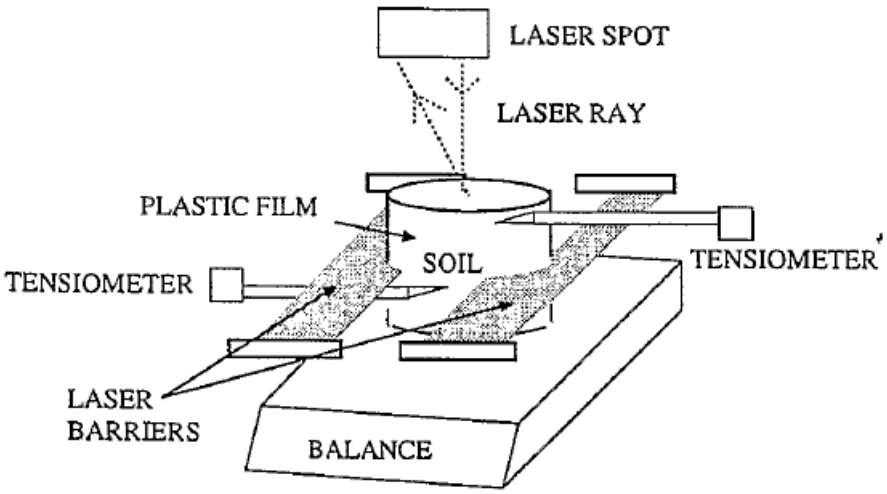

Figure 2.10: Schematic of the experimental setup for simultaneous determination of SSCC, WRC and CC (Garnier et al., 1997)

One of the disadvantages of core methods is the extraction process. The extraction can cause reorientation of clay particles on the core walls by shear stress during extraction. Cornelis et al. (2006b) and Crescimano and Provenzano (1999) identified this problem. Cornelis et al. (2006b) observed a much larger void ratio as compared to the balloon method of Tariq and Durnford, 1993a (see further) and the paraffin method of Lauritzen and Stewart (1941) (Fig. 2.12).

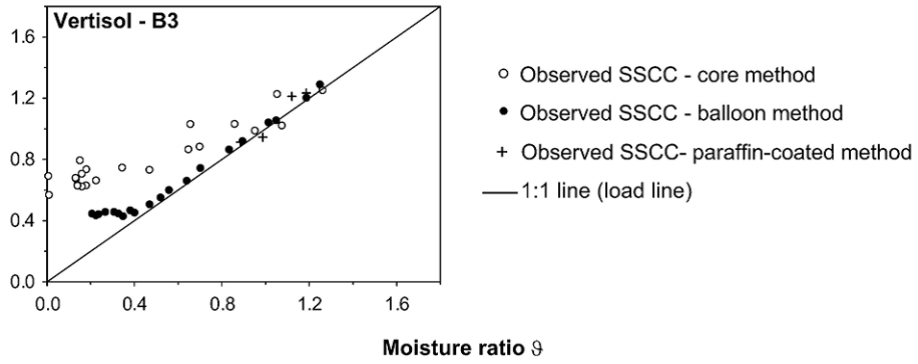

Figure 2.11: Experimental soil shrinkage curves determined with the core method, the balloon method and the paraffin method. B3 refers to the horizon. Adapted from Cornelis et al. (2006b)

Crescimano and Provenzano (1999) attributed this behaviour to the fact that shrinkage is

sometimes an anisotropic rather than an isotropic process as is assumed when using the core method of Berndt and Coughlan (1976) or Garnier et al. (1997). This anisotropy is confirmed by the observation of the anisotropy factor r_s by Cornelis et al. (2006b), which shows r_s increasing gradually with ϑ. A second reason could be, the reorientation of particles caused by sheer stress on the sample walls. A third explanation, given by Cornelis et al. (2006b), is the occurrence of small cracks inside the undisturbed samples. Aggregates are built of several millimetric domains and the number of domains increases with sample size. Thus, the large soil cores are more susceptible to these millimetric cracks. This is not a problem for disturbed samples or small aggregates as long as the aggregates are separated from undisturbed samples, after they were subjected to shrinkage. In Cornelis et al. (2006b), the core method also showed much higher scatter. This could be reduced however by the use of more precise measurement devices such as laser sensors. The most accurate method of volume measurement, however, remains fluid displacement with a high accuracy balance (0.0001 g). One advantage that core methods do possess however is the ability to determine the r_s factor.

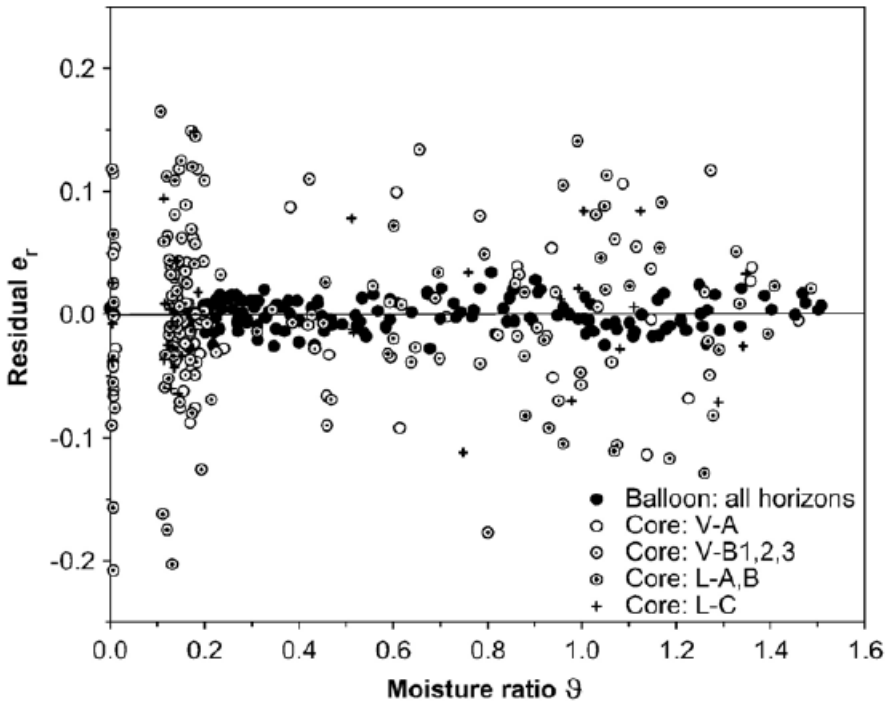

Figure 2.12: The residuals e_r associated with the core method and the balloon method (Tariq and Durnford, 1993a)

Disturbed methods

Some other methods that have been used are disturbed methods, where the soil structure is not preserved. There are two main setups used in the literature. Either the disturbed soil can be packed into soil cylinders (Schafer and Singer, 1976), or into rubber ballons (Tariq and Durnford, 1993a). Schafer and Singer (1976) filled columns with disturbed soil and followed the decrease in length of the drying rod-shaped soil column.

The limitations with many methods (millimetric cracking, non-elastic coatings, handling difficulties, etc.) led Tariq and Durnford (1993a) to design a simple method, similar to Boivin et al. (1991) called the "rubber balloon" method. Disturbed or undisturbed soil samples are dried and then placed in an ordinary rubber balloon with water and sealed with a rubber stopper. The soil is unconfined due to the elasticity of the balloon. The sample is left to saturate for several days and then the stopper is replaced with one with a plastic air inlet and outlet. The sample is dried by air flowing at low pressure over the sample. At given times, the balloon and soil are submerged in water and weighed hydrostatically.

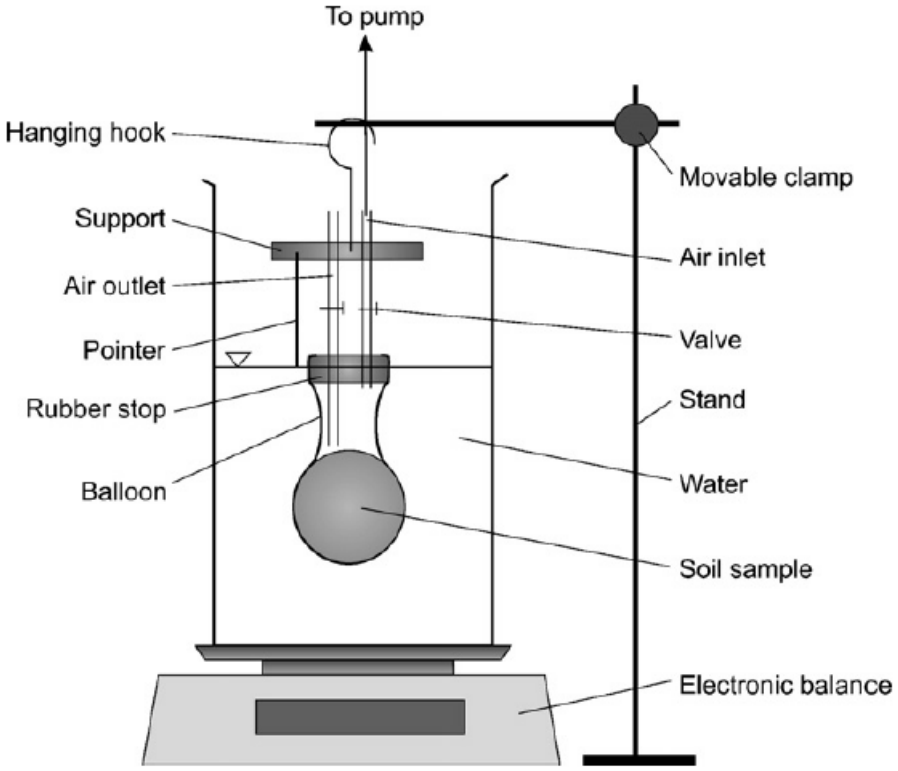

Figure 2.13: Experimental setup for the rubber balloon method (Tariq and Durnford (1993a), adapted from Cornelis et al. (2006b))

When comparing the void ratios obtained with the balloon and the paraffin method, Cornelis et al. (2006b) found them to be in very good agreement. This indicates that the balloon method, though not physically realistic as it uses sieved soil, is more accurate and reliable than the core method for measuring shrinkage. Given that it is easy to use, non-labour intensive, and that it provides well reproducible data using one single sample, it is a good alternative to the paraffin method or other coating methods.

2.4.2 IN-SITU METHODS

Transducer methods

Measurements done in the field require measuring soil subsidence, horizontal soil shrinkage, or both. Vertical methods usually employ a system of rods, anchored at different depths in the

soil. The relative movement of the top ends of these rods then gives the subsidence of each soil layer. There exist many methods of anchoring these rods.

Aitchison and Holmes (1953) were the first to measure thickness variations of swelling soils using steel rods anchored in a plaster of Paris plug. In order to model water flow within a clay soil, Bronswijk (1988) measured subsidence of the soil surface and of layers at different depths. Subsidence of the soil layer was measured relative to a benchmark anchored at 7 m depth. Also, since direct measurement of crack volume is not possible, subsidence of several layers was measured: rotating disks were installed at six depths in the soil. On turning, both halves of the disk are driven into the undisturbed soil (Fig. 2.14). With a thin steel probe and a telescope level indicator, the position of the disks in the soil relative to each other can be measured. For translating into horizontal shrinkage, a r_s factor of 3.0 is considered.

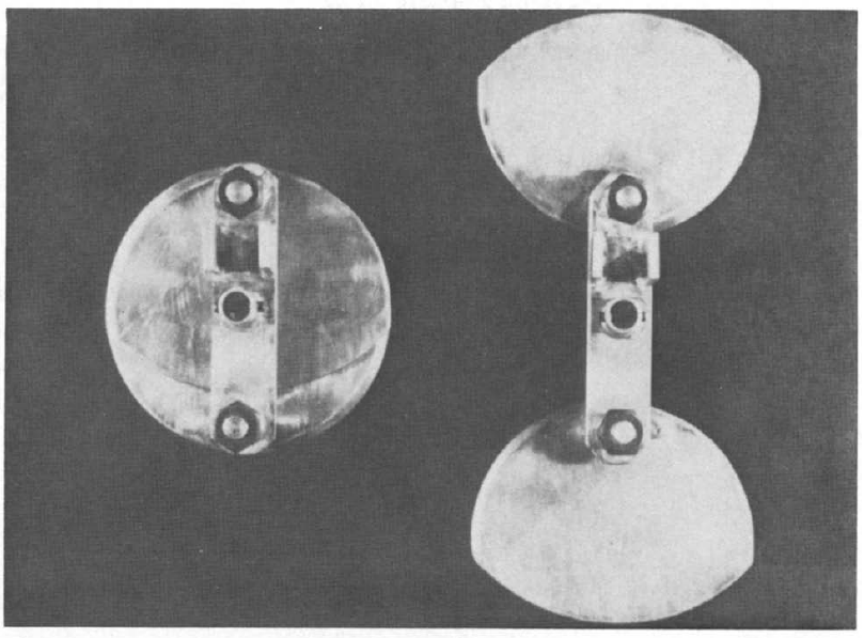

Figure 2.14: Disks for measuring changes in layer thickness, viewed from above (Bronswijk, 1988)

In order to map shrink-swell behaviour of soil across a Vertisol catena, Dinka et al. (2012) employed a similar method. They anchored 10 mm thick steel rods at the bottom of separate 50 mm diameter holes with concrete footings, all within 1 m distance of one another and at different depths. The deepest rod (4.5 m) served as a reference for overall subsidence.During the experiment, the height of each rod was measured within 1.5 mm accuracy with a tripod-mounted level and a stadia rod.

Measuring the hydraulic properties of a soil accurately can be very difficult. In order to do this as effectively as possible, Cabidoche and Ozier-Lafontaine (1995) developed a transducer called THERESA (Transfert Hydriques Évalués par le REtrait des Sols Argileux). THERESA is a new type of transducer capable of measuring soil water content via the variation of thickness of soil layers. Changes in water content during the normal shrinkage phase can be calculated from vertical deformation measurements if the ratio between vertical and horizontal shrinkage

is known. Although the main purpose of the transducer is to provide information on soil water content, and thus on the soil's hydraulic properties, it can obviously be used for establishing a shrinkage curve.

The transducers used by Bronswijk (1988) featured disks with a large insertion surface. These disks can have two drawbacks (Cabidoche and Ozier-Lafontaine, 1995): (1) large diameter bore-holes have to be drilled and then back-filled with remoulded soil. Transfer properties of the soil above the layer whose thickness is being measured are disturbed for a length of time which is hard to be determined. This is minimised by the use of spreading disks but is still a problem. (2) Inserting either disks or plaster plugs like Aitchison and Holmes (1953) cuts roots. That is a source of bias because the root sink function is the main dessication factor in soils with a low hydraulic conductivity. The THERESA transducer solves several of theses concerns.

The transducer is made of three components (Fig. 2.15): (1) a rod with a 14 mm outer diameter. The lower 2 cm of this rod bears a thread which protrudes 2 mm. This thread joins the bottom of the rod to the lower part of the layer being investigated; (2) a pipe with a 20 mm outer diameter slides without friction along the rod. The lower 2 cm of this pipe also bear a 2 mm thread. The thread joins the base of the pipe to the top of the layer being investigated; (3) a pipe with a 25 mm outer diameter fills the bore-hole above the layer under investigation.

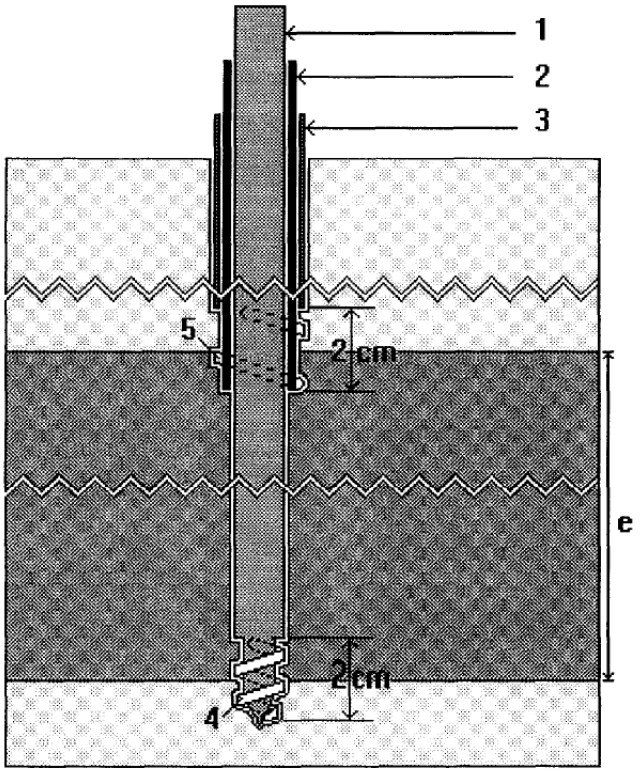

Figure 2.15: Schematic of the THERESA soil layer thickness transducer. 1. Central cylindrical PVC rod joined to the bottom of the layer by the thread 4. 2. Peripheral PVC pipe joined to the top of the layer by the thread 5. 3. PVC pipe. e is the actual thickness of the layer. (Cabidoche and Ozier-Lafontaine, 1995)

The apparatus is suitable for Vertisols: (1) a small outer diameter avoids inducing cracks too

quickly; (2) slight shrinkage around the insertion zones does not affect the soil-thread binding; (3) the diameter enables it to be applied to soils which are very heterogeneous in the horizontal direction; (4) many transducers can be deployed because of their low cost and ease of use; (5) The apparatus fills the entire bore-hole, avoiding water intake artifacts; (6) binding the transducer to the soil with two narrow threads does not disrupt root systems. The specific volume of matric water is given by Eq. 2.8.

$$\nu_{mw}(t) = (\nu_{mw}^{AE} + \nu_s)(e(t)/e^{AE})^3 - \nu_s \tag{2.8}$$

Where ν_{mw}^{AE} is the specific volume of matric water at the air-entry point, ν_s is the specific volume of solids, and e^{AE} is the void ratio at the air-entry point.

Gauge methods

Favre et al. (1997) use soil linear shrinkage mapping in order to quantify bulk linear shrinkage at different depths at the study site. They measured width and depth of cracks intersecting a transect of 20 m. Crack width at different depth was estimated assuming sections of cracks to be isosceles triangles.

In parallel to this, subplots were delimited and separated with metal sheets. Water was applied using simulated rainfall or surface irrigation, depending on the plot. Ultra-thin tensiometer cups were installed in the topsoil to follow the position of the wetting front. During this infiltration experiment, the dynamics of crack closure in time was monitored using simple 3:1 swelling gauges. The two pins of each 3:1 gauge were carefully installed at opposite sides from the soil crack, down to a depth of 5 cm. By monitoring the distance D (Fig. 2.16), the welling movement of the two soil peds at opposite sides of a crack are multiplied by a factor 3, allowing an accurate estimation of the variations in distance D. The swelling of the immediate border of the crack (i.e. D-C) is not measured but can be derived using the increase in border width as it compares to the initial border width.

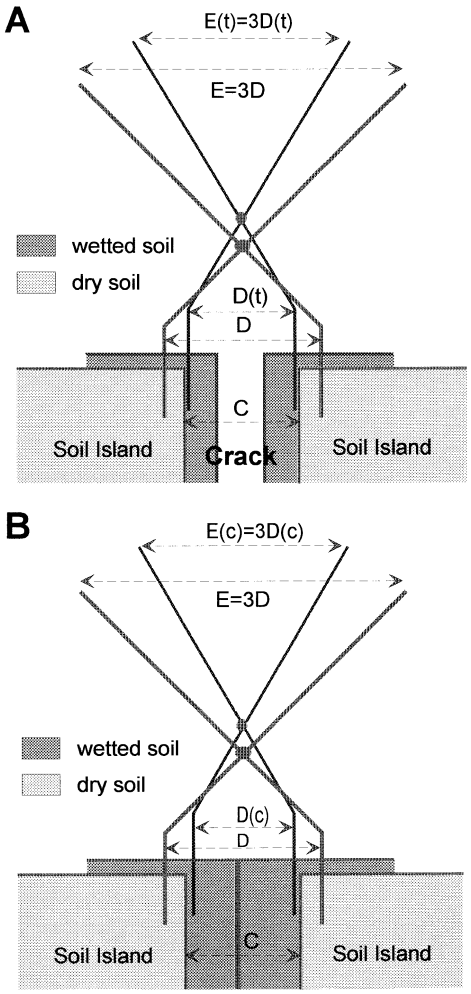

Figure 2.16: Schematic of the 3:1 shrinkage gauge used by Favre et al. (1997)

2.5 HYDRAULIC CHARACTERIZATION

Because of the shrink-swell nature of Vertisols, it is very difficult to measure the hydraulic characteristics of these soils, since cracking causes traditional sensors to lose contact (Cabidoche and Ozier-Lafontaine, 1995). Because cracks are present, it is difficult to measure the hydraulic conductivity and to determine its significance. The representative elementary volume should represent several cubic meters, and naturally occurring water flow inside cracks cannot be described by Darcy's law. Structural and matric flows are actually almost independent. It is therefore necessary to separate structural and matric conductivities (Ruy and Cabidoche, 1998). Methods for characterising the hydraulic properties can be divided into laboratory methods (i.e. evaporation methods or tension table and pressure plates, etc.) and in-situ methods (i.e. soil-water transducers).

2.5.1 LABORATORY METHODS

Many of the first efforts in characterizing the hydraulic parameters used traditional methods, developed for rigid soils. For example, Bronswijk (1988) used the sandbox and pressure plate methods for determining the WRC while using the traditional evaporation method (Boels et al.,

1978) for characterizing the CC.

Ritchie et al. (1972) determined the hydraulic conductivity of undisturbed, unsaturated Vertisol cores in the laboratory using the pressure plate outflow method to measure water diffusivity in the soil without taking into account soil movement. Many other others worked on clay pastes using a material coordinate system which assumes that soil deformation occurs in one direction only (Douglas and McKyes (1978), Douglas et al. (1980), and Smiles and Harvey (1973)).

Garnier et al. (1997) developed a fairly simple method for simultaneously determining the shrinkage curve, the moisture retention curve and the hydraulic conductivity curve using an evaporative method. The experiment is conducted in a controlled-atmosphere chamber. A soil core is placed on a balance to monitor moisture loss by mass. The core is wrapped in a plastic film to inhibit evaporation from the lateral sides and the core shrinkage in all directions is measured by laser. The WRC and CC are obtained by inversion of a water flow model that takes into account the deformation of the soil. The results from this experiment were compared with those from a multistep outflow experiment. Good agreement was found between the results of the two procedures.

The evolution of tension h is monitored using two tensiometers with 2-cm-long-cups. For the water flow model, water fluxes were described in a Lagrangian coordinate system.

$$\frac{1}{1+e}\frac{\partial \vartheta}{\partial t} = \nabla_s(\bar{\bar{K}}\nabla_s(H)F_s^{-1})F_s^{-1} \tag{2.9}$$

where $\bar{\bar{K}}(cmh^{-1})$ is the hydraulic conductivity tensor relative to the solid phase, $H(cm)$ is the soil water head, the operator ∇_s indicates that the spatial derivatives are with respect to Lagrangian coordinates. The terms of the transformation gradient tensor F_s are $F_{sij} = \partial x_i/\partial X_j$, that express the ratio between the spatial coordinate x_i and the material coordinate X_j. This equation is developed further by expliciting F_s but this won't be explained here. The shrinkage curve is described by Braudeau (1987). Garnier's experiment satisfies the condition set by Ruy and Cabidoche (1998), that is that hydraulic characterization in the laboratory should be conducted as the soil dries.

When determining the hydraulic conductivity of undisturbed unsaturated swelling soils in the laboratory, one must do so as the soil dries. When the soil rewets and swells, it can be laterally limited by the rigid sides of the core sampler, thus inducing a bias in the determination of the soil's characteristics. Ruy and Cabidoche (1998) criticized the method of Kim et al. (1992a) for this reason since they use the falling head method on a saturated clay paste with different moisture ratios but where the core is not allowed to swell.

Kim et al. (1992c) propose another method for determining simultaneously the WRC and the CC which is very similar to Garnier et al. (1997). This method also relies on the evaporation method but uses a predetermined shrinkage behaviour to include the effect of changes in the moisture content on the soil matrix. Disturbed soil samples are packed into PVC cylinders of 10 cm in height and 10 cm diameter. In the middle of each 2.5 cm layer, a microtensiometer cup was installed and allowed to move downward by subsidence of each layer. In this way, weight and

tension were recorded throughout the evaporation process in order to establish the WRC. The vertical shrinkage of each layer was established by inserting metal sticks at different depths in the core. Horizontal shrinkage was also measured by assuming the soil has a cone shape as it dries, with a maximum diameter at the base and a minimum diameter at the surface. The hydraulic conductivity is determined from the evaporative flux and the hydraulic gradient between two adjacent layers. The hydraulic gradient between two layers should be calculated by taking into account the variation in height between the two layers. Generally, the evaporation flux is calculated from the changes in moisture content for the depth considered using the continuity equation. However, in this method, it is calculated directly from the volume change of each layer. This method is compared with the traditional evaporative method established by Boels et al. (1978), and the one-step outflow method.

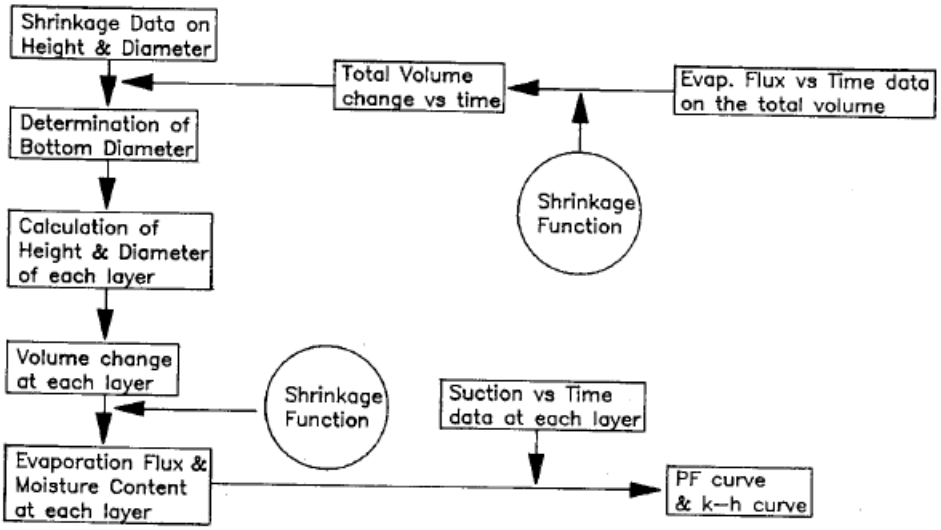

Figure 2.17: Diagram for the computation of $\theta(h)$ and $k(h)$ relationships in Kim's proposed method (Kim et al., 1992c)

2.5.2 IN-SITU METHODS

Tensiometers were successfully used for swelling soils by Jarvis and Meeds-Harrison (1987). Nevertheless, the range of suctions made it possible to only determine the conductivity of the structural porosity.

Jarvis and Meeds-Harrison (1987) tried to investigate water content variations with a neutron probe but their measurements could not be recorded over a broad range of water contents because of soil cracking and random detachment around the access tube, as also stressed by Yule and Ritchie (1980b). Huang and Fityus (2008) did, however, manage to establish theoretical calibration curves for neutron probes for a variety of complicated conditions that are likely to be encountered under field conditions, such as changes in soil dry density and the development of shrinkage cracks. These relationships are genereated using a numerical study that models the neutron probe measurement of soil moisture, based on a 7-group diffusion theory and it uses a finite element method to solve boundary-value problems of the diffusion equations. The

relationships obtained are non-linear, but can be easily obtained for situations that would be difficult to create under field or laboratory conditions.

As mentioned in section 2.4, a method for calculating soil water content from soil deformation was developed by Cabidoche and Ozier-Lafontaine (1995) and Cabidoche and Voltz (1995). Using this method, changes in the water content of swelling soils can be estimated from vertical deformation measurements provided two tools are available: (1) an appropriate device for measuring vertical deformations and (2) a model relating thickness to water content, which is simply a shrinkage curve which takes cracks into account (See Cabidoche and Voltz, 1995 for the development of the mathematical equations). See section 2.3.2 for a description of the device used, the THERESA transducer (Fig. 2.15).

The model of Cabidoche and Voltz (1995) relies on the following assumptions: (1) only structural and normal phases of shrinkage are present. This is important because it restricts the range of water contents that can be measured since the air entry point has not been reached, (2) shrinkage is equidimensional, (3) there are no horizontal cracks, all vertical shrinkage is attributed to a decrease in thickness.

Ruy and Cabidoche (1998) go further than this and relate soil layer shrinkage to soil conductivity using measured soil water gradients. In their study, they measure the matric hydraulic conductivity in the laboratory and in the field and compare the two. The laboratory method determines conductivity under drying conditions by using an Eulerian coordinate system taking into account soil movements in every direction. This means that both solid flows and water flows are described. In the field, matric flow was described in a material or Lagrangian coordinate system using transducers as described by Cabidoche and Ozier-Lafontaine (1995). Soil flow is given by the Eq. 2.10.

$$\left(\frac{\partial \vartheta}{\partial t}\right) = \frac{\partial}{\partial z_m}\left(\boldsymbol{K_m}\frac{\partial(\Psi_m - z + \Omega)}{\partial z_m}\right) \tag{2.10}$$

with

$$\boldsymbol{K_m} = \frac{K_{w/s}}{1+e} \tag{2.11}$$

where $\boldsymbol{K_m}$ is the hydraulic conductivity tensor which reduces to Eq. 2.11, $K_{w/s}$ is the hydraulic conductivity, Ψ_m is the matric potential, z is the depth, and Ω is the overburden potential.

The laboratory tests were conducted on soil cylinders of 4.5 cm in height and 8.5 cm in diameter. These cylinders were saturated and left to dry. The bottom face was sealed while the sides were smoothed and covered with silicon grease to inhibit lateral evaporation. Measurements of vertical shrinkage were made with a vernier while the actual shrinkage curve was established with small aggregates and buoyancy tests in petroleum. The water retention curve was established using the ultrafiltration method of Tessier and Berrier (1979) for low pressures and the pressure plate apparatus for high pressures. Using several replicates, soil moisture content was determined in the soil profiles by gravimetric method. Using soil deformation and water content gradient, diffusivity and hydraulic conductivity can be calculated.

As mentioned, the field tests were conducted in-situ using the THERESA transducer. A reduction of the total macroporosity to the macroporosity producing normal shrinkage was considered. Thirty transducers were installed, investigating five layers. This permitted the calculation of a soil hydraulic gradient. By using the instantaneous profile method, the vertical material hydraulic conductivity could be estimated from Eq. 2.10 and 2.11.

Differences were found between the laboratory and field methods however, especially near saturation. For wet soils, the ratio between the hydraulic conductivity measured in the field and that measured in the laboratory was around 10. Because of the large spatial variability of water content however, no final conclusion would be drawn to explain these differences.

2.6 MODEL SELECTION AND DESCRIPTION

2.6.1 MODEL SELECTION

This specific objective of this master's thesis is to model hydraulic behavior of the Vertisols in the PVNP. In order to do this, a mathematical soil water flow model, specifically designed for Vertisols must be implemented.

Mathematical modeling has become an important tool to support water management planning and decision-making. For managers of water resources, soil water balance models provide an essential support for planning and screening of alternative policies, regulations, and engineering designs affecting ground-water flow and contaminant transport. However, all mathematical models are, by nature, an approximation of reality. For that reason, a successful application of soil water flow models requires a combined knowledge of scientific principles, mathematical methods, and site characterization (EPA, 1998). In general, the selection and application of mathematical models follow the following steps: (1) the definition of the model application objectives; (2) the design of the project management; (3) the development of a conceptual model; (4) the selection of a specific model; (5) the model setup and input parameter estimation; (6) the definition of simulation scenarios; (7) the post simulation analysis; and (8) the assessment of overall effectiveness.

Model selection is especially important. Since the model is only an approximation, the model selected must reflect reality as best as possible. In this sense, model selection is critical for ensuring an optimal trade-off between project effort (such as model calibration, run-time, etc.) and the quality of the result. The US Environemental Protection Agency define three major criteria for selecting a soil water transport model (EPA, 1998): (1) suitability for the intended use; (2) reliability; (3) efficiency.

A mathematical model must be able to meet the needs of the conceptual model. This means, it must be able to express the initial and boundary conditions, hydrogeological properties, biological properties and inputs of the problem. This can be expressed in terms of applicability for various site conditions such as surface ponding, surface runoff, rainfall and irrigation, the presence of multiple layers, wetting and evaporation, vegetation cover, etc. (EPA, 1998).

The model reliability must also be considered. This means that the model's theoretical

framework must be credible and work for a variety of conditions.

Finally the model must be efficient in terms of parameter assessment and computational time.

For our case study, the soil profile considered is homogeneous. The bottom boundary is the water table while the upper condition is a variable rainfall. The initial conditions are a soil at equilibrium with the water table. Thus, the model must be able to calculate water table levels and use rainfall as input. Surface runoff is also considered because it constitutes a water input into surface cracks. No irrigation or drainage is considered however. Finally, and most importantly, the model must be able to calculate variable macropore volume according to soil moisture, i.e. soil shrinkage and swelling. Preferential flow must also be considered within the cracks that appear as a result of shrinkage.

The SWAP model developed by Alterra and the University of Wageningen complies with all these requirements. The model is physically based and solves the Richard's equation for the soil matrix using an implicit, backward finite difference numerical scheme, making it efficient as well. A disadvantage of the model is that the model is very complex, which means that many parameters must be determined.

2.6.2 GENERAL MODEL DESCRIPTION

SWAP (Soil-Water-Atmosphere-Plant) is the successor of the agrohydrological model SWATR (Feddes et al., 1978) and some of its numerous derivatives. Earlier versions were published as SWATR(E), SWACROP, and SWAP93 (Belmans et al. (1983) and Dierkx et al., 2009). SWAP 2.0 was published by Van Dam et al. (1997). The version used is the latest version of SWAP, SWAP 3.2. It introduces additional changes such as improved numerical stability, macropore flow, and detailed rainfall and evapotranspiration.

SWAP simulates the transport of water, solutes and heat in the vadose zone in interaction with vegetation development, during entire growing seasons. The model employs the Richards equation including root water extraction to simulate soil moisture movement. Concepts are added to account for macropore flow and water repellency. SWAP considers for solute transport the basic processes of convection, dispersion, adsorption and decomposition. It can also generate water fluxes to be used as input in more detailed models such as PEARL or ANIMO. SWAP simulates heat capacities and thermal conductivities. The module WOFOST is integrated for simulating leaf photosynthesis and crop growth. The soil moisture, heat and solute modules exchange information each time step to account for interactions. For example, crop growth is affected by soil moisture and salinity on a daily basis.

In the vertical direction, the model's domain of application extends from the top of the canopy to the shallow groundwater, where transport processes are mainly vertical. Below this domain, below the groundwater level, lateral drainage fluxes may appear as well as regional groundwater fluxes. This extends SWAP's horizontal domain to the field scale.

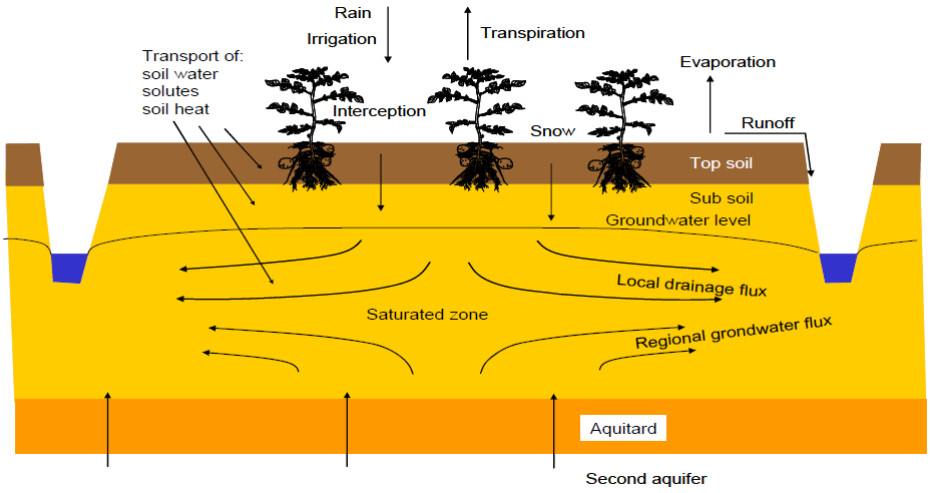

Figure 2.18: SWAP model domain and transport processes (Kroes et al., 2008)

2.6.3 WATER FLOW

As previously stated, water moisture variation with time is based on Richards equation, given by Eq. 2.12.

$$\frac{\partial \theta}{\partial t} = \frac{\partial \left[K(h) \left(\frac{\partial h}{\partial z} + 1 \right) \right]}{\partial z} - S_a(h) - S_d(h) - S_m(h) \tag{2.12}$$

where θ is given in $cm^3 cm^{-3}$, time in $days$. $S_a(h)$ is the water extraction rate by plant roots $[cm^3 cm^{-3} d^{-1}]$, $S_d(h)$ is the extraction rate by discharge to drains$[d{-}1]$, and $S_m(h)$ est the exchange rate with macropores$[d^{-1}]$.

Richards is combined with the common soil physical relationships given by the Van Genuchten - Mualem equations. This yields Eq. 2.13.

$$C = \frac{\partial \theta}{\partial h} = \alpha m n |\alpha h|^{n-1} (\theta_{sat} - \theta_{res}) \left(1 + |\alpha h|^n\right)^{-(m+1)} \tag{2.13}$$

The variables are not explicited here. SWAP permits the specification of several soil layers, each with their set of parameters for Eq. 2.13.

Modifications to the Mualem - Van Genuchten function are made for near saturation conditions, with the introduction of a small capillary height h_e (Eq. 2.14).

The lower boundary can be specified in different ways: Dirichlet condition (constant pressure head), Neumann condition (imposed flux, constant or variable), Cauchy condition (flux as function of pressure head), seepage face, and free drainage.

$$S_e = \begin{cases} \frac{1}{Se}[1 + |\alpha h|^n]^{-m} & h < h_e \\ 1 & h \geqslant h_e \end{cases} \tag{2.14}$$

Scaling of main drying and wetting curves describe hysteresis in the retention function. Impacts of frozen soil moisture on water flow is described by a reduction of the hydraulic conductivity, but this is not needed in our case. Hysteresis is also disregarded to reduce the number of parameters.

SWAP solves the Richards equation numerically with an implicit, backward, finite difference scheme. The Newton-Raphson iterative procedure ensures mass conservation and rapid convergence.

2.6.4 UPPER BOUNDARY CONDITIONS

SWAP is very flexible in terms of input data at the top of the column. In general, daily rainfall data is sufficient. A daily rainfall with duration can also be used. Alternatively, weather records can be specified with short, constant time intervals. A third option, for more detailed simulation, is detailed rainfall data. In this case, the rainfall intensity follows the format of a tipping bucket device. For nordic conditions, the model also has an optional snow storage module.

Rainfall interception is then calculated by SWAP in the case of a crop/grass cover following Von Hoyningen-Hüne and Braden. The interception concept of Gash is also available for forests.

For evapotranspiration, the Penman-Monteith equation can be used to calculate the potential evapotranspiration, using daily weather data such as temperature, wind speed, air humidity and solar radiation. An alternative exists of providing an input of reference evapotranspiration in combination with crop facors. From these, the potential transpiration and evaporation fluxes fluxes are derived, takeing into account interception and soil cover. Actual transpiration and evaporation depend respectively on soil moisture and salinity and on the capacity of the soil to transport water to the surface (Fig. A1).

2.6.5 RUNOFF, INTERFLOW AND DRAINAGE

SWAP distinguishes between two different runoffs: Horton overland flow when rainfall rate exceeds infiltration. Surface runoff is calculated only when the ponding layer (Eq. 2.15) exceeds a critical depth. A second form occurs awhen the groundwater table has reached the soil surface. The rate of runoff depends on a specified surface resistance.

$$\frac{\Delta h_0}{\Delta t} = q_{prec} + q_{irr} + q_{melt} + q_{runon} + q_{inun} + q_1 - q_{e,pond} - q_{runoff} + I_{ru} \tag{2.15}$$

where q_{prec} is the precipitation flux, q_{irr} is the irrigation flux, q_1 is the flux from the surface soil layer to the ponding layer, q_{melt} is snowmelt, q_{runon} is runon, q_{inun} is flow from surface water, q_{runoff} is the runoff flux, $q_{e,pond}$ is evaporation from ponding layer and I_ru is runoff into macropores. All units are $cm.d^{-1}$.

Interflow is defined as near-surface flow resulting in seepage to a stream channel within the time frame of a storm hydrograph. Interflow can be saturated or unsaturated and is simply governed by differences in hydraulic potential.

Drainage can be calculated via the Hooghoudt or Ernst equations, either with a table relating drainage flux and groundwater level, or with drainage resistances per drainage system. The drainage resistances are distributed vertically constituting separate "discharge" levels.

The SWAP model can account for interactions between surface and groundwater by describing runoff as a non-linear function of water storage in the field, interflow as a non-linear funciton of the groundwater elevation when it has reached the near-surface zone and the discharge to

a series of drainage systems. This provides the possibility to describe feedback and the close interconnection between groundwater and surface water in stream valleys and polders.

Even if drainage isn't applicable to our study, runoff nad ponding is certainly interesting in the modeling a seasonal wetland. Additionally, the methods for describing drainage are relatively detailed and may potentially be adapted in order to describe regional groundwater flow that happens at the study site.

2.6.6 SURFACE WATER MANAGEMENT

Surface water management options have also been implemented in SWAP by accounting for a surface water balance described at the scale of the horizontal subregion. Again, this could prove extremely useful for modeling in a seasonal wetland, adjacent to a river (Tempisque). The simulation is extended to the subregion by assuming the subregion as a single representative groundwater level and that the soil profile occupies the whole surface area.

Surface water levels can be imposed, or simulated using a control unit and by setting soil moisture criteria (groundwater level, pressure head, minimum storage) in combination with a weir.

The variation of regional surface water storage within the control unit is given by Eq. 2.16.

$$\frac{dV_{sur}}{dt} = q_{sup} - q_{dis} + q_{drain} + q_{crackfl} + q_{runoff} \tag{2.16}$$

where, q_{sup} is the external supply, q_{dis} is the discharge, q_{drain} is regional drain flow, $q_{crackfl}$ is bypass flow through cracks, and q_{runoff} is surface runoff.

Regional surface water storage, V_{sur} is given by Eq 2.17.

$$V_{sur} = \frac{1}{A_{reg}} \sum_{i=1}^{n} l_i A_{d,i} \tag{2.17}$$

where, A_{reg} is the total area of the sub-region $[cm^2]$, l_i the total length of channels/drains of order i in the sub region $[cm]$, and $A_{d,i}$ is the wetted area of a channel vertical cross section $[cm^2]$.

SWAP is able to calculate multi-level drainage with imposed surface water levels or with simulated water levels (using a control unit). The model also makes provision for the modeling with fixed weirs and controlled weir management.

2.6.7 MACROPORE FLOW

Version 3.2. of the SWAP model saw the introduction of MacroPore flow. More time will be spent on explaining this component of the model because it is not included in most other infiltration models.

In structured soils such as clay, preferential flow can occur through large pores (or macropores). Macropores are defined as pores with a diameter or width equal to or larger than 100 μm. Macroporosity can be caused by shrinking and cracking of the soil, by plant roots, by soil fauna, or by tillage operations. Due to very rapid flow through these macropores, water and

solutes can reach large depths very quickly after the start of a shower, bypassing the capacity of the soil matrix for storage, adsorption and transformation of certain pollutants.

The simulation of these processes in SWAP are based on the description of macropore geometry proposed by Hendriks et al. (1999).

In SWAP the geometry of macropore structure is described by characterizing maccropore volume according to three main properties:

1. Continuity: continuous, interconnected macropores vs discontinuous, unconnected macropores ending at different depths.

2. Persistency: static, permanent macropores and dynamic, temporary macropore volume depending on soil moisture.

3. Horizontal distribution: distribution in the horizontal plance of macropore volume over cracks and holes.

Continuity

With respect to continuity, SWAP divides macropores into two classes or domains:

1. Main Bypass (MB)flow domain: the network of continuous, horizontal interconnected macropores;

2. Internal Catchment (IC) domain: discontinuous non-interconnected macropores, ending at different depths.

The macropores of the MB are horizontally interconnected and penetrate deeply into the soil profile, enabling fast drainage of soil water. The IC domain represents macropores that are not interconnected or connected to the MB domain and that end at different depths. In these pores, water is trapped at the bottom of the individual macropores, forcing lateral infiltration into the soil.

The volumetric proportions of each domain as a funciton of depth are described using four basic input parameters: Z_{AH} representing the bottom of the A-horizon, Z_IC representing the bottom of the IC domain, $P_{IC,0}$ of the IC domain at the soil surface, and power $m[-]$ a shape factor. In order to calculate the IC domain macropores, the domain is divided into sub-domains. This is strictly an aspect of numerical implementation however. The effect of the$m$ shape factor is shown in Fig. 2.20.

$P_{IC,0}$ is an important parameter because it determines how much water is routed into each domain at the soil surface, which is the major source of macropore water. In fact, FIGURE shows that the model is more sensitive to this parameter than the other three.

It is assumed that the IC macropore volume consists of many individual small macropores that originate at the soil surface and end at different depths. The cumulative frequency distribution of the depth z at which the functional IC macropores end in concept is described by Eq.

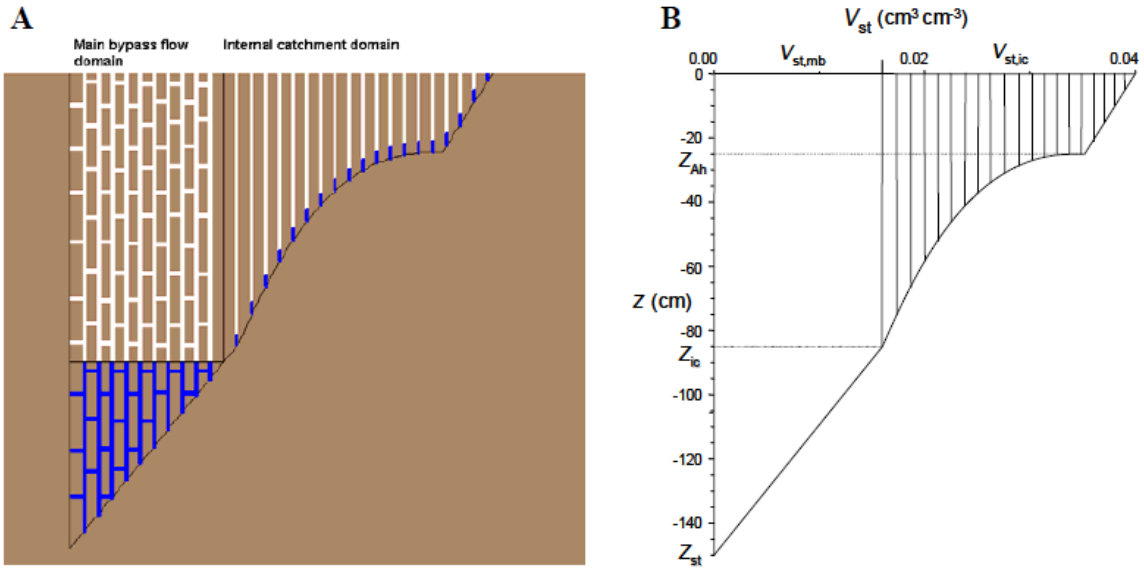

Figure 2.19: A: Schematic representation of the two domains; B: Mathematical representation of the two domains. (Kroes et al., 2008)

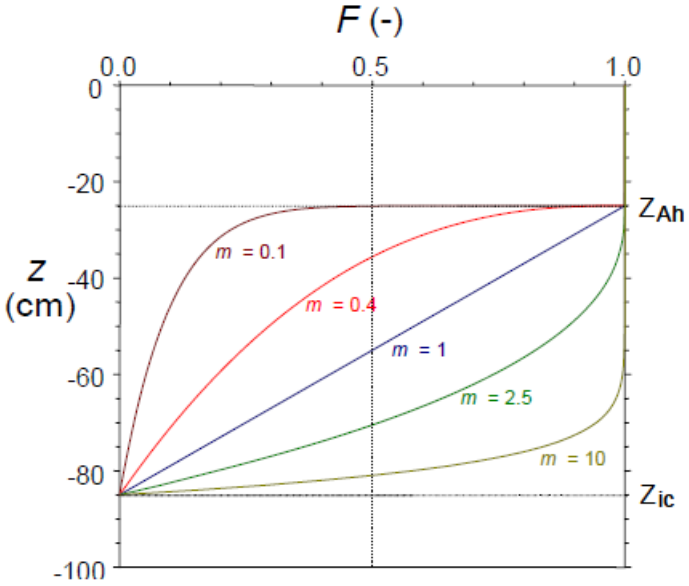

Figure 2.20: Schematic representation of the effect of a variation of m on macropore distribution with depth (Kroes et al., 2008)

.

2.18.

$$R = R_{Z_{Ah}} \frac{z}{Z_{Ah}} \qquad for \quad 0 \geq z > Z_{Ah} \tag{2.18a}$$

$$R = R_{Z_{Ah}} + (1 - R_{Z_{Ah}})(\frac{Z_{Ah} - z}{Z_{Ah} - Z_{IC}})^m \qquad for \quad Z_{Ah} \geq z \geq Z_{IC} \tag{2.18b}$$

where Z_{Ah} and Z_{IC} are defined negative downwards. Power $m < 1$ describes shallow IC systems, while $m > 1$ describes deep IC systems. When $m = 1$, the distribution between Z_{Ah} and Z_{IC} is linear. In Fig. 2.19, $m < 1$. $R_{Z_{Ah}}$ is an additional parameter with which a linear decrease of the R-curve over the thickness of the A-horizon can be described. Its default value is zero. F, the complement of R, is the fraction of IC macropores that is still functional at depth z:

$$F = 1 - R \tag{2.19}$$

Using Eq. 2.18 and 2.19, the volumetric proportion of IC macropores as a function of depth can be defined:

$$P_{IC} = \frac{F}{\frac{1}{P_{IC,0}} + F - 1} \qquad for \quad 0 \geq z > Z_{IC} \qquad and \quad 0 < P_{IC,0} \leq 1 \tag{2.20a}$$

$$P_{IC} = 0 \qquad for \quad z \leq Z_{IC} \qquad and/or \quad P_{IC,0} = 0 \tag{2.20b}$$

Persistency

With respect to persistency, SWAP divides the macropore volume into to fractions:

1. Static macropore volume: Volume of macropores that are permanently present and whose distribution as a function of depth is constant in time.

2. Dynamic macropore volume: Volume of macropores that appear because of soil shrinkage (i.e. cracking). The dynamic volume is not a constant in time.

The total macropore volume is not only distributed over the dynamic and static fractions but also over the MB and IC domains:

$$V_{mp} = V_{st} + V_{dy} \tag{2.21a}$$

$$V_{mb} = P_{mb} V_{mp} = P_{mb}(V_{st} + V_{dy}) = V_{st,mb} + P_{mb} V_{dy} \tag{2.21b}$$

$$V_{ic} = P_{ic} V_{mp} = P_{ic}(V_{st} + V_{dy}) = V_{st,ic} + P_{ic} V_{dy} \tag{2.21c}$$

Static macroporosity

The volume fraction of static macropores V_{st} as a function of depth z is described with the constant $P_{IC,0}$n the function F and the two additional parameters, $V_{st,0}[-]$, describing the volume fraction of static macropores at the soil surface, and $Z_st[cm]$, the maximum depth of static macropores. As stated previously, the volume of static macropores is distributed over the MB and IC domains:

$$V_{st,mb} = V_{st,mb,0} \qquad for \quad 0 \geq z > Z_{ic} \tag{2.22a}$$

$$V_{st,mb} = V_{st,mb,0}\frac{z - Z_{st}}{Z_{ic} - Z_{st}} \qquad for \quad Z_{ic} \geq z > Z_{st} \tag{2.22b}$$

$$V_{st,mb} = 0 \qquad for \quad z \leq Z_{st} \tag{2.22c}$$

$$V_{st,ic} = FV_{st,ic} \qquad for \quad 0 \geq z > Z_{ic} \tag{2.22d}$$

$$V_{st,ic} = 0 \qquad for \quad z \leq Z_{ic} \tag{2.22e}$$

where,

$$V_{st,ic,0} = P_{ic,0}V_{st,0} \qquad and \qquad V_{st,mb,0} = (1 - P_{ic,0})V_{st,0} \tag{2.23}$$

Dynamic macroporosity

As already expressed in section 2.3.2, in order to model soil shrinkage, or the variation of dynamic macropore volume, a relationship is established between the moisture ration of a soil at a given time and its void ratio, so that $e = f(\vartheta)$. Several functions can be used to establish this relationship. The SWAP model uses the function developed by Kim as expressed in Eq. 2.24. This function is a combination of an inverse exponential and a linear model. Input of the shrinkage curve in SWAP be done either by specifying typical points of the shrinkage curve (i.e. void ratio at $\vartheta = 0$ and air-entry point ϑ_r) or the parameters of the Kim equation.

For our purposes, we chose to use the parameters of Kim's equation. In order to obtain these parameters Kim's model will be inverted using an experimental shrinkage curve.

$$e = \alpha_K exp(-\beta_K\vartheta) + \gamma_K\vartheta \quad for \quad 0 < \vartheta < \vartheta_s \quad where \quad \vartheta_s = \frac{\theta_s}{1 - \theta_s} \tag{2.24}$$

where $\alpha_K(cm^3cm^{-3})$ is the e_0 the void ratio at $\vartheta = 0$; β_K is a dimensionless fitting parameter, proportional to the moisture ratio at the air-entry point (ϑ_R, Fig. 2.6) and so the transition between exponential and linear models; γ_K is another dimensionless fitting parameter and is equal to the slope of the linear portion of the model.

Horizontal distribution

In the horizontal plane, macropores are distributed over a variety of different forms, from holes with a diameter of $100\mu m$ to cracks a few cm wide and several dm long. The function shape of the macropores influences several processes:

1. The lateral exchange of water between macropores and the soil matric (via vertical area of macropores walls per unit of volume and the distance from macropore wall to center of matrix polygons.

2. The lateral hydraulic conductivity of cracks in case of rapid drainage.

This macropores distribution is not explicitly distinguished. Instead, it is expressed implicitly via an effective functional horizontal macropore shape that is described by an effective matrix polygon diameter $d_{pol}(cm)$, as a function of depth. It is assumed that d_{pol} is minimal at the soil surface, where macropore density is maximal, and maximal deeper in the profile, where macropore density is minimal. d_{pol} as a function of depth is given by Eq. .

$$d_{pol} = d_{p,min} + (d_{p,max} - d_{p,min})(1 - M) \tag{2.25a}$$

where M [-], the relative macropore density as a function of depth, depends on the static macropore volume if present:

$$M = \frac{V_{st}}{V_{st,0}} \qquad for \quad V_{st,0} > 0 \tag{2.25b}$$

If no static macropore volume is present, M depends ont the volumetric proportion of the IC domain:

$$M = \frac{P_{ic}}{P_{ic,0}} \qquad for \quad V_{st,0} = 0 \qquad and \quad P_{ic,0} > 0 \tag{2.25c}$$

If no static macropore volume and no IC domain are present, M can be defined as a function of depth with Z_{dpmax} as the depth below which d_{pol} equals $d_{p,max}$:

$$M = max\left(0.1 - \frac{z}{Z_{dpmax}}\right) \qquad for \quad V_{st,0} \qquad and \quad P_{ic,0} = 0 \tag{2.25d}$$

Water flow and balance

SWAP organizes macropore water flow and balance as follows:

1. Storage of water in macropore domains S_{mp}

2. Infiltration of water into macropores at the soil surface, by precipitation directly into macropores I_{pr}, and by runoff into the macropores $I_{ru}[cmd^{-1}]$

3. lateral infiltration into the unsaturated soil matrix $q_{lu}[cmd^{-1}]$

4. lateral infiltration into and exfiltration out of the saturated soil matrix $q_{ls}[cmd^{-1}]$

5. Lateral exfiltration out of the saturated soil matrix by interflow out of a zone with perched groundwater $q_{li}[cmd^{-1}]$

6. Rapid drainage to drainage systems $q_{rd}[cmd^{-1}]$

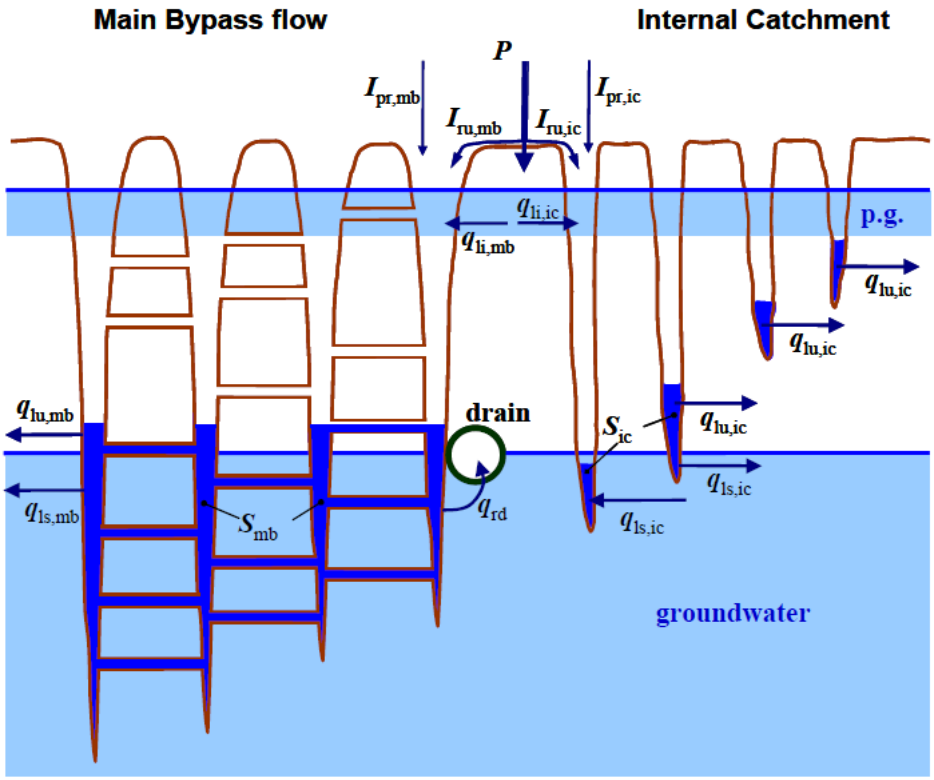

Figure 2.21: Schematic representation of water flow and balance with the macroporosity and divided over the MB and IC domains. (Kroes et al., 2008)

All of the processes above won't be detailed here, only those that are of particular interest for interpreting infiltration later on or those that require parameter input (See Tab. 3.3), i.e. Lateral infiltration into the unsaturated matrix, infiltration and exfiltration into and out of the saturated matrix, exfiltration out of perched saturated matrix.

Infiltration of water into macropores at the soil surface

The total rate of infiltration at the soil surface is the sum of precipitation, irrigation and snowmelt water routed directly into the macropores at the soil surface (I_{pr}) and of the runoff from the ponding layer into the macropores (I_{ru}).

$$I_{pr} = A_{mp} P \tag{2.26}$$

where A_{mp} is the surface of macropores at the soil surface and P is the intensity of precipitation.

$$I_{ru} = \frac{h_0}{\gamma_{Iru}} \tag{2.27}$$

where h_0 is the pressure head at the soil surface that equals the ponding height, and γ_{Iru} is the resistance for macropore inflow at the soil surface:

$$\gamma_{Iru} = \frac{h_{0,max}}{k_{ver,mp}} \quad \text{with} \quad k_{ver,mp} = 14.4 \times 10^8 \frac{w_{mp,0}^3}{d_{pol,0}} \tag{2.28}$$

where $k_{ver,mp}$ is the vertical conductivity of macropores at the soil surface, $w_{mp,0}$ is macropore width at the soil surface and $d_pol, 0$ the polygon diameter at the soil surface.

Once infiltrated into the macropore domain, the inflowing water is instantaneously added to water storage at the bottom of the domain.

Lateral infiltration into unsaturated soil matrix

This lateral infiltration only takes place over the depth where stored macropore water is in contact with the soil matrix. This infiltration depends upon two mechanisms, depending on soil matrix humidity: absorption of macropore water when capillary forces dominate and Darcy flow due to a pressure head gradient from polygon wall to center. Absorption is dominant at low soil moisture contents and is described by Philip's sorptivity. Under wet conditions with a large pressure gradient, Darcy flow will be dominant.

Lateral absorption with Philip's sorptivity:

$$I^*_{ab,t} = \frac{4 S_P \sqrt{t - t_0}}{d_{pol}\sqrt{1 - V_{mp}}} \tag{2.29}$$

where, $I^*_{ab,t}$ is the lateral absorption per unit of depth $[cmcm^{-1}]$ over time interval $t \rightarrow t_0$, S_P is Philip's sorptivity $[cmd^{-0.5}]$.

Philip's sorptivity is given by:

$$S_P = S_{P,max}\left(\frac{\theta_s - \theta_0}{\theta_s - \theta_r}\right)^{\alpha_s} \tag{2.30}$$

where, $S_{P,max}$ is the maximum sorptivity when $\theta_0 = \theta_r$ and α_s is a fitting parameter [-]. Both are SWAP input parameters.

Average absorption rate $q^*_{lu,ab}$ per unit of depth $[cmcm^{-1}d^{-1}]$ for time interval $t_1 \rightarrow t_2$:

$$q^*_{lu,ab} = \frac{I^*_{ab,t_2} - I^*_{ab,t_1}}{t_2 - t_1} \tag{2.31}$$

Infiltration rate by Darcy flow per unit of depth $q^*_{lu,D}[cmcm^{-1}d^{-1}]$:

$$q^*_{lu,D} = \frac{f_{shp} 8 K_h (h_{mp} - h_{mt})}{d^2_{pol}} \tag{2.32}$$

where, $K_h[cmd^{-1}]$ is the hydraulic conductivity as a function of pressure head, $(h_{mp} - h_{mt})/x_{pol}$ is the lateral pressure head gradient between macropores and the centre of the matrix polygon, and $f_{shp}[-]$ is a shape factor to account for uncertainties in the theoretical description of infiltration. Depending on whether the polygons are more plate or cylinder shaped, f_{shp} should be somewhere between 1 and 2. f_{shp} is a SWAP input parameter.

Finally, the lateral infiltration flux density per unit of depth $q^*_{lu}[cmcm^{-1}d^{-1}]$ is:

$$q^*_{lu} = max(q^*_{lu,ab}, q^*_{lu,D}) \tag{2.33}$$

Lateral infiltration into and exfiltration out of saturated soil matrix

Lateral infiltration into and exfiltration out of saturated soil matrix takes place over the depth where stored macropores water is in contact with the matrix. This only concerns static macropores since dynamic macropores will be swollen to their maximum volumes.

In case of water filled macropores:

$$q^*_{ls,D} = \frac{f_{shp} 8 K_{sat} (h_{mp} - h_{mt})}{d^2_{pol}} \tag{2.34}$$

In case of empty macropores, exfiltration into these macropores:

$$q^*_{ls,seep} = -\frac{h_{mt}}{\gamma_{seep}} \tag{2.35}$$

where, γ_{seep} is the seepage resistance.

Lateral exfiltration out of saturated matrix as interflow

This process is a special case of exfiltration from a saturated zone into the macropores and is described in a similar way. The perched groundwater zone is defined as a saturated zone above groundwater level and separated from the saturated zone below groundwater level by an unsaturated zone which contains at least a critical value $V_{undsat,crit}$, a SWAP input parameter.

2.7 INVERSE PROBLEM AND WELL POSEDNESS

2.7.1 INVERSE PROBLEM

An inverse problem is the process of calculating, from a set of observations, the causal factors that produced them[3]. Inverse problems are extremely useful because they give us information about parameters that we cannot always directly observe. In this case, the inverse problem enables us to avoid the difficulties linked to the swelling nature of Vertisols.

The inversion problem uses an optimization algorithm in order to run the model subsequently with different parameter values. For each parameter value the modeled data is compared to the observed data using an objective function which evaluates the maximum likelihood of a set of parameters. Assuming that the parameters are normally distributed, independent, and homoscedastic, the maximum likelihood reduces to a classical least squares problem (Eq. 2.36) (Lambot et al., 2002).

$$\phi(b) = (\theta^* - \theta)^T (\theta^* - \theta) = e^T e \tag{2.36}$$

where θ^* is the vector of observed data, θ is the vector of modeled data, and e is the difference between the two, called error.

[3]Wikipedia: Inverse problem, `https://en.wikipedia.org/wiki/Inverse_problem`, accessed on 22/07/2015

2.7.2 WELL-POSEDNESS OF THE INVERSE PROBLEM

The success of the inverse approach depends on the appropriateness of the forward model, the identifiability of the model parameters, the uniqueness and stability of the inverse solution, and the robustness of the optimization algorithm (Lambot et al., 2004).

The appropriateness of the forward model to be used in an inverse procedure will depend on the existence of the solution of the model in the parameter domain, on parameter identifiability, on the sensitivity of the model to parameters, and on the adequacy of the model to reproduce an observed system response.

Firstly, the forward solution must exist for specified parameters, boundary conditions, and initial conditions. Secondly, different parameter sets must lead to different solutions; if not, the parameters are unidentifiable. The model response for a certain parameter response must also be unique. This means specifying the parameter ranges, boundary conditions and initial conditions so that the problem can have a unique solution. Sensitivity means that the model should depend on the parameters, i.e. a variation in parameter value should induce a system response.

Model adequacy can never be known a priori (Lambot et al., 2004). Adequacy and confidence in its parameters can only be evaluated relative to the uncertainty in the observations. The model must be a valid model for describing real-world data. It may be possible that numerically validated inversion methods, that have been shown to converge on unique and stable parameter solutions, may fail when model errors are too large. This is particularly important when applying inverse modeling to real-world data where system behaviour may be influenced by a series of processes that are not included or not well concieved in the model.

2.7.3 METHODS FOR ASSESSING THE WELL-POSEDNESS OF THE INVERSE PROBLEM

Several methods exist for assessing the well-posedness of the inverse problem. A first method is response surface analysis. Response surface analysis allows one to assess the problems related to nonuniqueness, model sensitivity, and parameter dependency in an objective and transparent way. Response surfaces are two-dimensional contour plots representing the objective function as a function of two parameters. They represent therefore only cross sections of the full M-dimensional parameter space.

A measure of identifiability can usually be given by calculating the sensitivity of the model to the parameter in question. Calculating sensitivity is important because it distinguishes between sensitive and identifiable parameters and insensitive non-identifiable parameters. The former are important to identify accurately because of the effect of their variation on the model response. The latter can be fixed to an approximate value because the model is less sensitive to them. It would also be more difficult to the determine them by inversion. Finally, a sensitivity analysis descretized according to depth gives an indication to the most sensitive depths at which to optimally place the moisture probes. Thus, a sensitivity analysis provides valuable insight to optimize experimental design and determine which parameters can be optimized.

Elements $S_{i,j}$ of the sensitivity matrix $\mathbf{S}$ (size $n \times p$, where n is the number of observations and p is the length of the parameter vector) are computed as follows:

$$S_{i,j} = b_j J_{i,j} \tag{2.37}$$

where $\mathbf{J}$ is the Jacobian matrix (size $n \times p$) whose elements $J_{i,j}$ are defined as the partial derivatives $\partial\theta_i/\partial b_j$. Elements of $J_{i,j}$ represent the change in model response θ to a change of 1% of the parameter b_j. $\mathbf{J}$ is normalized by b_j in order to be able to compare sensitivities.

Model adequacy can be evaluated using a maximum liklehood estimator (Lambot et al., 2004). At the global minimum, the objective function follows a chi-square distribution and the probability of model adequacey is expressed as:

$$p_{adeq} = 1 - Q(min\phi(b), n - p) \tag{2.38}$$

where $Q(min\phi(b), n - p)$ is the chi-square cumulative density function.

Unidentifiable parameters (due to either poor sensitivity or parameter correlation) can be measured by parameter uncertainty. Parameter uncertainty can originate from model errors (non-adequacy or non-validity) or experimental errors. Parameter uncertainty is determined on the basis of the parameter variance-covariance matrix $\mathbf{C}$ (Kool et al., 1988).

$$\boldsymbol{C} = \frac{\boldsymbol{e}^T \boldsymbol{e}}{n - p} \boldsymbol{H}^{-1} \tag{2.39}$$

Where $\mathbf{H}$ is the Hessian matrix ($p \times p$), e is the error between model response and real data, n is the number of observations and p is the number of parameters. The elements $H_{i,j}$ of $\mathbf{H}$ are determined as follows:

$$H_{i,j} = \frac{\partial\phi(b)}{\partial b_i \partial b_j} \tag{2.40}$$

where b_i and b_j are parameters.

Parameters that are strongly correlated lead to un-identifiabiability and non-uniqueness. The elements of the correlation matrix are given by:

$$A_{i,j} = \frac{C_{i,j}}{\sqrt{C_{i,i}}\sqrt{C_{j,j}}} \tag{2.41}$$

Approximate confidence intervals for each parameter can then be given by:

$$b_i - t_{1-\alpha/2}^{n-p}\sqrt{C_{i,i}} \leq b_i \leq b_i - t_{1-\alpha/2}^{n-p}\sqrt{C_{i,i}} \tag{2.42}$$

where $t_{1-\alpha/2}^{n-p}$ is the value of Student's distribution with $(n - p)$ degrees of freedom and confidence level $(1 - \alpha)$.

The series of test simulations to assess the well-posedness of an inverse problem are referred to as numerical experiments.

3

Materials and methods

3.1 EXPERIMENTAL DESIGN

3.1.1 SAMPLING PROTOCOL

Based on existing soil and land cover maps of the PVNP, the location of an existing network of surface and groundwater dataloggers currently recording water the temporal dynamics of water level, and the knowledge of the system by local experts, six sites were determined for assessing the soil hydraulic parameters and modeling the soil water flow. These sites are all near the six groundwater dataloggers (Fig. 3.1) set up within the framework of the UF PhD study of A. Alonso (personal communication).

Table 3.1: Coordinates of the sampling sites (WGS84)

Site	X	Y
Laguna	-85.34023815	10.34478085
Tempisque	-85.34043868	10.32633098
Chamorro	-85.36577073	10.34331655
Posaverde	-85.37602526	10.37798304
Varillal	-85.34429066	10.40235892
La Bocana	-85.27457677	10.34797322

The sites chosen are all georeferenced and named (Tab. 3.1)

A soil profile was dug at each site to an approximate depth of 1 m. Because of the hardness of the soil, a hydraulic digger was used (Fig. A2). Photos were taken using a DSLR camera and the soil horizons were delimited on the base of visual observation . Disturbed samples of approximately 100-200 cm^3 were taken from each horizon. If the profile was visually homogeneous, three samples were taken at regular intervals. This rendered the sampling given by Tab. 3.2.

Two soil aggregates were collected at -10cm, -20cm and -45cm in order to perform SSCC tests.

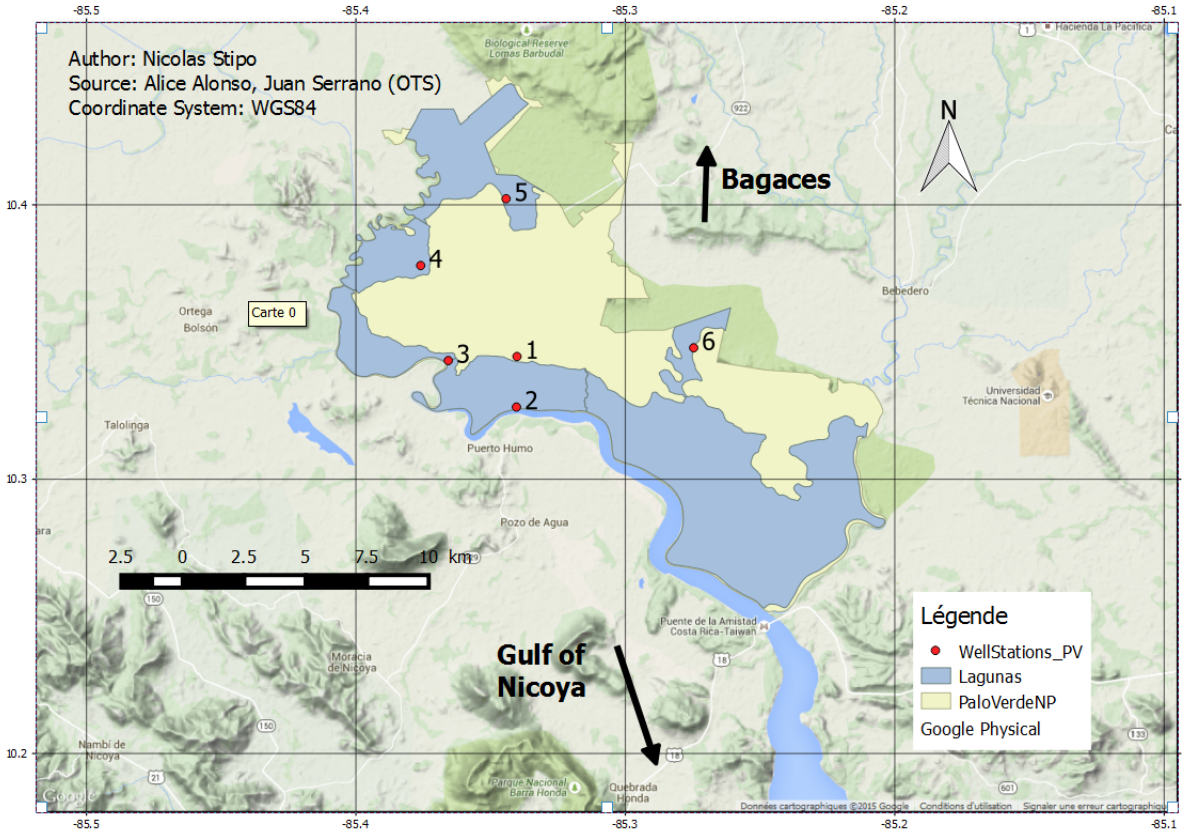

Figure 3.1: Map of the location of groundwater dataloggers and thus of our experimental sites. 1. Palo Verde Laguna, 2. Tempisque, 3. Chamorro, 4. Posaverde, 5. Varillal, 6. La Bocana

Table 3.2: Sampling depths for each site

Site	Depths
Laguna:	-30, -60, -85 cm
Chamorro:	-10, -20, -45 cm
Posaverde:	-10, -45, -80cm
Varillal:	-30, -60, -100cm
La Bocana:	-10, -45, -75, -100cm
Tempisque:	-10, -45, -80 cm

3.1.2 PHYSICO-CHEMICAL CHARACTERIZATION

Soil samples were transported back to Belgium in plastic ziplock bags. These bags were placed in hermetically sealed metal cases.

Once in the laboratory (ACME,UCL), the soil samples were air-dried for a few days before being sieved at 2 mm. pH in an aqueous solution was measured using a pH probe. CEC and exchangeable bases (Na^+, K^+, Ca^{++}, and Mg^{++}) were measured using the Schollenberger method (Schollenberger and Simon, 1945). The soil columns were rinsed successively with NH_4^+ to saturate the sample, then removal of the excess by washing with alcohol, and finally displacement with KCl. The displaced NH_4^+ was measured using colorimetry with a NH_4^+ test kit. The soil cations were determined using ICP-MS.

Soil texture was measured by sedimentation using Stokes law according to the Raviller method used for soils containing smectite (Raviller et al., 1972). First the sand fraction was sieved out using ultrasounds to detach all silt and clay particles. Then the clays were dispersed using resins before mixing and letting the soil/water solution settle. Samples were taken after 1 min, 4 min 48 s and 24 hours. These give the fractions of coarse silt, fine silt and clay respectively. Clay mineralogy was not determined in order to reduce costs and analysis time. Instead, the type of clay minerals was inferred from soil texture, organic matter content and CEC. For example, an idea of clay mineralogy can be given by Eq. 3.1 (Baize, 2000).

$$CEC_{clay} = \frac{CEC - (\%OM \times 2)}{\%Clay} \times 100 \tag{3.1}$$

If $CEC_{clay} < 25\ meq/100g$ than the majority of clays are kaolinite. If $CEC_{clay} > 45\ meq/100g$ than the majority of clays are swelling smectite. If $25 < CEC_{clay} < 45\ meq/100g$ than the situation is ambiguous and difficult to determine.

The effective cation exchange capacity is calculated as the sum of the exchangeable bases.

For the Laguna site at depths of 30, and 60 cm and for La Bocana site at 100cm, soil minerals were determined by x-ray diffraction using the D8 Advance diffractometer from Bruker (CuKa, I = 0.15418 nm , 40KV, 30mA and 2 theta= 1°/min).

Carbon content was determined by the Walkley & Black method (Walkley and Black, 1934). The Walkley & Black method is a method for estimating organic carbon and total organic matter from the total oxidizable carbon using conversion factors. The total oxidizable carbon is found by complete oxidation using potassium dichromate in the presence of sulfuric acid. The excess dichromate is titrated using ammonium ferrous sulfate.

3.1.3 CHARACTERIZATION OF SSCC

The method used for determining the shrinkage characteristics was the hand-spray aggregate method described in section 2.4. Indeed, of all the methods considered, aggregate methods seemed to be the best adapted. The first reason for this is purely practical. Because of the extreme hardness of some of the soils in the Palo Verde National Park, soil core extraction was extremely difficult and only disturbed samples and soil aggregates were possible to extract. Core

methods also tend to underestimate shrinkage and the volume measurements that accompany them tend to be less precise.

In-situ methods were also considered but presented a few problems. Installation requires digging small diameter boreholes. This must be done cleanly in order for there to be a good contact between the transducer and the soil. In addition to this, the Palo Verde National Park was visited in the middle of the dry season (February-March) when the soil was exceptionally dry and hard. This implies that a hand-held auger would not allow installation of gauges. For this method, more expensive equipment would have been needed and was finally not available.

Aggregates were sampled at three depths for each site, the three depths at which soil moisture probes are installed (see next section). Two aggregates were measured for each soil depth to increase statistical validity, which adds up to 36 samples in total (6 sites, 3 depths, 2 replicates). Each sample was mounted on a tripod made from nails pushed through a styrofoam board (Fig. 3.2). Each aggregate was then coated with two coats of spray-on plaster (of the brand Hansaplast). The coating was left to dry for an hour and then the aggregates were sanded on a belt sander to expose a small flat surface. The aggregates were weighed before and after application of the coating, and the mass was corrected. A density of $0.77 gcm^{-3}$ (Liu and Buzzi, 2014) was used in order to calculate the volume of coating. The aggregates were then saturated in a vacuum chamber. The perforated ceramic plate of the chamber was lined with nylon meshing and the aggregates were placed on this meshing. Water was brought up to a level just over the meshing and the aggregates were left to saturate by capillarity for three days. If after the three days, some aggregates weren't saturated, a vacuum was applied to the desiccator to aid in the capillary wetting of the samples.

Figure 3.2: Image of HSP used and the spraying setup

The aggregates were then recoated with two layers of plaster before being weighed hydrostatically in a plastic cup of water on a high precision balance ($1e^{-4}$ g) which had been tared with the weight of the cup and water. A metal support was welded to support a thin metal wire. The extremity of the wire was bent into a ring to accommodate the sample so it could be lowered into the water. The metal support sits around the balance, not on it.

The soil aggregates were weighed in air and in water every day for sixteen days. The

first measurement gives the total mass of the sample, while the second gives the total volume. According to Archimedes' principle, the volume of an object immersed in water is equal to the volume of fluid (or mass in the case of water) that it displaces. In the first few days, a few aggregates were lost because they were badly sealed, meaning that they fell apart upon contact with the water. For aggregates that only lost one or two small pieces, they were recoated and reweighed. The experiment was then continued and previous measurements were not kept.

The moisture ratio was calculated by Eq. 2.4b while the void ratio was calculated using Eq. 2.5. Specific density was calculated using the Standard Test for Specific Gravity of Soil Solids by Water Pycnometer (ASTM D 854-00). For this method, three measurements are made: (1) mass of the dry soil sample (W_0), (2) mass of pycnometer filled with water to a given level (W_A)), (3) mass of pycnometer filled with soil and water to the same level (W_B). From these three measurements the specific density can be derived:

$$\rho_s = \frac{W_0}{W_0 + (W_A - W_B)} \tag{3.2}$$

Once the experimental soil shrinkage curve was established, Kim's equation for shrinkage was fitted to the data points using the GMCS optimization algorithm. This yielded the three parameters to Kim's equation used as input for the SWAP model.

3.1.4 HYDROLOGICAL CHARACTERIZATION (WRC, CC)

Generally speaking, for hydraulic characterization, in-situ methods were favoured from the get-go, because they enable measurements to be made on real soils, in the field, and so avoid problems such as soil disturbance and having to determine a minimal representative volume.

For this reason, methods using disturbed soils or clay pastes such as (Douglas and McKyes (1978), Douglas et al. (1980), Smiles and Harvey (1973), and Kim et al. (1992c)) were not considered. Traditional methods such as the sandbox, pressure plate, and evaporative methods (Boels et al., 1978) are approximate because of surface smoothing and the fact that they don't account for shrinkage. They can be adapted though by coupling with a shrinkage curve for mass calculations and by careful manipulation. Soil surface smoothing is a major problem. Fig. 3.3 shows the degree of effect that surface smoothing can have on evaporative fluxes. Ruy and Cabidoche (1998) countered smoothing by blow drying the core surface and chipping away micro-aggregates to expose the soil's natural porosity). For hydraulic conductivity, the methods of Garnier et al. (1997) and Ruy and Cabidoche (1998) seem to be the best laboratory methods since they account for shrinkage and do not destructure the soil.

All laboratory methods do destructure the soil to some degree however, which is why in-situ methods were favoured. The THERESA method of Cabidoche and Ozier-Lafontaine (1995), Cabidoche and Voltz (1995), and Ruy and Cabidoche (1998) was considered. However, it wasn't used for the same reasons specified in the previous section.

We implemented an in-situ rainfall infiltration experiment, and monitored soil water at different depths using capacity probes, which measure the dielectric permittivity of the soil.

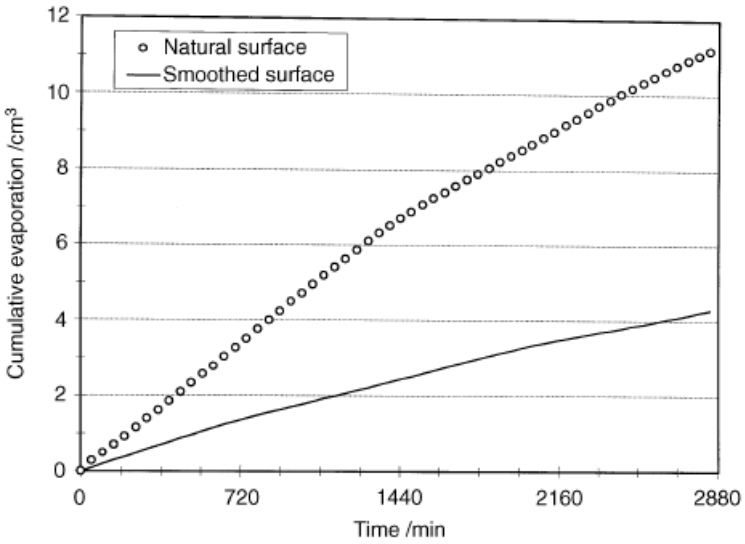

Figure 3.3: Graph of the effect of smoothing on the evaporative flow of a soil core (Ruy and Cabidoche, 1998)

The data collected from these experiments was used to obtain the hydraulic parameters of the soil via inversion of the SWAP model.

The probe used is the Ech2o EC-20 probe, developed by Decagon. The Ech2o EC20's are capacitance-type probes which means that they determine the dielectric permittivity of a medium by measuring the charge time of a capacitor, which uses the medium as a di-electric. Using a Campbell Scientific CR1000 datalogger, a 25V excitation was created with a frequency of $60Hz$ and the probe response was recorded every minute. The response of the probe is given as a potential (in Volts). This potential is directly linked to the soil humidity via a calibration curve established at the factory (Eq. 3.3).

$$\theta = 1.75 * U - 0.29 \tag{3.3}$$

The validity of this calibration curve was questioned, even though Decagon ensures that their factory calibration gives ±3-4% accuracy and that a soil specific calibration only increases this accuracy to ±1-2%. However, soil specific calibration requires packing a specific mass of soil at a known volumetric moisture ratio into a known volume. This is done to recreate the soil bulk density in the field which is important because dielectric probes establish a link between the dielectric constant and volumetric water content. However, bulk density varies with moisture in a shrinking-swelling soil. For this reason, the soil calibration was not feasible in the field because the shrinkage curve first needs to be established in order to plot bulk density according to soil moisture. For this reason, soil was brought back in order to perform a calibration in the laboratory if needed. This calibration was not done, for reasons discussed later on.

The soil probes were placed at depths of 10, 20, and 45 cm. In order to insert the probes, a metal sheet was used to create pilot holes. This was necessary because of the hardness of the soil and the flexible nature of the probes. Based on hydraulic conductivity estimates, 45 cm was chosen as the lowest depth possible to keep simulation times relatively short in order to

minimize water usage. Indeed, water usage was limited by reservoir size. The first two probes were placed close to the surface to obtain more information on preferential macropore flow at these shallow depths.

Rainfall was simulated according to the methodology of Humphry et al. (2002). Humphry et al. (2002) developed a rainfall simulation method designed to be easy to operate and transport to and from the field while maintaining critical intensity, distribution, and energy characteristics of natural rainfall. It was developed within the context of a project studying the link between soil phosphorous levels and phosphorous in runoff. The project was funded by USDA-NRCS, USDA-ARS, and USEPA. Their rainfall simulator was designed according to three characteristics: kinetic energy of the drops upon impact, intensity, and uniformity.

Our rainfall simulator was not designed to the same level of detail because the kinetic energy aspect was not needed. Indeed, the method of Humphry et al. (2002) was developed to relate soil phosphorous to runoff phosphorous. For our purposes (setting a known and stable boundary condition for the model) only intensity and uniformity were considered.

The simulator was made up of a gas powered non-submersible pump, a pressure regulator and a square 50 WSQ nozzle, all supplied by the University of Florida (Fig. 3.4). The setup also came supplied with manometer for measuring pressure head at the nozzle. The manometer broke however during transport meaning that a known intensity couldn't be set for all sites. Instead, pressure was approximated based on pressure regulator bolt position and pump settings and intensity was measured after each infiltration experiment from 16 points over a 2 m x 2 m surface. The water supply was provided by a 2000 liter trailer-tank which was filled prior to each infiltration from irrigation canals, with the help of the park rangers.

Figure 3.4: Photos of rainfall simulator components. Upper left: pump; Upper right: threaded coupling for easy assembly; Bottom left: pressure regulator; Bottom right: 50WSQ nozzle

The simulator frame was constructed from 1" stainless steel tubing sourced in Costa Rica. The tubing was welded together with the help of a local technician into a 2x2x2 m frame. Due to extremely strong winds (March being the windiest month in the PVNP) tarps had to be securely attached to the structure with rope and anchored to the ground (Fig. 3.5). This proved to be quite challenging as previous attempts, with thinner tubing, resulted in bent and broken structures.

Figure 3.5: Photo of rain simulator setup

Because of the lack of manometer, intensity was initially approximated based on initial tests and then measured after each infiltration experiment. The intensity needed was determined based on several factors: (1) intensity needed to saturated at least the top two probes, in order to obtain information on saturated hydraulic parameters; (2) Reservoir size; (3) Natural rainfall episodes. Based on simulations with estimated hydraulic parameters (HYPRES database) made prior to the field work and natural tropical precipitation intensities (Humphry et al. (2002), Favre et al. (1997)) it was estimated that intensity should be around 50-70 mmh^{-1}. For a nozzle spread of approximately 2.5 m, that equals about 0.34 m^3h^{-1}. Test simulations showed that for this intensity, all three probes should be saturated after four hours, or 1.4 m^3, which is still less than the capacity of the 2000 L reservoir.

3.1.5 MACROPOROSITY DISTRIBUTION AND FLOW

The macroporosity parameters identified as important in section 3.3.2 were also identified via the same model inversion as the hydraulic properties. This is because numerical experiments revealed that certain macropore parameters, such as Z_{IC}, m and $P_{IC,0}$ were in fact important for describing macropore flow, even in the absence of static macroporosity. This is far from optimal for several reasons that will be discussed later but chief of which is that it increases the number of parameters that must be inverted from 3 to 6.

3.2 MODEL SETUP

In order to accurately model reality and ensure well-posedness of the inverse problem, the model parameters must be defined accurately. Many model parameters, such as those pertaining to the numerical solution or soil discretization, could be defined right from the start (See section 3.3.1). For other parameters, the results of preliminary numerical experiments and soil analysis were needed before deciding which parameters could be defined and how.

Before defining certain model parameter values, the general model setup should be defined. This includes describing boundary (such a meteorological data and drainage data) and initial conditions precisely, as well as the discretization of the soil profile.

The infiltration experiments were usually conducted for four hours, or until the last probe reached saturation followed by a 30 min period of zero rainfall. This 30 minute period created an inflection point in the soil moisture evolution curve, providing more information for the inversion. The total duration of the experiment is the duration used for defining the time domain. The minimum time step is limited to $10^{-5}(d)$ and the maximum time step to $10^{-2}(d)$, as recommended by Kroes et al. (2008) for soils with macropore flow.

The depth of the soil profile is fixed at 50 cm. This was defined by the depth of the third probe, which is 45 cm. Each layer was divided into sublayers depending on the height of the soil compartments used for the numerical solution. In general, in order to ensure accurate calculations and according to SWAP literature, the thickness of these compartments were 1.0 cm for the first 10 cm and 2.5 cm for a depth of 10-50 cm. Thin compartment thickness is needed for accurate calculation of macropore flow.

The top boundary condition corresponds to a step function with a constant rainfall until saturation is reached at the last probe. Precipitation is then reduced to zero and soil moisture is monitored for another 30 minutes. For realistic rainfall intensities, rainfall option SWRAIN 3 is preferred, which provides detailed rainfall intensities as opposed to daily intensities. Daily intensities greatly underestimate macropore inflow at the soil surface (Kroes et al., 2008). Evapotranspiration was not considered because of the the experimental conditions at the site. No transpiration took place because of the lack of vegetation directly over each profile. Also, the presence of the rain simulator structure, wrapped in tarps, greatly reduces wind speed as well as reducing *direct* solar radiation to zero. In addition to this, the relative humidity is greatly increased because of the enclosed space around the infiltration site. Finally, the time-period during which precipitation is equal to zero and evaporation takes place is relatively short (30 min).

The bottom boundary condition is specified as free drainage. The initial conditions are described as the pressure head of each compartment being in hydrostatic equilibrium with initial groundwater level [1].

[1] This data is obtained from the University of Florida's Hydrobase Server (version 3.0).

3.3 INVERSE PROBLEM

3.3.1 NUMERICAL EXPERIMENTS

In order to get an idea of which parameters must be optimized and which can be fixed, a general sensitivity response was conducted in the same manner as Lambot et al. (2002). However instead of analyzing the change in objective function response, the change in direct model response was analyzed. Both water content and the derivative of water content were analyzed. The initial values used were those described in section 3.3.2.

The robustness of the inversion method and algorithm was tested by inverse parameter estimation using a series of simulated data instead of real data. The algorithm is deemed robust if it is able to find the initial parameters, even when a large parameter space is specified. The parameters used were estimated manually in order to try and approximate the infiltration data from the Chamorro site 3.4. This ensured that the sub-space of the main parameter space tested was relatively close to reality.

The modeled data was simulated using the parameter values specified in section. 3.3.2. An inversion was first made for K_{sat} and α with all other parameters fixed. The parameters Z_{IC}, m, and $P_{IC,0}$ for macropore distribution were then added and a second inversion was performed. Finally, $V_{st,0}$ relative to static macroporosity was added and a third inversion was performed. Each time, the quality of the inversion was assessed by studying the optimized parameter values, their confidence intervals and the coefficient of determination R^2 of the fit. In order to progressively test robustness, inversions were performed for an increasing number of parameters, from two to six. The parameters that were inverted and their ranges are defined in Tab. 3.5.

Parameter identifiability was assessed via response surface analysis and sensitivity analysis. The response surfaces were constructed by calculating the two dimensional matrices of objective function values for all combinations of parameter values within a given range. This was done two parameters at a time, but in order to reduce the number of parameter combinations, Van Genuchten-Mualem parameters and macropore distribution parameters were considered separate groups. The objective function was evaluated for parameters within the ranges defined in Tab. 3.5.

The sensitivity analysis was done using two methodologies in order to qualify and quantify parameter sensitivity. The first is the method that was described above and gives a quantified notion of sensitivity but gives little information on the nature of the effect of each parameter on the model response. For this, a model response was produced for parameter values in the vicinity of the optimized parameter set. Then, each parameter was modified separately and manually to produce a new model response. Graphs of different model responses were compared in order to get a feeling for the effect of each parameter on the simulated data.

Finally, model validity was evaluated by manually changing parameter values in order to try to reproduce the same dynamics as those observed in the measured data. The quality of the fit as well as a comparison of the dynamics of modeled and measure infiltration curves were used

to assess the validity of the fit.

3.3.2 MODEL PARAMETERIZATION

Now that the model domain and boundaries have been defined, we can identify all the parameters that must be found by inversion or that may be fixed at arbitrary values. These parameters are grouped in Tab. 3.3. Regarding soil hydraulic functions, saturated hydraulic conductivity is relative to the conductivity of the matrix only.

Based on the preliminary sensitivity analysis and response surfaces, presented in the Results section, on soil observations and on advice taken from the SWAP documentation (Kroes et al., 2008), the parameters that must be determined by inversion were defined: K_{sat}, α, $alpha_K$, β_K, γ_K, Z_{IC}, m, $P_{IC,0}$, and $V_st, 0$.

Other parameters were fixed at plausible values. PondMAX and RSRO were fixed at default values of 0.1 cm and 0.1 days respectively. RSRO was fixed at 1. θ_s was fixed to measured values determined during the SSCC characterization. θ_r was set to an arbitrarily low value. λ was set to the often used value of 0.5. For the sites, where static macroporosity was modeled, the number of parameters was decreased by fixing n using ROSETTA pedotransfer functions.

The anisotropy ratio r_s was fixed at 3.0, assuming isotropic shrinkage. θ_{CrMP} was fixed at 95% of θ_s and z_{crack} was set to 0. An A horizon was not considered meaning R_{ZAh} and Z_{Ah} were fixed to zero. The number of subdomains was set to 4, the value recommended by the SWAP documentation. Despite high sensitivity, Z_{st} was not estimated by inversion because it can usually be approximated. SWAP literature advises taking Z_{st} at or a few decimeters above the highest annual groundwater level. For our model, Z_{st} was either set to the bottom of the profile (-50 cm) or higher based on infiltration curve observation.

$d_{p,min}$ and $d_{p,max}$ were set to values observed in the field, usually between 15 and 20 cm. Z_{dpmax} was set to -50 cm, the bottom of the profile.

Because the Parlange shape factor was used, $S_{p,max}$ and α_s did not need to be defined. Based, on sensitivity results and infiltration curve analysis, $SFacParl$ was set to a value of 75. Darcy flow for lateral flow was not defined, removing the need to define f_{sh} and $V_{undsat,crit}$.

Finally, for further numerical experiments and for defining accurate parameter ranges for parameter inversion, the most sensitive parameters, defined above, were manually set so that the model response approximated the Chamorro infiltration data. These parameter values are given by Tab. 3.4.

Table 3.3: List of SWAP parameters that must be defined

Equation	Parameter	Definition
Ponding	$PondMAX$	Min thickness for runoff
	$RSRO$	Drainage resistance for surface runoff
	$RSROEXP$	Form parameter for runoff
Mualem - Van Genuchten	θ_s	Saturated water content
	θ_r	Residual water content
	K_{sat}	Saturated conductivity
	α	Form parameters
	λ	
	n	
Dynamic macroporosity	α_K	Void ratio in dry conditions
	β_K	Air-entry point
	γ_K	Slope for normal shrinkage
	r_s	Shrinkage geometry
	θ_{CrMp}	Threshold moisture content below which horizontal shrinkage exists
	z_{crack}	Depth at which surface crack volume is computed
Static macropore geometry	R_{ZAh}	Distribution factor IC domain in horizon A
	Z_{Ah}	Depth horizon A
	Z_{IC}	Depth IC domain
	m	Power shape factor for IC distribution
	$P_{IC,0}$	Proportion IC domain at surface
	$NumSbDm$	Number of sub domains for numerical implementation
Static macropore distribution	$V_{st,0}$	Volume ratio of static macropores at surface
	Z_{st}	Max depth static macropores
Horizontal crack distribution	$d_{p,min}$	Min diameter of shrinkage polygons
	$d_{p,max}$	Maximum depth of soil polygons
	$Z_{dp,max}$	Depth below which $d_{pol} = 0$
Macropore flow	SFacParl	Parlange's shape factor for determining sorptivity from hydraulic characteristics.
	$S_{p,max}$	Max sorptivity at θ_r
	α_s	Philip's sorptivity shape factor
	f_{sh}	Shape factor for lateral Darcy flow
	$V_{undsat,crit}$	Critical volume for unsaturated matrix under perched groundwater

Table 3.4: Table of approximate parameter values used for numerical experiments

Parameter	Value
K_{sat}	30 cm/d
α	0.02 cm^{-1}
Z_{IC}	-20 cm
m	10 [-]
$P_{IC,0}$	0.4 [-]
$V_{st,0}$	0.4 cm^3cm^{-3}

3.3.3 DESCRIPTION OF THE INVERSION PROBLEM

The optimization algorithm used is the Global Multilevel Coordinate Search (GMCS) algorithm (Huyer and Neumaier, 1999), combined sequentially with the Nelder-Mead Simplex algorithm (NMS) (Lagarias et al., 1999). GMCS is designed to overcome the problem of complex topography of the objective function, without requiring excessive computing resources. GMCS itself does a global and local minimum search. However, to improve accuracy, and speed, the amount of time that GMCS spends looking for a local minimum is reduced and the algorithm is combined sequentially with the Nelder-Mead algorithm. The operation of the GMCS algorithm won't be described in detail here. For more information, see Huyer and Neumaier (1999).

The objective function used in this study is the sum of the square residuals, defined by Eq. 2.36. Because of the errors present in the data, it was decided to perform the model inversion on the variation of soil moisture content instead of the actual moisture content measured. Indeed, the use of capacitance type probes for measuring volumetric moisture content in a swelling soil most likely systematically underestimates the moisture content, if the probes are not calibrated (Kim et al., 2000). In our case, probes were not calibrated because of a lack of time. In order to calibrate the Ech2o EC-20, soil must be packed to field bulk density at different moisture contents. Measurements are made for each moisture content and then validated by gravimetric moisture content determination. However, because soil bulk density varies with moisture, the soil shrinkage curves were needed first. By the time they were acquired, and accounting for the time for the soil to equilibrate at each calibration stage, not enough time was left to perform the calibration. In addition to this, the probes were only designed to measure a maximum water content of 40%. This is confirmed by observation of the infiltration data which seems to be capped at 40%.

Because of these errors, it was decided to invert the model using the variation of soil moisture content, AKA the derivative of the raw curve. For both the measured data and the modeled data, this was obtained by substracting each element of the data vector from the following element and dividing by the time step of 2 min. This gives us a variation of water content in $cm^3cm^{-3}min^{-1}$. Before doing this, the raw data was smoothed by fitting a multi-sigmoid function to the data using Eq. 3.4 and the GMCS algorithm. Data occurring before the first jump in water content and data corresponding to the saturation plateau were removed.

$$y = H_0 + \sum \frac{(B_i t + H_i)}{(1 + exp(-K_i(t - t_i)))} \tag{3.4}$$

where t position vector (in our case length(t) was equal to the number of observations), H_0 is the starting value for t=0, H_i is the height of the sigmoid, B_i is the slope of the upper tangent (reduces to 0 for a perfect sigmoid), K_i is the growth rate, t_i is the t at the sigmoid's inflection point.

The choice of the parameters to estimate by inversion was made using the results of the a global sensitivity analysis. The results of this sensitivity analysis led to a model parameterization (section 3.3.2) which determined that the parameters that had to be estimated by inversion were: K_{sat}, α, Z_{IC}, m, $P_{IC,0}$, $V_{st,0}$ except for La Bocana site. For this site, the infiltration data showed no preferential flow so macroporosity was not taken into account. Because the number of parameters was lower, n was estimated by inversion with K_{sat} and m. For all the other sites, n was estimated using Rosetta pedotransfer functions. The parameter ranges are defined in Tab. 3.5.

For reasons stated above and in infiltration and inversion results sections, most of the sites yielded very poor inversion results. After many tries for different GMCS parameterizations, it was decided that the problem was too ill-posed. For this reason, the parameters were estimated manually, while trying to reproduce the dynamics observed in the infiltration data as closely as possible. The main parameters that were manipulated were K_{sat}, α, n Z_{IC}, m, $P_{IC,0}$, $V_{st,0}$ and Z_{st}.

Table 3.5: Parameter ranges for model inversion and response surfaces

	K_{sat}	α	Z_{IC}	m	$P_{IC,0}$	$V_{st,0}$
Lower value	5	0.01	-49	0.1	0.1	0.01
Higher value	100	0.05	-1	10	0.9	0.5

The quality of the inversion was estimated using several indicators. First a graphical assessment of the fit was made. If this was satisfactory, then parameter values and their respective confidence intervals were studied. The coefficient of determination was also used as an indicator of the quality of the fit with measured data.

3.4 DIRECT MODELING SCENARIO

Once the results of the inverse parameter estimation were obtained, direct modeling scenarios were simulating and analyzed. Because of the lack of time towards the end of the thesis, this was only done for one site. The site modeled was the Tempisque site, based on the usefulness for future studies, notably its proximity to the main marsh, and on the quality of the parameters values obtained by inversion for this site.

The model setup was the same as for model inversion (section 3.3.2). Groundwater level was not simulated because of the lack of soil property data for the depth between 45 cm and

groundwater level. Instead, soil moisture content, was observed on a bi-hourly basis, while the drainage flux and the ponding layer were studied on a daily basis. The duration of the forward modeling experiment was one full year, from the February to February in order to be sure to encompass a full wet season. Precipitation and reference evapotranspiration data was retrieved from the OTS database[2]. The data used dates from 2002-2003 because that was the latest daily data, downloadable from the database. Meteorological data was specified on a daily basis with daily pre-calculated evapotranspiration and precipitation.

Four scenarios were considered. The first scenario considered a non-rigid soil and used the parameters estimated by model inversion, including dynamic and static macroporosity. The second scenario used estimated hydraulic properties but did not model macroporosity, in order to determine its effect on soil water balance. The third scenario considered the soil to be rigid and used Mualem - Van Genuchten parameters determined from Neural Network prediction with Rosetta pedotransfer equations in HYDRUS. This was done to provide a benchmark for analysis given the poor results of the inverse parameter estimation and to assess the importance of a change in hydraulic properties on soil water balance as opposed to other factors such as runon/runoff and groundwater level.

In order to study the dynamics of groundwater levels in response to precipitation at the soil surface, a fourth scenario was considered. This scenario supposed the entire soil profile, down to the groundwater level to be homogeneous. This enabled a forward simulation taking into account the groundwater level. The bottom boundary condition can be described as a bottom flux which is a function of groundwater level:

$$Q_{bot} = A * exp(B * abs(groundwaterlevel)) \tag{3.5}$$

where A and B are form parameters.

However, because of a lack of data needed to establish a correlation between Q_{bot} and the groundwater level (GWL), significant results could not be simulated.

The soil parameters given by the Rosetta pedotransfer equations are:

Table 3.6: Table of estimated parameters for the Tempisque site using Rosetta pedotransfer functions built in to HYDRUS-1D

Parameter	Value
θ_s	0.4999
θ_r	0.1004
$K_{sat}\ cm/d$	24.25
$\alpha\ cm^{-1}$	0.0176
$n\ cm$	1.2503

[2]OTS meteorological database, `http://www.ots.ac.cr/meteoro/default.php?pestacion=1`, accessed: 15/07/2015

4

Results and Discussions

4.1 EXPERIMENTAL RESULTS

4.1.1 PHYSICO-CHEMICAL RESULTS

The results of the physico-chemical assessment are assembled here and grouped by site.

Palo Verde Laguna

This site is situated on the northern limits of the main Palo Verde laguna. The profile dug was approximately 100 cm deep and was delimited into three horizons.

- 0-45 cm: Dry, hard, soil, rich in clay. Cracks were visible in the profile face. Dark grey in color.
- 45-75 cm: More friable soil, less rich in color. Tan to brown in color.
- 75+ cm: Rich in clay with a black color.

This profile does not have lithic contact with the 100 cm sampled, the lowest clay content percentage is 56%, seasonal cracks are observable and a gilgaï topography combined with the presence of wedge-shaped aggregates is observed. Based on these observations, the soil can be classified as a Vertisol, according to the *American Soil Taxonomy* defined in the Vertisol theory chapter.

The physico-chemical data for the Laguna site can be found in Tab. 4.1 and shows that the profile is very rich in clay, in general, even with the presence of a soil horizon from 45-75 cm that has slightly less clay. This is compensated by higher sand and silt contents as well as a much higher percentage of calcination[1] from 550 - 1100°C. This is usually correlated to the oxidation of carbonates since most of the water between the clay sheets has already evaporated, and thus gives an indication of the amount of carbonates in a soil. Indeed, for temperatures of over 1000°C, 44% of the mass of $CaCO_3$ is lost (Baize, 2000):

[1]The percentage of calcination is calculated relative to the dry soil mass at 105°C

$$CaCO_3 \rightarrow CaO + CO_2 \nearrow \tag{4.1}$$

The effective CEC is given by Tab. B1. However, for the second layer, we see that the ECEC is higher than the CEC. This coincides with an increase in calcination at 1100°, likely meaning a higher percentage of carbonates. The difference between ECEC and CEC can thus be explained by a dissolution of carbonates in the second horizon, increasing the amount of Ca present (Tab. B1).

Using Eq. 3.1, the CEC for clay is calculated and is greather than 45 meq/100g for all horizons. Thus, it can be inferred that the majority of clay minerals are smectites. This is verified by the fact that smectites usually have a CEC between 80 and 150 meq/100g (Baize, 2000).

This is confirmed by the DRX analysis.

Table 4.1: Table of physico-chemical data for the Laguna site

Site	Depth(cm)	ECEC	CEC	CEC_{clay}	$\%C_{org}$	%S	%Si	%C	% Calcination 550-1100°C
Laguna	30	70.86	94.15	117.55	2.70	7.84	18.02	74.15	2.63
	60	73.90	40.18	68.98	0.50	13.77	29.84	56.39	11.35
	85	65.04	63.23	90.52	0.98	11.06	21.89	67.05	3.33

Figure 4.1: Laguna profile

Chamorro

The soil profile at Chamorro was *extremely* dry and presented severe shrinkage cracks to depths of 60 cm (Fig. 4.2). In addition to this, the physico chemical analysis (Tab. 4.2) showed high levels of clay that increased with depth (67-74%). Sand content is exceptionally low in this soil (<2%). The clay CEC shows that the clay mineralogy is mainly smectite clays. Oblique slickensides were observed as well as a gilgaï topography and large wedge shaped aggregates. Of all the sites, this one exhibited the strongest Vertisol characteristics. While in the national park, we also had the chance to observe a complete flooding of the site following an episode of overflow of the Tempisque River due to a particularly strong high tide. Despite the large cracks, this confirmed the very low conductivity of the soil, the ponding water was still present more than a week later. It was observed that the cracks swelled shut fairly quickly.

The profile dug was approximately 90 cm deep. The profile on the whole was very homogeneous with no visible horizons, except for a thin orange layer at 15-20 cm, demonstrating the presence of oxidized iron. This is understandable since the site is seasonally flooded. The rest of the horizon was light grey.

Table 4.2: Table of physico-chemical data for the Chamorro site

Site	Depth(cm)	ECEC	CEC	CEC_{clay}	$\%C_{org}$	%S	%Si	%C	% Calcination 550-1100°C
Chamorro	10	40.08	59.41	77.99	2.60	1.23	31.21	67.57	2.48
	20	43.33	58.06	81.93	0.69	1.06	30.25	68.69	2.52
	45	46.94	63.35	84.09	0.55	1.97	24.39	73.65	2.44

Figure 4.2: Chamorro profile

Posaverde

The Posaverde profile exhibited much less shrinkage cracks than the previous sites. No cracks were visible at the soil surface, however once a profile wall had been exposed, small cracks were visible at depths of up to 40-50cm. The reason for the small cracks might be due to the fact that less shrinkage had occurred than other sites. The site was well shaded, on the edge of the tropical dry forest. For this reason, the profile was not excessively dry. In addition to this, tree roots could be found throughout the profile with a high density of fine roots in the top 15 cm. This could also explain the reduced shrinkage.

The profile dug was 90 cm deep and was very homogeneous all the way through with a black color from top to bottom, indicating a possibly high carbon content throughout the profile, which might also diminish shrinking (Fig. 4.3).

The physico-chemical analysis (Tab. 4.3) still reveals a very high clay content that increases with depth. Despite this high clay content however, the soil has a relatively high sand content (10-16%). Posaverde also exhibited the highest clay CEC of all sites investigated. Based on the fact that the clay CEC is always higher than 100 meq/100g, it can be inferred that the clay mineralogy is a mix of smectites and vermiculites (Baize, 2000). Organic carbon content is also relatively high and homogeneous throughout the profile, verifying our visual observations.

Table 4.3: Table of physico-chemical data for the Posaverde site

Site	Depth(cm)	ECEC	CEC	CEC_{clay}	$\%C_{org}$	%S	%Si	%C	% Calcination 550-1100°C
Posaverde	10	65.39	90.80	135.40	1.69	15.28	20.90	63.82	2.12
	45	76.28	86.55	116.66	1.36	16.40	12.42	71.18	4.86
	80	74.56	93.34	117.34	1.35	10.41	13.01	76.58	3.23

Figure 4.3: Posaverde profile

Varillal

Varillal exhibited much of the same characteristics as Posaverde, which was to be expected because of their geographical and topological locations. Indeed both are situated outside of seasonally flooded zones, in the dry forest and at slightly higher altitudes. The soil profile was also largely homogeneous but with slightly larger cracks than Posaverde. The clay content is high throughout, decreasing slightly with depth.

The profile dug was 100 cm deep and the profile a homogeneous dark grey. Physico-chemical analyses reveal a high carbon content througout the profile (2.5-2.6%). There was also a thick humic layer at the top (Fig. 4.4). Clay CEC is also high as at Posaverde indicating a mix of smectite and vermiculite clays.

Table 4.4: Table of physico-chemical data for the Varillal site

Site	Depth(cm)	ECEC	CEC	CEC_{clay}	$\%C_{org}$	%S	%Si	%C	% Calcination 550-1100°C
Varillal	30	75.28	93.50	109.95	2.54	6.55	14.40	79.06	2.80
	60	76.87	92.00	110.50	2.56	8.83	13.91	77.27	4.06
	100	77.44	99.88	120.96	2.62	8.65	14.37	76.98	4.16

Figure 4.4: Varillal profile

La Bocana

The soil at La Bocana presented shrinkage cracks at the soil surface descending to about 20-30 cm in depth. Although the profile exhibits high clay content (50-60 meq/100g), increasing with depth except at the very bottom of the profile (Tab. 4.5), these values are lower than for any of the other sites. The profile depth was 115 cm and a clear color gradient was observable in the profile:

- 0-35: Uniform grey, very dry
- 35-85: Grey with orange streaks (oxidized iron), humid
- 85-115: Brick red with beige streaks, wet

The humidity gradient can be explained by the fact that the site is seasonally flooded and was situated not far from marshes that were still filled with water. This physico-chemical data also clearly show a gradient of clay CEC which drops from 106.95 meq/100g at 45 cm to only 42.95 meq/100g at 75 cm, meaning that it can no longer be determined exactly what type of clay minerals are present. An increase in sodium content is also observed in the lower part of the profile (Tab. B1). These characteristics make us hesitant to qualify the soil as a Vertisol. The results of the DRX analysis confirm the heavy presence of smectites (Fig. A11). They also show a large presence of sulfate minerals and some hematite, which explains the reddish color of the soil.

Table 4.5: Table of physico-chemical data for La Bocana site

Site	Depth(cm)	ECEC	CEC	CEC_{clay}	$\%C_{org}$	%S	%Si	%C	% Calcination 550-1100°C
La Bocana	10	42.58	51.18	76.34	3.77	18.38	27.36	54.26	1.92
	45	70.76	65.02	106.95	2.38	19.03	25.94	55.03	2.40
	75	64.31	34.11	42.95	2.52	17.16	18.60	64.24	3.04
	100	44.43	32.04	41.50	3.42	25.32	18.76	55.92	4.09

Figure 4.5: La Bocana profile

Tempisque

The Tempisque site is along the edge of the main laguna, although slightly elevated and situated in a Palo Verde tree grove. This site was the last site sampled and showed clear Vertisol characteristics with a gilgaï topography, the presence of wedge shaped aggregates and a high clay content (Tab. 4.6).

The profile dug was 90 cm deep and homogeneous from top to bottom with a grey color (Fig. 4.6). The bottom of the profile was soft and saturated up to a depth of about 80-90 cm (the bottom of the profile hole was filled with water). The clay CEC was moderately high (65-99 meq/100g) confirming the presence of smectites.

Table 4.6: Table of physico-chemical data for the Tempisque site

Site	Depth(cm)	ECEC	CEC	CEC_{clay}	$\%C_{org}$	%S	%Si	%C	% Calcination 550-1100°C
Tempisque	10	46.65	49.91	68.29	4.15	12.30	30.34	57.36	2.25
	45	51.44	50.99	65.20	3.30	8.80	26.08	65.13	2.18
	80	56.31	66.80	99.11	2.71	4.08	35.60	60.32	2.22

Figure 4.6: Tempisque profile

4.1.2 SSCC RESULTS

The results of the shrinkage curve characterization experiment are displayed in Fig. 4.7. An initial observation reveals very similar dynamics between the different sites. All sites exhibit virtually non existent zero shrinkage stages with very long normal and residual shrinkage stages.

Table 4.7: Saturated moisture content measured from soil aggregates

Site	Saturated water content [-]
Palo Verde Laguna	0.6358
Chamorro	0.5841
Posaverde	0.5431
Varillal	0.6265
La Bocana	0.6116
Tempisque	0.5995

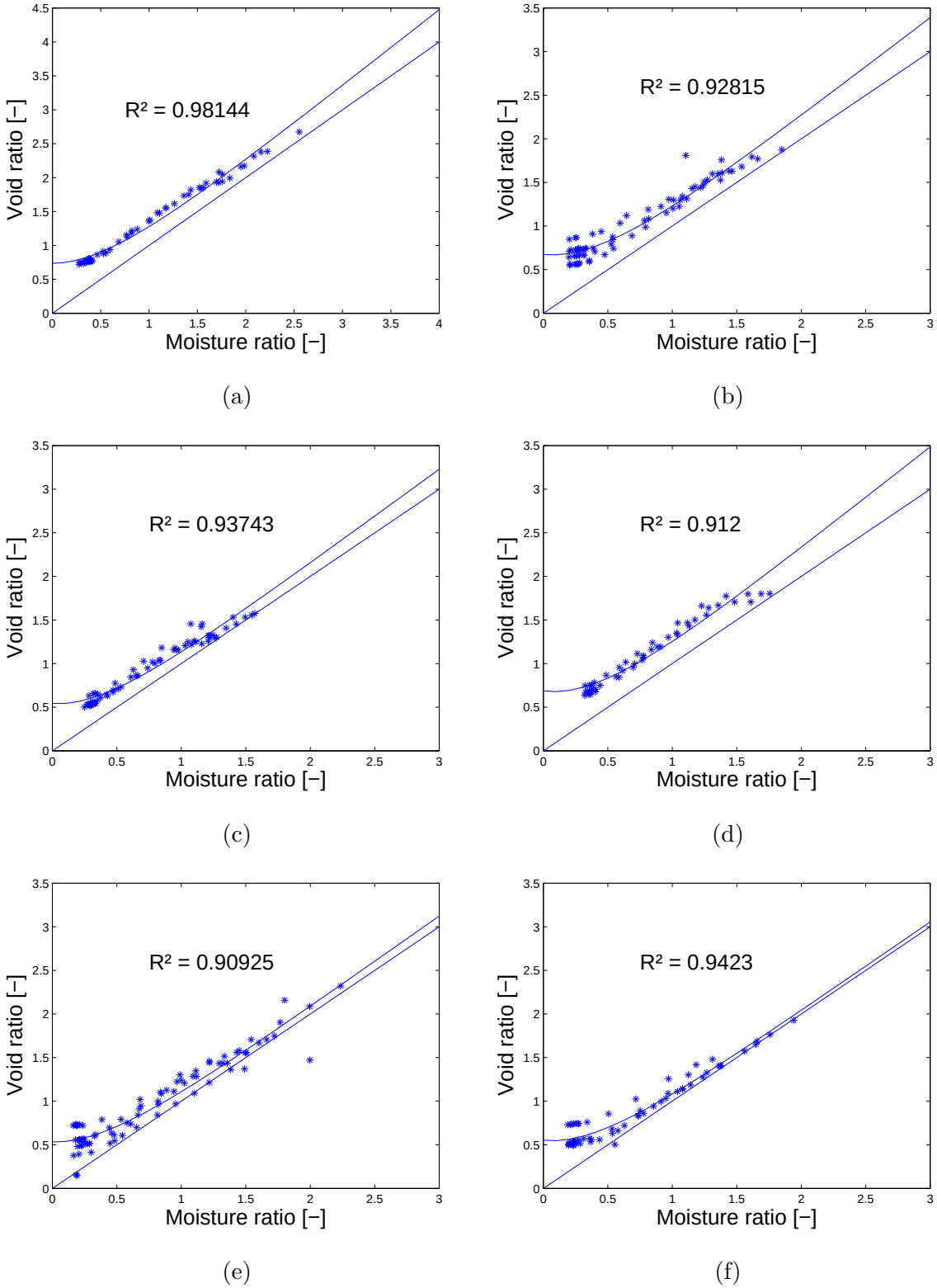

Figure 4.7: Shrinkage curves: (a) Laguna; (b) Chamorro; (c) Posaverde; (d) Varillal; (e) La Bocana; (f) Tempisque

The results of the inverse parameter estimation are shown in Tab. 4.8. As indicated in the table, α_K was not found by inversion but was measured since it has a tangible physical meaning. It is the void ratio at a moisture ratio of zero. It's important to note that even though theoretically incorrect, the parameter γ_K was allowed to go over 1. The reason for this is a condition imposed by the SWAP model where the moisture of the air-entry point, ϑ_a cannot be larger than the saturated moisture ratio. This is assured for larger values of γ_K. However, the moisture ratio at air-entry point is given by:

$$\vartheta_a = \left[-log\left(\frac{\gamma_K - 1}{\alpha_K \times \beta_K}\right)\right]/\beta_K \tag{4.2}$$

Where $\gamma_K \leq 1$ is impossible, meaning that γ_K had to be limited to values above 1. This is a potential source of error because when $\gamma_K > 1$, saturation can never truly be attained because γ_K is the slope of the linear portion of the shrinkage curve. However, a $\gamma_K > 1$ was observed in Kim et al. (1992c) as well and so was accepted here.

Table 4.8: Inversely estimated parameters and their sensitivities for the six sites considered

		α_K (measured)	β_K	γ_K	R^2
Laguna	Parameter values	0.7367	1.5325± 0.1377	1.1185± 0.0153	0.9814
	Sensitivity	N/A	0.2036	1.1150	
Chamorro	Parameter values	0.6735	1.9073± 0.2261	1.1290± 0.0267	0.9282
	Sensitivity	N/A	0.1903	0.7814	
Posaverde	Parameter values	0.5441	2.2114± 0.2708	1.0759± 0.0216	0.9374
	Sensitivity	N/A	0.1508	0.7861	
Varillal	Parameter values	0.6865	1.9961± 0.2492	1.1612± 0.0275	0.9120
	Sensitivity	N/A	0.2004	0.9057	
La Bocana	Parameter values	0.5329	2.0585± 0.3751	1.0407± 0.0262	0.9093
	Sensitivity	N/A	0.1335	0.8063	
Tempisque	Parameter values	0.5525	2.1471± 0.2593	1.0182± 0.0225	0.9423
	Sensitivity	N/A	0.1503	0.6961	

Tab. 4.8 shows that, except for the Laguna site, all of the sites present very similar values for β_K. In fact, all of the values for beta are included in within the the confidence intervals of other sites. This can be explained by the much lower sensitivity of the model to this parameter. Thus, a change in the value of β_K has less effect than a change in the value of γ_K. This can be observed in Fig. A3.

4.1.3 INFILTRATION RESULTS

The results of the infiltration experiments can be observed in Fig. 4.8. Initial observation seem to confirm the presence of multiple porosities, leading to jumps on the infiltration curves. The dynamics observed from site to site differ greatly however.

Laguna

The Palo Verde Laguna site demonstrates a clear double or even triple porosity. The probes at 20 and 45 cm show an initial small jump attributed to the filling of the macroporosity at that depth. This first jump is then followed by a second, attributed to a partial saturation of the soil matrix by lateral infiltration from the macroporosity into the soil matrix. The infiltration curve at 45 cm does not exhibit the first bump, but does show signs of a slight saturation due to lateral infiltration. Finally, all curves demonstrate a third jump attributed to the arrival of the wetting front. Because of the the instantaneous nature of drainage in the macropores, the presence or lateral infiltration is only possible along the portions of lateral soil wall below the water storage level in the macropores. This suggest a shallow IC domain and/or a small m to enable early lateral infiltration at 10 cm. The MB domain ends at around 20-30 cm which enables early saturation at 20 cm and the 45 cm. The infiltration curves seem to be inconsistent conceptually, however. The main wetting front arrives later at 10 cm than at 20 and 45 cm. The curves also seem to be artificially capped at a water content of about 40%, especially the 10 cm curve. The result of the stop in precipitation is clearly visible at 150 min, at a depth of 10 cm.

Chamorro

The probe at 45 cm is the first to start to saturate which suggests an MB domain that ends at around this depth. The probe at 20 cm exhibits a jump starting at 100 minutes, also due to flow from macropore to soil matrix, due to the IC domain ending around this depth. Lateral infiltration at 45 cm is relatively slow and the soil does not reach saturation before the end of the precipitation period. Finally, the curves show the arrival of the main wetting front at each probe in the order of depth, which is to be expected. There appears to be an offset in the arrival of the main wetting curve however. When comparing the transfer time from surface to 10 cm and from 10 cm to 20 cm, there is a large discrepancy. This difference could be due to differences in soil conductivity or local soil-probe contact issues.

Posaverde

The Posaverde site shows very little preferential flow, except very slightly to a depth of 20 which is indicative of a large portion of macropores ending around this depth. The MB domain most likely ends deeper than 45 cm because no lateral infiltration from macropores to the soil matrix is observed in the lower part of the profile. The maximum water content for each probe is drastically different however, suggesting a problem with at least some of the probes. The probe at 10 cm only attains a maximum water content of 25% for instance. Thus, the data for this probe was neglected.

Varillal

The Varillal site shows temporal dynamics similar to those observed at Chamorro. The soil at 45 cm starts to saturate very early in the experiment, suggesting an MB domain that ends around this depth. The soil at 20 cm also reveals macropore flow attributed to the IC domain ending at this depth, or lower if the value of m is small. The progession of the main wetting front is more plausible here than at Chamorro.

La Bocana

The first thing that is noticed for La Bocana site are the large differences in saturated water contents between the different depths, especially for the probe at 10 cm, much like at the Posaverde site. For this reason, the data was also disregarded for the probe at 10 cm when estimating the hydraulic parameters by inversion. This discrepancy can be explained by the fact that the cable for the 10 cm probe was too short. To lengthen it, it was spliced together with another cable and the connection was covered tightly in several layers of electrical tape, however the water tightness of the connection might not have been perfect. Very little macropore flow is observed for this site, which is consistent with visual and physico-chemical observations made before which confirmed that the soil at La Bocana is different from other sites and exhibits less macroporosity. This results in all probes showing very simple dynamics with only the arrival of the main wetting curve being observed.

4.1.4 TEMPISQUE

The Tempisque site shows infiltration curves that arrive much earlier than other sites, possibly indicating a higher soil conductivity. The main wetting front displays a conceptually plausible progression, as opposed to other sites like the Laguna. Macropore flow to the depths of 20 and 45 cm is visible as small jumps in the infiltration curves, indicating that large portions of macropores end around these two depths, most likely IC and MB domains respectively.

General discrepancies

In general, the infiltration data contains several inconsistencies that must be addressed. Three out of the six sites (Laguna, Chamorro, Posaverde) display a large delay of the arrival of the main wetting front. For the Laguna and Chamorro sites, the probes at 10 cm show wetting fronts arriving exceptionally late compared to the other depths, and in the case of the Laguna, the front seems to arrive at 10 cm after it arrives at 20 and 45 cm.

This is attributed to the nature of the probes and their degree of effectiveness in a shrinking-swelling soil. Capacitance probes of this type require a good contact between the probe and the soil in order to be efficient. This is difficult in a shrinking soil. In addition to this, all probes that measure soil di-electric properties are sensitive to the soil volume within the area of influence of the probe (Kim et al., 2000). Kim et al. (2000) show the importance of using a corrected volumetric moisture content, which has been corrected for soil shrinkage or swelling.

In contrast, it was shown that using an uncorrected water content when establishing the ratio between the dielectric constant ϵ and water content θ resulted in a systematic underestimation of θ for a given ϵ. These corrections were not made for our model for reasons described in section 3.3.3.

The documentation for the Decagon Ech2o EC-20 states that the maximum measurable water content is 40% which is lower than the saturated water contents measured in the laboratory. Indeed, some of the infiltration curves seem to plateau rather abruptly.

These problems render the interpretation of the data difficult. For example, the difference between the 'distance' between the curves at 10 and 20 cm and the curves at 20 and 45 cm could simply be caused by a period of non contact between the soil and the probe, rather than a difference of conductivity between the two layers. Also, what may be interpreted as a saturated state, may only be due to the limits of the moisture probe, resulting in a loss of information for the inversion of θ_s and K_{sat} if saturation is in fact not attained.

In an attempt to reduce the impact of the errors, especially the error induced by non-corrected volumetric water content, the model inversion was performed on the variation of water content rather than the water content itself, as described in section 3.3.3.

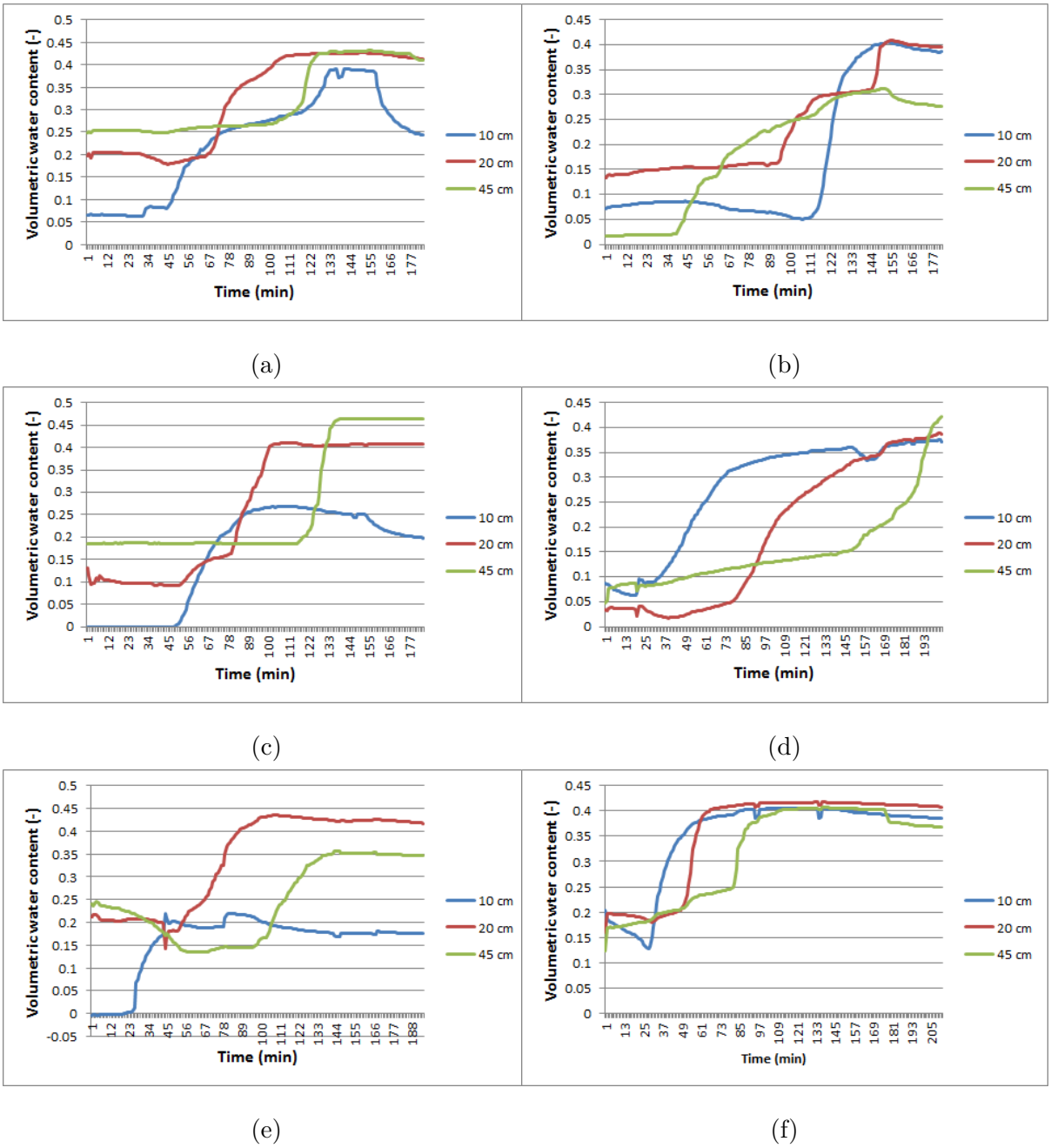

Figure 4.8: Infiltration curves: (a) Laguna; (b) Chamorro; (c) Posaverde; (d) Varillal; (e) La Bocana; (f) Tempisque

4.2 NUMERICAL EXPERIMENT RESULTS

4.2.1 GENERAL SENSITIVITY

The results of the general sensitivity analysis are given by Fig. 4.9 and Fig. 4.10. Each parameter sensitivity is distinguished by its number, defined in Tab. 4.9. Tab. 4.9 also shows the exact sensitivity values for each parameter. These figures show three main groups of parameters that show non zero sensitivity values. These three groups correspond to: 1. Mualem-Van Genuchten parameters; 2. shrinkage parameters; 3. macroporosity distribution parameters. The sensitivity analysis for the variation of moisture content shows the same dynamics but their values are intensified.

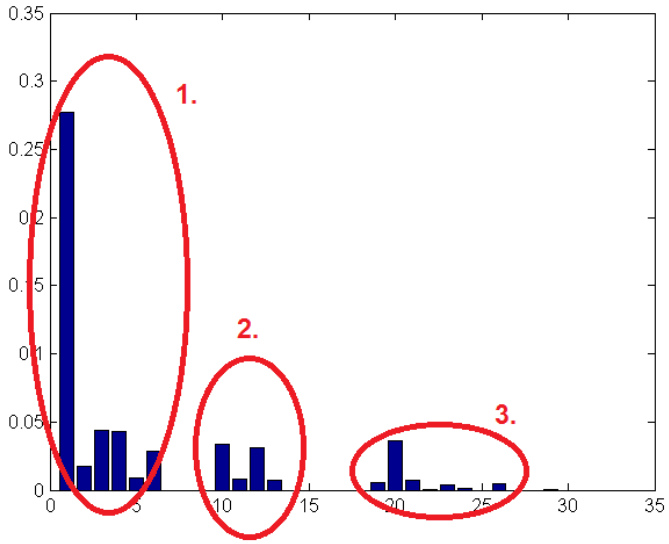

Figure 4.9: Graph of total sensitivity calculated from modeled soil water content. 1. Van Genuchten - Mualem parameter; 2. Shrinkage parameters; 3. Macropore distribution parameters

This analysis shows that for the first group, θ_s, K_{sat}, α and n are the most sensitive parameters. θ_s, despite being extremely sensitive, can be fixed using measurements (Tab. 4.7) and λ can be fixed as well. For the second group, Kim's parameters and θ_{CrMP} are the most sensitive parameters. Kim's parameters were determined via SSCC characterization while θ_{CrMP} is set at 95% of the saturated water content. Finally, for the third group, the most sensitive parameters are Z_{IC}, $P_{IC,0}$, V_{st0}, Z_{st}, and to a certain extent m. m was also defined as having to be estimated from model inversion. While the preliminary sensitivity analysis shows that m is relatively insensitive, response surface analysis as well as manual simulations show that depending on the location within the parameter space, m can have a strong effect on the model response.

Table 4.9: Table of parameter sensitivities relative to water content and water content variation

Number	Parameter	Sensitivity for moisture content	Sensitivity for the variation of moisture content
1	θ_s	0.3150	0.0346
2	$theta_r$	0.0082	0.0054
3	K_{sat}	0.0630	0.0118
4	α	0.0623	0.0133
5	λ	0.0053	0.0040
6	n	0.1002	0.0093
7	PondMAX	0.0000	0.0000
8	RSRO	0.0000	0.0000
9	RSROEXP	0.0000	0.0000
10	α_K	0.0100	0.0057
11	β_K	0.0210	0.0083
12	γ_K	0.0533	0.0116
13	r_s	0.0025	0.0016
14	θ_{CrMP}	0.0091	0.0050
15	z_{crack}	0.0000	0.0000
16	R_{Zah}	0.0000	0.0000
17	Z_{Ah}	0.0000	0.0000
18	Z_{IC}	0.0382	0.0081
19	m	0.0033	0.0020
20	$P_{IC,0}$	0.0826	0.0099
21	$V_{st,0}$	0.0949	0.0134
22	Z_{st}	0.0190	0.0061
23	$d_{p,min}$	0.0000	0.0000
24	$d_{p,max}$	0.0000	0.0000
25	$Z_{dp,max}$	0.0000	0.0000
26	SfacParl	0.0002	0.0002
27	$S_{p,max}$	0.0000	0.0000
28	α_s	0.0000	0.0000
29	fsh	0.0000	0.0000
30	Vundsat	0.0000	0.0000

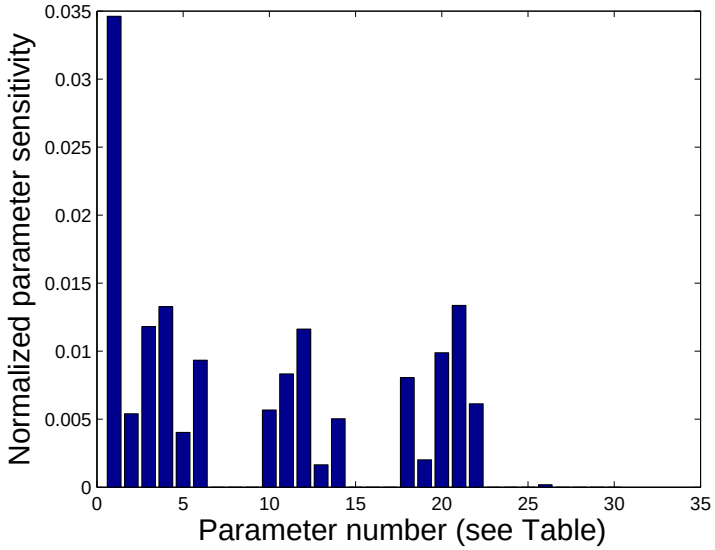

Figure 4.10: Graph of total sensitivity calculated from the variation rate of modeled soil water content

4.2.2 IDENTIFIABILITY, UNIQUENESS, AND SENSITIVITY

The results of the manual variation of parameter values are visible in Fig. A7 and A8. These have been summarized in Tab. 4.10.

The results of the surface response analysis can be shown in Fig. A9 and A10. These graphs confirm the observations made in Fig. 4.10, how ever they give us more information about the sensitivity over the entire range of parameter space. It is important to note however that these 2D graphs are only slices through a 5 parameter space and so don't show all the information that may be present. Also, the graphs were produced by varying parameters two-by-two as specified in section 3.3.1. However, the proper way to proceed would have been to calculate all OF values for the 5 parameter space simultaneously and then plot 2D slices of this parameter space.

Fig. A9 confirms that K_{sat} and α are both sensitive, however this sensitivity varies throughout the parameter range. In fact, both parameters are more sensitive for lower values. This figure also shows that K_{sat} and α are negatively correlated. This is verified using Eq. 2.41 which gives a value of -0.2517. Fig. A10 also confirms the relative insensitivity of m and $FacParl$ but reveals that both are very sensitive for small values. $FacParl$ becomes sensitive for values under 1. This is not realistic for our soils however as high sorptivities were observed for all sites. This means that for the ranges that are of interest to us, $FacParl$ is relatively insensitive. m is sensitive under values of about two, which is plausible for our soils and describes shallow IC domains. For this reason, m cannot be fixed but might be difficult to estimate by inversion if the true value is greater than 2.

Fig. A10 also reveals a slight correlation between Z_{IC} and m for low values. An inverse correlation was observed for $m - V_{st,0}$, $P_{IC,0} - FacParl$, and $V_{st,0} - FacParl$. These correlations are fairly weak however. Their values calculated from Eq. 2.41 confirm this.

Results, that are not presented here, show a very strong correlation between θ_s and K_{sat}.

Table 4.10: Summary of effects of separate parameter variation on the model output

Parameter	$Value_1$	$Value_2$	Effect
K_{sat} [cm/d]	30	300	An increase in decreases the distance between infiltration curves and also decreases the maximum moisture content because of increased drainage.
α [1/cm]	0.02	0.01	A decrease in α increases the water retention capabilities of soil. The effect on infiltration is an increase in initial moisture content and a delay in the arrival of the wetting front.
n [-]	4	2	A decrease in n decreases the severity of the slope of the WRC. This results a decrease in infiltration rate.
Z_{IC} [cm]	-20	-45	Because of the instantaneous nature of macropore drainage, lateral infiltration takes place majoritively at the bottom of the domain. An decrease from -20cm to -45 cm increases lateral infiltration at -45 cm.
m [-]	10	1	A decrease in m results in a shallower IC domain which moves lateral infiltration up in the profile.
$P_{IC,0}$ [-]	0.4	0.6	An increase leads to a routing of more water into the IC domain, resulting in increased lateral infiltration along this domain, especially at the bottom.
$V_{st,0}$ [-]	0.4	0.1	An decrease leads to a general decrease in macropore volume and thus a decrease in lateral infiltration.
$FacParl$ [-]	75	1	A decrease results in a decrease in sorptivity and thus lateral infiltration.

This, as well as an effort to reduce the number of parameters, led us to use measured values for θ_s.

These results show that parameters m and $FacParl$ are relatively insensitive, making them less identifiable. While $FacParl$ can arbitrarily be set high, without much effect on the model output, m must be estimated by inversion. This will most likely lead to larger confidence intervals, diminishing the quality of the inversion. The correlation discussed above, between certain parameters also makes them less identifiable.

4.2.3 OPTIMIZATION ALGORITHM ROBUSTNESS

The results of the three robustness test inversions are shown in Tab. 4.11 and Fig. A4-A6.

These tests show that despite a relatively large parameter space (see section 3.3.1) the optimization algorithm is entirely capable of converging on parameter values relatively close to

the actual values. One exception is the parameter m which is very different from the initial value and also between tests. This can be explained by m's low sensitivity for values above 2. Although none of the parameter values found are exactly the same as the initial values, they are very close and the coefficient of determination R^2 remains relatively high for all tests.

In conclusion, the robustness tests seem to confirm the ability of the optimization algorithm to converge on an adequate solution.

Table 4.11: Table of estimated parameters and their confidence intervals derived from robustness tests

Parameter	Initial values	Test 1	Test 2	Test 3
K_{sat} [cm/d]	30	29.6248 ± 0.3942	26.8983 ± 0.0450	29.0750 ± 0.0551
α [1/cm]	0.02	0.0187 ± 3.0825e-4	0.0188 ± 2.47e-5	0.0194 ± 4.262e-5
$Z_{IC}[cm]$	-20	/	-22.5859 ± 0.0446	-23.5221 ± 0.0113
m	10	/	3.2037 ± 0.0099	2.6297 ± 0.0083
$P_{IC,0}$	0.4	/	0.4457 ± 9.6707e-4	0.4254 ± 7.7485e-4
$V_{st,0}[-]$	0.4	/	/	0.4137 ± 9.6961e-4
R^2	1.0000	0.9874	0.9975	0.9962

4.2.4 MODEL VALIDITY

Model validity was assessed on the basis of the graphs in Fig. A7 and A8. The SWAP model seems to be able to reproduce the dynamics observed in the infiltration data relatively well from a qualitative points of view. The modeling of macropore volume results in rapid drainage and lateral infiltration from the macroporosity to the soil matrix. The model accurately recreates the dynamics observed at the Chamorro and Posaverde sites where lateral infiltration at 20 cm is observed before the arrival of the main wetting front. This is plausible because for 15 cm soil polygons, the water only has to travel a maximum of 7-8 cm, often less, to the center of the polygon instead of the 20 cm from the soil surface. Dynamics such as those at the Laguna, Chamorro, Varillal and Tempisque sites were also reproduced where the drainage to the probe at 45 cm is the first to be observed.

The model is not capable of reproducing the curve jumps that were attributed to the filling of macroporosity, observed at the Laguna and Tempisque sites. This is because the water content expressed by SWAP corresponds only to matric water content, while the soil moisture probes measure total soil water content. SWAP is also incapable of reproducing the delayed nature of lateral infiltration observed for most sites at 20 cm. This can be attributed to two things. The first is the lack of a conductivity parameter for macropore flow. SWAP is not a traditional dual porosity model with separate sets of hydraulic parameters. Instead, SWAP specifies only a resistance of water flow at the entrance of the macroporosity. Once in the macropore domain, water is added instantaneously to the bottom of the macropore domain. For this reason, there is no delay in the beginning of lateral infiltration. Second, the delay could be due to the fact

that in reality, the majority of macropores end at a depth lower than 20 cm. The delay is the time it takes for the macroporosity to fill to this level. This was difficult to reproduce in the model because the data clearly show the arrival of the main wetting front at all three depths within the simulation period. In order to reproduce this, conductivities had to be taken on the higher end of plausible conductivities for our clay heavy soil (20-30 cm/d, based on the Rosetta pedotransfer functions and our soil texture). This increased conductivity decreases water storage levels in the macropore domain. This is impossible to quantify however because SWAP does not provide an output for the macropore domain storage water balance.

4.3 INVERSION RESULTS

The results of the SWAP parameter estimation are presented in Tab. 4.12. Examples of inversion results are given in Fig. 4.12 and for the Varillal and La Bocana sites, where the results of the inversion were best.

Table 4.12

Parameter	Laguna	Chamorro	Posaverde	Varillal	La Bocana	Tempisque
K_{sat} [cm/d]	50	30	70	100	511	200
α [1/cm]	0.01	0.02	0.02	0.03	0.0159	0.03
n	4	4	2.5	3	2.489	1.75
$Z_{IC}[cm]$	-20	-20	-30	-45	/	-20
m	10	10	1	10	/	10
$P_{IC,0}$	0.7	0.4	0.6	0.4	/	0.6
$V_{st,0}[-]$	0.4	0.4	0.3	-45	/	0.2
Z_{st}	-20	-50	-30	-45	/	-45

The results of manual parameter estimation are shown in Fig. 4.13.

Despite trying many different parameterizations for the GMCS algorithm, increasing the number of iterations and trying different parameter ranges for inversion, the results of the inverse parameter estimation for the various sites remained very poor. This suggests that the ill-posedness of the problem is not only due to model errors but also measurement errors.

The measurement errors were attributed to five main causes. The first cause is the problem of contact between the probe and the soil. The variable volume of the soil matrix has the potential to create contact problems between the probe and the soil. This was considered not to be a problem during experimentation because the infiltration experiments were to be done only once and along the wetting curve. It was believed that any contact problems would be resolved by the swelling soil. This is the case, but the time it takes for the soil to swell and create a good contact with the probe was longer than expected and seems to vary from probe to probe, creating the impression of multiple conductivities in the soil. The time it took to establish contact was increased by the additional space that was created when inserting the probes. The extremely hard soils meant that the pilot holes were not always created as cleanly

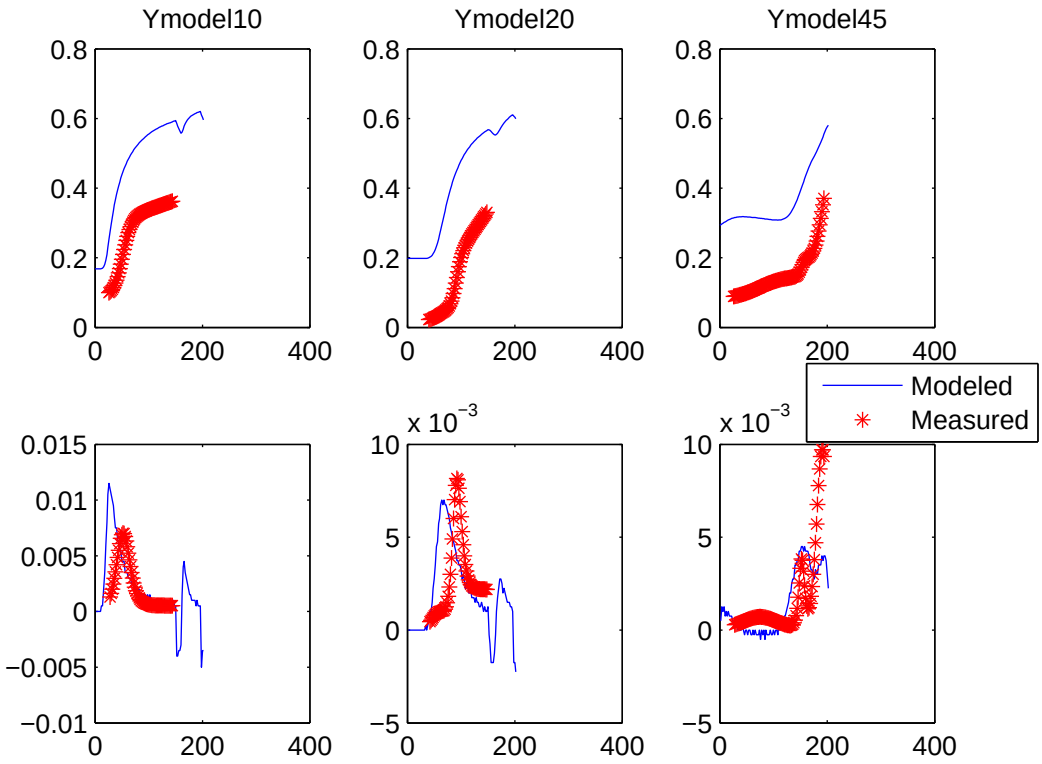

Figure 4.11: Results of the inverse parameter estimation for the Varillal site

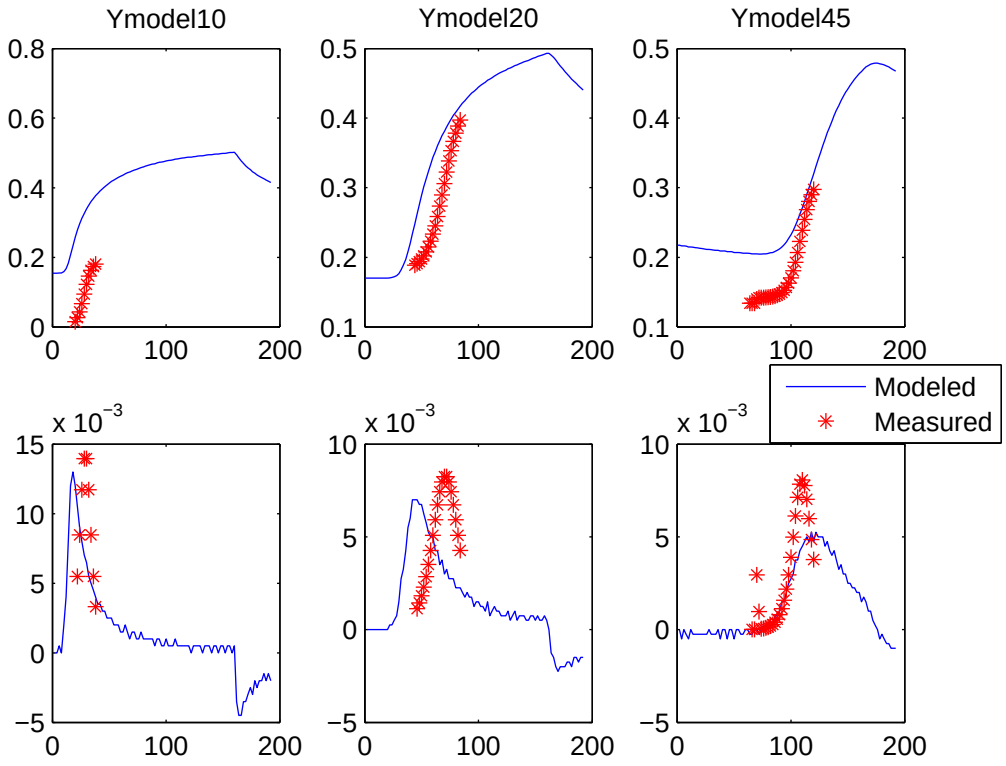

Figure 4.12: Results of the inverse parameter estimation for La Bocana site

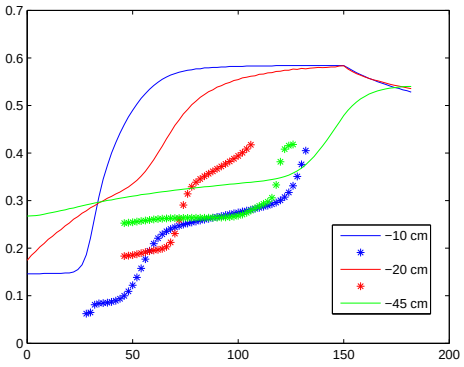

(a) Laguna

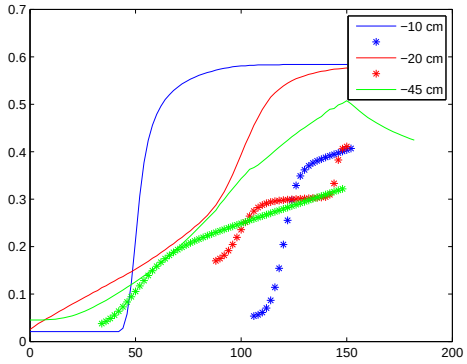

(b) Chamorro

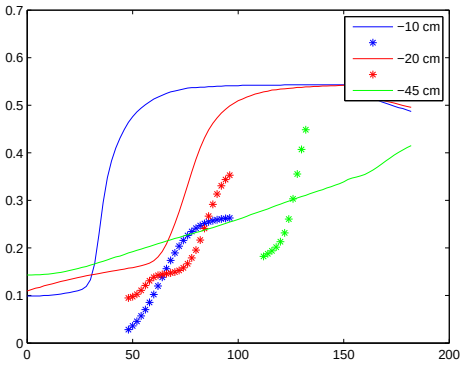

(c) Posaverde

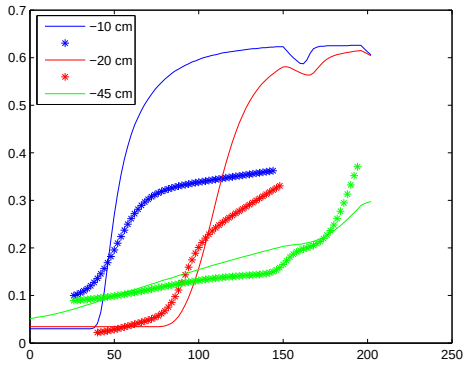

(d) Varillal

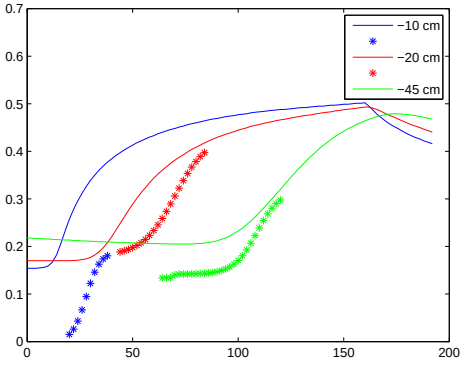

(e) La Bocana

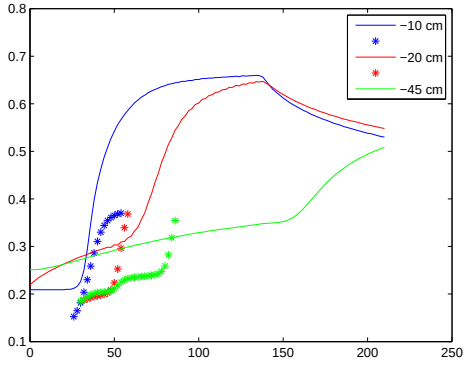

(f) Tempisque

Figure 4.13: Graphs of model response for manually estimated parameters (solid lines: model)

as they should have been.

The second cause is a lack of proper calibration. Because of a lack of time as described before, the potential-water content calibration was not corrected. This introduces a systematic error into the measurements. However, the infiltration data still presents correct dynamics of water content change.

A third cause was the effective maximum saturation level of the probes. The probes are specified to measure only a maximum of 40%, potentially causing data loss for the estimation of K_{sat}. This is confirmed by the infiltration data which seems to be capped at 40%.

A fourth cause is the possibility of poorly represented parameters. What we mean by this is that the data measured does not necessarily contain enough information about certain parameters that need to be estimated. This is surely the case for the macroporosity parameters. Conceptually, it is not known if the 20x2cm EC-20 probe comes into contact with a large enough section of the macropore domain to be able to extract significant data during model inversion.

The fifth cause is soil disturbance. The extreme hardness of the soil meant that the soil profiles had to be dug using a hydraulic digger which created large "blocks" of soil. When the hole was refilled, this created artificial macroporosity that was not present in the naturally structured soil. This problem is mitigated in longterm experiments where the soil has time to reorganize itself through shrinking and swelling due to rainfall. In our case, however, infiltration experiments were done only a matter of days after backfilling the holes. This might be the cause for the fast infiltration times. Indeed, in order to fit the data, the value range for saturated soil hydraulic conductivity had to be increased to values that are not plausible for clayey soils (Fig. 4.12). The same is true with the values for α and n which are high for most of the soils but that needed to be in order to fit our data. Plausible parameter values for our soil are given in Tab. 3.6.

4.4 FORWARD MODELING SCENARIO

The precipitation and evapotranspiration data used for forward modeling scenarios is shown in Fig. 4.14.

The dual nature of the precipitation periods is clearly visible with the wet season spreading from mid-May to mid-November. The evapotranspiration is relatively stable throughout the year with slightly higher values in the beginning of the year, during the dry season. The total precipitation and evapotranspiration are 1041.8 mm and 1861.2 mm respectively. The actual total amount of water reaching the wetlands however is larger than this due to heavy runon from the surrounding mountains and hills. This runon was not simulated but its impact may be significant.

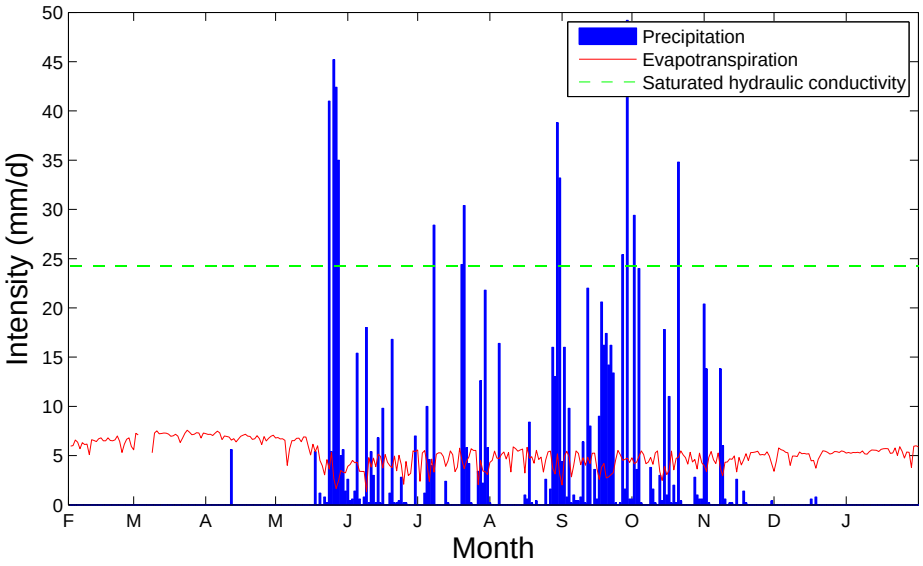

Figure 4.14: Precipitation and evapotranspiration data for 1st Feb. 2002 - 31st January 2003

4.4.1 SWELLING SOIL WITH INVERSE PARAMETERS

The results of the forward simulation using estimated parameters from the infiltration experiment are shown in Fig. 4.15 and 4.16. The soil moisture results show that despite the heavy amounts of rainfall, the soil fails to even achieve saturation. This means that no ponding is observable. Because saturation is not attained, the bottom flux fluctuates greatly with $K(h)$. The bottom flux is defined as positive in the downwards direction, for the sake of constructing the graphs.

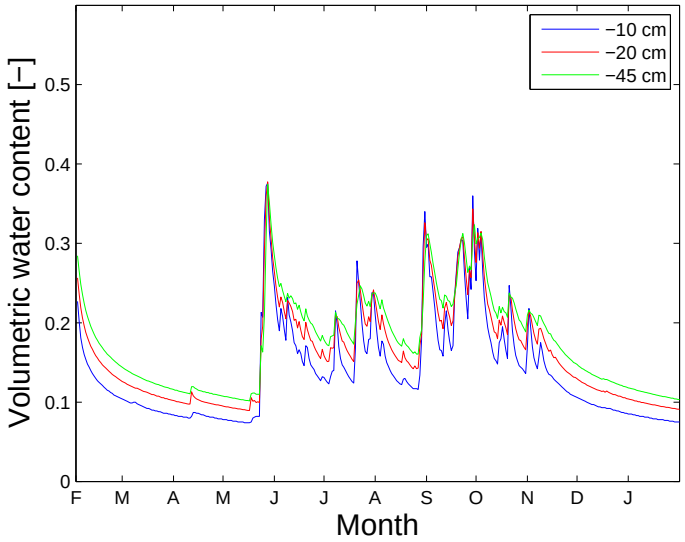

Figure 4.15: Graph of soil water content at depths of 10, 20 and 45 cm for swelling soil with inverse parameters

This lack of soil saturation and ponding is attributable in part to the higher conductivity

that was derived from parameter estimation. However, this is not the only factor, nor even maybe the major factor in determining soil saturation and ponding levels, as is observed further down.

The soil flux balance given by Tab. 4.13 shows that despite the relatively high conductivity for our soil type, when looking at annual water balance, the majority of soil moisture is lost as evaporation rather than as drainage to deeper layers (62.80 and 45.69 %, where the difference contributes to a change in soil water storage).

Table 4.13: Overview of soil water balance for a swelling soil with inverse parameters

Water balance components (cm)			
In		Out	
Rain + Snow:	104.18	Interception:	0.00
Runon:	0.00	Runoff:	0.00
Irrigation:	0.00	Transpiration:	0.00
Bottom flux:	-47.60	Soil evaporation:	65.42
Sum:	56.58	Sum:	65.42

The amount of precipitation routed into the macropore domain is given by Tab. 4.14.

Table 4.14: Overview of macropore water balance

Macropore water balance components (cm)							
Input	MB	IC	Total MP	Output	MB	IC	Total MP
Initially present:	0.00	0.00	0.00	Finally present	0.00	0.00	0.00
Inflow top:							
- direct precipit.	19.38	29.07	48.45				
- overland flow	0.00	0.00	0.00				
Exfiltration matrix:				Infiltration matrix:			
- interflow	0.00	0.00	0.00	- unsaturated	19.38	29.07	48.45
- saturated	0.00	0.00	0.00	- saturated	0.00	0.00	0.00
				Rapid drainage	0.00		0.00
Sum	19.38	29.07	48.45	Sum	19.38	29.07	48.45

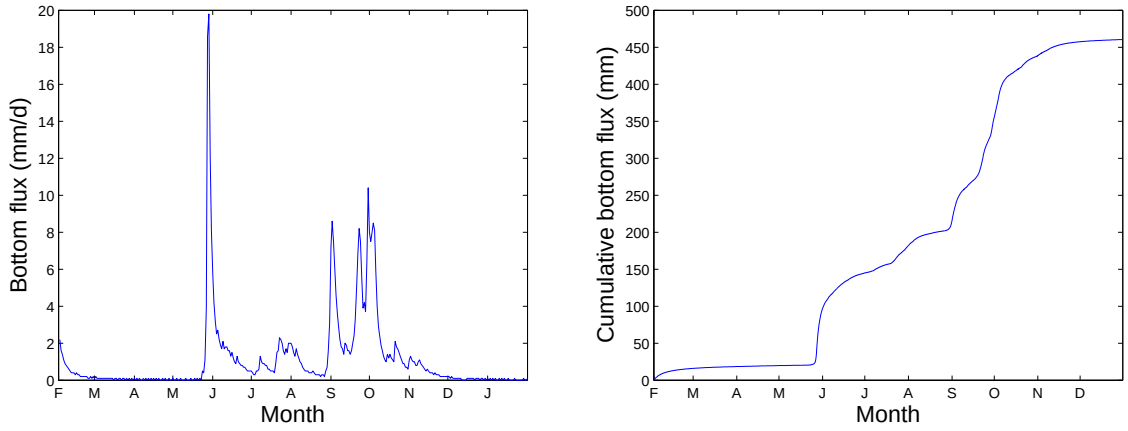

(a) Net bottom flux (mm/d)

(b) Cumulative bottom flux (mm)

Figure 4.16: Graph of bottom flux variation during the simulation period for a swelling soi with inverse parameters

4.4.2 RIGID, HOMOGENEOUS SOIL WITH INVERSE PARAMETERS

The results for forward simulation without macroporosity are given in Tab. 4.15. The results for soil moisture and bottom flux present relatively the same dynamics as before and so are not presented here. The only difference observed was a slightly lower moisture content for soil at -45 cm. The total moisture contents do not change, only their distribution with depth. However, when dynamic and static macroporosity are neglected, the ratio of total evaporation to bottom flux increases.

Table 4.15: Overview of soil water balance for a rigid soil with inverse parameters

Water balance components (cm)			
In		Out	
Rain + Snow:	104.18	Interception:	0.00
Runon:	0.00	Runoff:	0.00
Irrigation:	0.00	Transpiration:	0.00
Bottom flux:	-39.72	Soil evaporation:	74.39
Sum:	64.46	Sum:	74.39

4.4.3 RIGID, HOMOGENEOUS SOIL WITH ROSETTA PARAMETERS

The results when hydraulic properties are estimated from pedotransfer functions can be observed in Fig. 4.17 and 4.18. Fig. 4.17 shows that soil moisture is increased relative to the simulation with the same conditions but with inverse parameters. This shows that parameter values more appropriate to a clayey soil, notably a lower conductivity (24.25 cm/d), results in higher soil moisture. However, the soil still remains unsaturated. The soil water balance is presented in Tab. 4.16. The effect of the different hydraulic parameters is a further increase of evapotranspiration and decrease in bottom flux. This change was smaller than the one induced by neglecting

macropore flow however, which validates the importance of considering preferential flow through the macropore domain.

Table 4.16: Overview of soil water balance for a rigid soil with pedotransfer parameters

Water balance components (cm)			
In		Out	
Rain + Snow:	104.18	Interception:	0.00
Runon:	0.00	Runoff:	0.00
Irrigation:	0.00	Transpiration:	0.00
Bottom flux:	-34.47	Soil evaporation:	77.92
Sum:	69.71	Sum:	77.92

The fact that saturation was still not achieved was attributed to three things: the overestimation of soil hydraulic conductivity by the pedotransfer functions; the lack of runon which is an important water balance input in the field; and the condition of free drainage at the bottom of the soil profile.

The pedotransfer functions are, at best, only an approximation. They were used here because of the lack of valid parameter values. However, they might not be valid for use in Vertisols.

The situation of the Palo Verde marshlands in the lower part of the Tempisque-Bebedero basin as well as its topographical situation, surrounded by mountains, mean that the marshlands are subjected to runon generated from Tempisque overflow (which was witnessed, even in the dry season! See section 4.1.1) and runoff from the surrounding hills. This increases water input, saturating the soil and creating ponding conditions. While the Tempisque site itself might not be subjected to these conditions, other sites like Chamorro certainly are. In addition to this, when considering free drainage at the bottom of the soil profile, soil saturation from the bottom up becomes impossible. Thus, when modeling any hydrological system, it is important to take to assess the impact of groundwater levels on the soil profile studied.

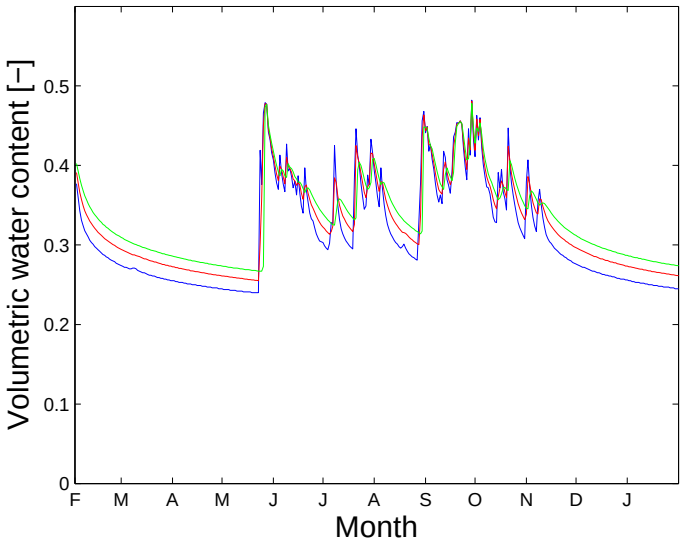

Figure 4.17: Graph of soil water content at depths of 10, 20 and 45 cm for a rigid, homogeneous soil

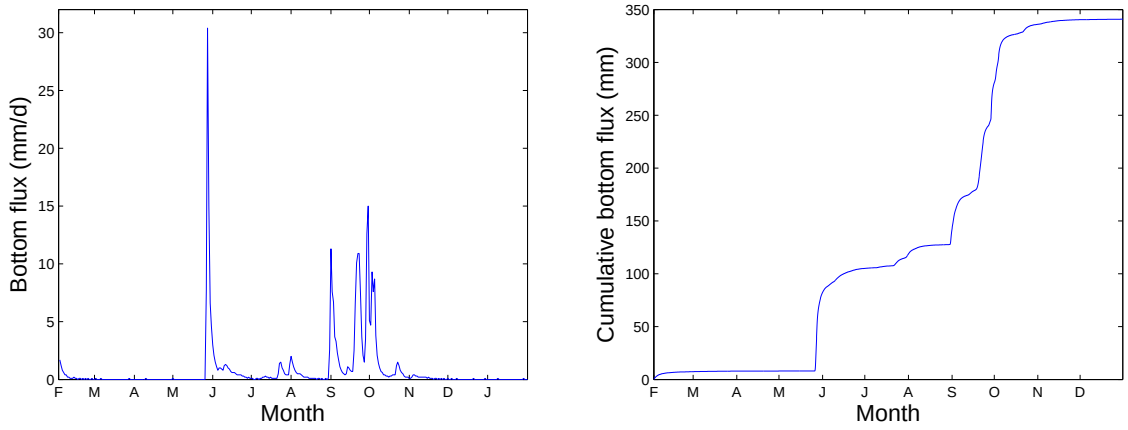

(a) Net bottom flux (mm/d)

(b) Cumulative bottom flux (mm)

Figure 4.18: Graph of bottom flux variation during the simulation period for a rigid, homogeneous soil

4.4.4 RIGID, HOMOGENEOUS SOIL WITH SIMULATED GROUNDWATER LEVEL

The results of a simulation which takes into account groundwater levels is given in Fig. 4.19 and 4.20. The results shown in these graphs don't necessarily represent reality. The A and B from Eq. 3.5 were simply taken at levels that enabled the model to converge and produce believable GWL's. However, they show the impact of saturation from the bottom for creating ponding. In Fig. 4.19, we see that the soil is quickly saturated. Once the soil is saturated, a ponding layer can be observed (Fig. 4.20).

It is important to note, however, that it is possible that for our soil, the relationship between groundwater level and soil water flow is fairly weak.

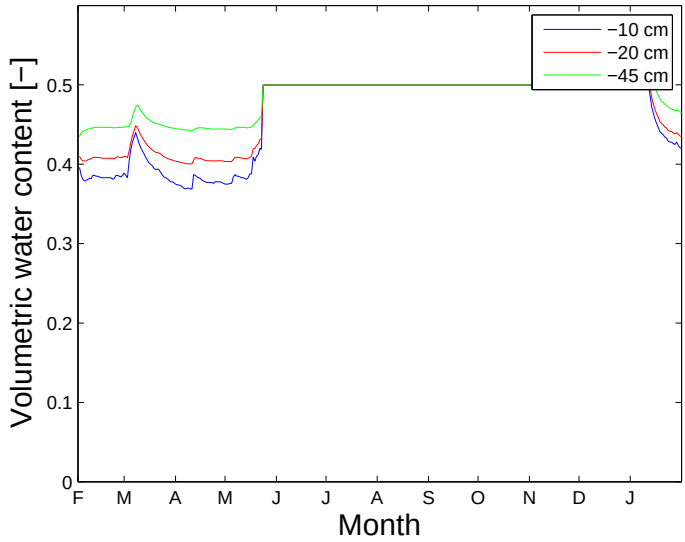

Figure 4.19: Graph of soil water content at depths of 10, 20 and 45 cm for a rigid, homogeneous soil with simulated GWL

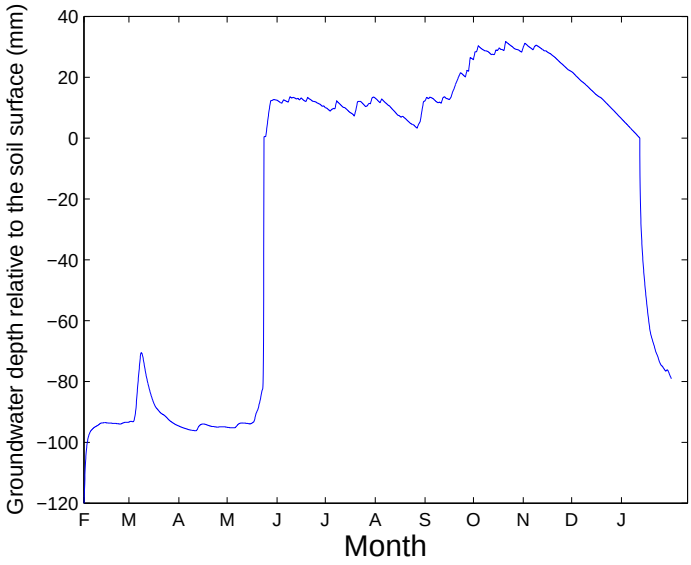

Figure 4.20: GWL relative to the soil surface

5

Conclusion

5.1 GENERAL CONCLUSION

During the course of this master's thesis, the main goal has been to select and properly characterize an infiltration model for the PVNP. In light of this, this master's thesis has helped advance the understanding of dynamics of the park's hydrological dynamics. This was especially the case when it came to understanding, characterizing and modeling unsaturated flow in systems containing swelling soils. While the main objective was the modeling, the central theme of the thesis ended up being measuring and dealing with the complexities of a shrinking-swelling soil. This was particularly difficult because of the lack of prior work done on the subject in the GERU research lab. This means that all protocols had to be established from scratch, based on the literature.

A physico-chemical analysis was done, mainly with the goal of producing pedotransfer functions for estimating soil shrinkage characteristics. However, time ran out and we were not able to complete this objective. It would likely prove to be beneficial to create pedotransfer functions adapted to Vertisols, based on the overestimation of hydraulic conductivity observed when using the Rosetta pedotransfer functions.

The physico-chemical data did enabled us to confirm the nature of the soils and contribute to the information database for future studies. High clay contents combined with high CEC values and low carbonate content indicate an important amount of swelling clays which was confirmed using DRX studies for some sites.

For modeling the soil water flow in the system, the SWAP model was selected, mainly because of its ability to integrate the shrinking behavior. However SWAP presents many other advantages that made it appealing. The model is highly flexible and very detailed. This level of detail enables very accurate modeling of water flow and macropore volume, making SWAP more accurate than a dual porosity model. This level of detail comes with a tradeoff which is the number of parameters. In order for the SWAP model to correctly model complex dynamics, which it is capable of doing, it must be accurately parameterized. Indeed, the number of parameters made the elaboration of an experimental protocol to produce data for the model inversion, challenging. This was complicated by SWAP's inability to reproduce certain behaviors

such as the delayed nature of lateral infiltration.

Estimation of the SWAP parameters proved to be extremely difficult. This was attributed to an ill-posed inversion problem. The ill-posedness was attributed to errors in the inversion setup and split into two categories: model errors and measurement errors. The optimization algorithm itself was proven to be well adapted to inverse parameter estimation with SWAP, even with a high number of parameters, as long as the algorithm was properly parameterized. Numerical tests and simulation analysis proved that SWAP was generally valid for reproducing the soil water flow dynamics, although unable to reproduce certain behaviors such as the delayed nature of lateral infiltration or the presence of a conductivity for the macropore domain.

The dominant source of error in the inversion setup was deemed to be measurement error. Indeed, errors in measurements produced data that was either impossible to reproduce with SWAP or required increasing the size of the parameter space to values that were not theoretically valid for our soils. Measurement errors were attributed to two factors considered flaws in the experimental protocol: the non-suitability of the moisture probes for the soil, and the low amount of information contained in the data relative to certain parameters.

The results of the four forward simulations showed that the presence of macropore flow increases the depth of infiltration, increasing bottom drainage and decreasing soil evaporation. This effect is larger for soils which have relatively poorly conductive soils. However, it was observed that for a profile with free drainage, soil saturation was never achieved using actual rainfall data. This was attributed to overestimation of the hydraulic conductivity values by the model inversion and the pedotransfer functions and to the importance of other inputs for creating ponding, such as runon and groundwater levels. Because of this, it would be very beneficial to establish pedotransfer functions specially adapted to use with Vertisols.

5.2 RECOMMENDATIONS

5.2.1 CHARACTERIZATION OF SHRINKAGE PROPERTIES

Even though the protocol selected enabled us to accurately and successfully characterize the shrinkage curves for our various sites, several recommendations can be made to make the process easier.

Saturation of the aggregates proved to be particularly difficult and was not described in detail in the literature. In our case, aggregates were brought to full saturation by capillarity in a vacuum chamber. However, despite the coating, the aggregates were very difficult to handle, notably during the reapplication of the coating after saturation. Because of the presence of normal shrinkage, which is linear, it is in fact not necessary to fully saturate the aggregates[1]. Instead, the aggregate can be equilibrated at a suction of -5 cm as much of the literature recommends or saturated and then equilibrated at field capacity (Stewart et al., 2012). Saturation should be

[1]It should be noted however that if this experiment is also used to determine saturated water content, that the aggregate should be fully saturated. There exist several water contents where the soil matrix is effectively saturated (Fig. 2.6). This measurement does not consider static macropore volume however and should be avoided if possible.

done using a traditional sandbox and a nylon meshin and a good contact with the nylon can be insured by using kaolin paste. This method was used previously by the ACME soil science lab and did not result in damaged aggregates.

The choice of coating could be revised as well, depending on the degree of saturation of the aggregates. Indeed, the coating did its job well, however the application of the hand-spray plaster was awkward and often resulted in soil loss because of the need to manipulate aggregates. Instead, a coating into which the aggregates can be dipped should be considered, such as PVA glue, which Krosley et al. (2003) proved to be efficient, especially when used on the drying curve. Also, smaller aggregates (< 10 g) should be favored as they facilitate handling and increase drying speed.

5.2.2 CHARACTERIZATION OF HYDRAULIC PROPERTIES

Where the shrinkage characterization protocol was valid but could stand to be improved, the hydraulic characterization protocol was very poorly adapted to determining the needed parameters. The flaws of the experimental protocol were described in the inversion results section and were attributed to five main factors: poor probe contact, probe saturation levels capped at 40%, non-correction of volumetric water content, soil disturbance and lack of information in the data.

For future studies, we would recommend using evaporation experiments such as Ruy and Cabidoche (1998) or Garnier et al. (1997) to determine to the hydraulic conductivity curve. This circumvents all the problems related to probe installation and soil-probe interaction and is accurate as long as a model that takes into account soil deformation is used. Care must also be taken to avoid smoothing of the evaporation surface. This method can be combined with a traditional sandbox and pressure plate apparatus for the water retention characteristic. Kaolin should be used with nylon meshing in order to ensure that proper suction is maintained on the sample. This can be applied on aggregates or soil cylinders and combined with a SSCC to calculate volumetric water content at each stage.

5.2.3 CHARACTERIATION OF MACROPORE DISTRIBUTION

Based on the results from the robustness test, model inversion based on the infiltration data was acceptable. However, from a practical point of view, for the same reasons as discussed above, this method should be avoided because of the heavy soil disturbance it causes. Conceptually, it is not certain if the 20x2 cm Ech2o EC-20 moisture probe comes into contact with a representative section of the macropore domain.

Instead, a infiltration test using a tracer or dye could be used, as described by Van Schaik et al. (2009). This method is of interest because it was developed specifically for SWAP and in collaboration with one of its authors (R.F.A. Hendriks).

During their tests, the authors applied a blue dye (4 gL^{-1} of Brilliant Blue FCF [CI 42090]) onto 1.5x1.5 plots. The soils studied were a combination of Cambisols and Leptosols. Rainfall was simulated at 44 $mm.h^{-1}$ for 1 hour to ensure good infiltration. Then each plot was excavated and studied. Infiltration patterns were plotted as a fraction of dye-stained area with depth. The

average curve of three profiles per plot was used.

5.3 FUTURE APPLICATIONS

The SWAP model can prove to be an invaluable tool for future studies in the PVNP. For example, the plant module, combined with solute transport can be invaluable for the *Typha* restoration project that is currently under way. SWAP is also able to model runoff or runon to surface water reservoirs such as rivers. Studies are also currently being done, for example by Chris Murray from Auburn university, on the impacts of pesticide and heat changes in soils on the determination of the sex of crocodile embryos. The solute and heat transport models of SWAP might prove to be valuable in establishing an understanding of the impact of soil flow to these processes.

All of these situations show that, once properly parameterized, the highly flexible and modular nature of SWAP enables it to be adapted to a large number of situations. It is important however to develop the right protocol for determining the model parameters.

Bibliography

Agriculture Canada, Research Branch (1984). "Analytical methods manual 1984 Land Resource Research Institute". In: ed. by B.H. Sheldrick. Chap. 3.3: Physical Analysis: Shrinkage.

Aitchison, G.D. and J.W. Holmes (1953). "Aspects of swelling in the soil profile". In: *Aust. Hournal of Applied Science* 4, pp. 244–259.

Baize, Denis (2000). *Guide des analyses en pédologie: 2ème revue et augmentée*. Ed. by INRA. INRA.

Belmans, C., J.G. Wesseling, and R.A. Feddes (1983). "Simulation of water balance of a cropped soil: SWATRE". In: *Journal of Hydrology* 63, pp. 271–286.

Berndt, R.D. and K.J. Coughlan (1976). "The nature of changes in bulk density with water content in a cracking clay soil". In: *Aust. J. Soil Res.* 15, pp. 27–37.

Boels, D. et al. (1978). "Theory and system of automatic determination of soil moisture characteristics and unsaturated hydraulic conductivity". In: *Soil Science* 126, pp. 191–199.

Boers, A.M. and J.B. Zedler (2008). "Stabilized water levels and *Typha* invasiveness." In: *Wetlands* Vol. 28, pp. 676–685.

Boivin, P., D. Brunet, and C. Gascuel-Odoux (1991). "Denisté apparente d'échantillon de sol: Méthode de la poche plastique". In: *Bulletin GFHN* 28, pp. 59–71.

Bradeau, E. et al. (1999). "New device and method for soil shrinkage curve measurement and characterization". In: *Soil Science Society of America* Vol. 63, pp. 525–535.

Brasher, B.R. et al. (1966). "Use of saran resin to coat natural soil clods for bulk density and water retention measurements". In: *Soil Science* 101, p. 108.

Braudeau, E. (1987). "Mesure automatique de la rétraction d'échantillons de sol non-remaniés". In: *Science du Sol* 25, pp. 85–93.

Bronswijk, J.J.B. (1988). "Modeling of water balance, cracking and subsidence of clay soils". In: *Journal of Hydrology* Vol. 97, pp. 199–212.

Cabidoche, Y-M. and H. Ozier-Lafontaine (1995). "THERESA: I. Matric water content measurements through thickness variations in vertisols". In: *Agricultural Water Management* Vol. 28, pp. 133–147.

Cabidoche, Y-M. and M. Voltz (1995). "Non-uniform volume and water content changes in swelling clay soil: II. A field study on a Vertisol". In: *European Journal of Soil Science* Vol. 46, pp. 345–355.

Cornelis, W.M. et al. (2006a). "A simplified parametric model to describe the magnitude and geometry of soil shrinkage". In: *European Journal of Soil Science* Vol. 57, pp. 258–268.

Cornelis, W.M. et al. (2006b). "Measuring and modelling the soil shrinkage characteristic curve". In: *Geoderma* Vol. 137, pp. 179–191.

Crescimano, G. and G. Provenzano (1999). "Soil shrinkage characteristic curve in clay soils: measurement and prediction". In: *Soil Science Society of America* 47, pp. 25–32.

Daniels, A.E. (2004). *Protected Area Management in Watershed Context: A case study of Palo Verde National Park, Costa Rica.*

Dexter, A.R. (1988). "Advances in characterization of soil structure". In: *Soil and Tillage Research*, pp. 199–238.

Dierkx, J., C. Belmans, and P. Pauwels (2009). "SWATRER, a computer package for modelling the field water balance". In: *Reference manual. soil and Water Eng Lab., KULeuven,Belgium*, 114pp.

Dinka, T.M. et al. (2012). "Shrink-swell behaviour of soil across a Vertisol catena". In: *Journal of Hydrology* 476, pp. 352–359.

Douglas, E. and E. McKyes (1978). "Compaction effects on the hydraulic conductivity of a clay soil". In: *Soil Science* 125, pp. 278–282.

Douglas, E. et al. (1980). "Unsaturated hydraulic conductivity of a tilled clay soil". In: *Canadian Agricultural Engineering* 22, pp. 153–161.

FAO (2005). *Classification and management-related properties of Vertisols.* URL: `http://www.fao.org/wairdocs/ilri/x5493e/x5493e05.htm`.

Favre, F. et al. (1997). "Water movement and soil swelling in a dry, cracked Vertisol". In: *Geoderma* Vol. 78, pp. 113–123.

Garnier, P. et al. (1997). "Determining the Hydraulic Properties of a Swelling Soil from a Transient Evaportation Experiment". In: *Soil Science Society of America* 61, pp. 1555–1563.

Giraldez, J.V. and Sposito (1983). "A general soil volume change equation: II. Effect of load pressure". In: *Soil Science Society of America* Vol. 47, pp. 422–425.

Giraldez, J.V., G. Sposito, and C. Delgado (1983). "A general soil volume change equation: I. The two-parameter model." In: *Soil Science Society of America* Vol. 47, pp. 419–422.

Groenevelt, P.H. and C.D. Grant (2001). "Re-evaluation of the structural properties of some British swelling soils". In: *European Journal of Soil Science* Vol. 113, pp. 469–477.

— (2002). "Curvature of shrinkage lines in relation to the consistency and structure of a Norwegian clay soil". In: *Geoderma* Vol. 106, pp. 235–245.

Guzman, J (2007). *Effects of land cover changes on the water balance of the Palo Verde Wetland, Costa Rica.* International Insitute for Geo-Information Science and Earth Observation. Enschede, The Netherlands.

Hazell, P et al. (2001). *Monitoring Systems for Managing Natural Resources: Economics, Indicators, and Environmental Externalities in a Costa Rican Watershed.*

Hendriks, R.F.A., K. Oostindie, and P. Hamminga (1999). "Simulation of bromide tracer and nitrogen transport in a cracked clay soil with the FLOCR/ANIMO model combination". In: *Journal of Hydrology* 215, pp. 94–115.

Huang, Wenxiong and Stephen Fityus (2008). "Numerical Study of Neutron Probe Measurement of Water Content in Expansive Soils". In: *The 12th Internation Conference of International Association for Computer Methods and Advances in Geomechanics*.

Humphry, J.B. et al. (2002). "A Portable Rainfall Simulator for Plot-Scale Runoff Studies". In: *American Society of Agricultural Engineers* 18 (2), pp. 199–204.

Huyer, W. and A. Neumaier (1999). "Global optimization by multilevel coordinate search". In: *J. Global Optimization* Vol. 14, pp. 331–355.

Jarvis, N. and P.B. Meeds-Harrison (1987). "Some problems associated with the use of the neutron probe in swelling/shrinking clay soils". In: *J. Soil Sci.* 38, pp. 149–156.

Jiménez, Jorge Arturo (2001). *Prospectives for Integrated Management of the Tempisque River Basin, Costa Rica*. Organization for Tropical Studies.

Kim, D.J. et al. (1992a). "A Numerical Model of water Movement and Soil Deformation in a Ripening Marine Clay Soil". In: *Modeling Geo-Biosphere Processes* Vol. 1, pp. 185–203.

Kim, D.J. et al. (1992b). "On the characterization of properties of an unripe marine clay soil. I. Shrinkage processes of an unripe marine clay soil in relation to physical ripening." In: *Soil Science* 153, pp. 471–481.

— (1992c). "On the characterization of properties of an unripe marine clay soil. II. A method on the determination of hydraulic properties". In: *Soil Science* 154, pp. 59–71.

Kim, D.J. et al. (2000). "Determination of moisture content in a deformable soil using time-domain reflectrometry (TDR)". In: *European Journal of Soil Science* 51, pp. 119–127.

Kool, J.B., and J.C. Parker (1988). "Analysis of the inverse problem for transient unsaturated flow". In: *Water Resources Res.* 24, pp. 817–830.

Kroes, J.G. et al. (2008). *SWAP version 3.2: Theory description and user manual. Alterra Report 1649*. Alterra. ISBN: 1566-7197.

Krosley, L., W.J. Likos, and N. Lu (2003). "Alternative Encasement Materials for Clod Test". In: *Geotechnical Testing Journal* 26.

Lagarias, J.C. et al. (1999). "Convergence properties of the Nelder-Mead simplex algorithm in low dimensions". In: *SIAM J. Optimization* Vol. 9, pp. 112–147.

Lambot, S. et al. (2002). "A global multilevel coordinate search procedure for estimating the unsaturated soil hydraulic properties". In: *Water Ressources Research* Vol. 38 (11), p. 1224.

Lambot, S., M. Javaux, and F. Hupet (2004). "Soil-Water Solute Process Characterization". In: ed. by CRC Press LLC. Chap. Inverse Modelling Techniques to Characterize Transport Processes in the Soil-Crop Continuum.

Lauritzen, C.W. and A.J. Stewart (1941). "Soil-volume changes and accompanying moisture and pore-space relationships." In: *Soil Science Society of America* 6, pp. 113–116.

Li, Jie and Gang Ren (2010). "Monitoring In-Situ Moisture Variations of Expansive Clay using Neutron Probes". In: *Deep Foundations and Geotechnical in Situ testing: Proceedings of the GeoShanghai 2010 International Conference, June3-5, 2010, Shanghai, China*.

Lishawa, S.C. et al. (2010). “Water Level Decline Promotes Typha X glauca Establishment and Vegetation Change in Great Lakes Coastal Wetlands.” In: *Wetlands* Vol. 30, No.3, pp. 676–685.

Liu, Xianfeng and Olivier Buzzi (2014). “Use of Hand-Spray Plaster as a Coating for Soil Bulk Volume Measurement”. In: *Geotechnical Testing Journal* 37 No. 3, pp. 1–7.

Loaiciga, HA and TH Robinson (1995). *Sampling of agrochemicals for environmental assessment in rice paddies: dry tropical wetlands, Costa Rica.* Groundwater Monit Rem 15:107-118.

McGarry, D. and K.W.J. Malafant (1987). “The analysis of volume change in unconfined units of soil.” In: *Soil Science Society of America* Vol. 51, pp. 290–297.

McIntyre, D.S. and G.B. Stirk (1954). “A method for determination of apparent density of soil aggregates”. In: *Aust. J. Agric. Res.* 5, pp. 291–296.

Newman, S. et al. (1998). “Factors influencing cattail abundance in the northern everglades.” In: *Aquatic Botany.*

Osland, Michael J. et al. (2011a). “Coastal Freshwater Wetland Plant Community Response to Seasonal Drought and Flooding in Northwestern Costa Rica”. In: *Wetlands* Vol. 31, No.2, pp. 641–652.

— (2011b). “Restoring diversity after cattail expansion: disturbance, resilience, and seasonality in a tropical dry wetland”. In: *Ecological Applications* Vol. 21, pp. 715–728.

Parker, J.C. (1982). “Water adsorption and swelling of clay minerals in soil systems”. In: *Soil Science Society of America Journal* 46, pp. 450–456.

Raviller, D. et al. (1972). “Bulletin ENSIA de Nancy. Tome XIV. Fascicule II: "La dispersion d’argiles pour l’analyse granulométrique”. In:

Ritchie, J.T., D.E. Kissel, and E. Burnett (1972). “Water movement in undisturbed swelling clay soil”. In: *Soil Science Society of America Proceedings* 36, pp. 874–879.

Robichaux, Estelle S. (2009). “Influence of soil and water chemistry on marsh plant communities in Palo Verde National Park, Costa Rica.” MA thesis. University of Florida.

Ruy, S. and Y-M. Cabidoche (1998). “Hydraulic conductivity of the matric porosity of an unsaturated vertisol: a field and laboratory comparison”. In: *European Journal of Soil Science* Vol. 49, pp. 175–185.

Ruy, S. et al. (1999). “Numerical modelling of water infiltration into the three components of porosity of a vertisol from Guadeloupe”. In: *Journal of Hydrology* Vol. 221, pp. 1–19.

Schafer, W.M. and M.J. Singer (1976). “A new method of measuring shrink-swell potential using soil pastes”. In: *Soil Science Society of America* 40, pp. 805–806.

Schollenberger, C.J. and R.H. Simon (1945). “Determination of exchange capacity and exchangeable bases in soil–Ammonium acetate method”. In: *Soil Science* 59, pp. 13–24.

Sibley, J.W. and D.J. Williams (1989). “A procedure for determining volumetric shrinkage of an unsaturated soil.” In: *Geotech. Test. J.* 12, pp. 181–187.

Smiles, D.E. and A.G. Harvey (1973). “Measurement of moisture diffusivity of wet swelling systems”. In: *Soil Science* 116, pp. 391–399.

Stewart, R.D. et al. (2012). "An Image-based Method for Determining Bulk Density and the Soil Shrinkage Curve". In: *Soil Science Society of America Journal* 76 No. 4, pp. 1217–1221.

Stirk, G.B. (1954). "Some aspects of soil shrinkage and the effect of cracking upon water entry into the soil". In: *Aust. J. Agric. Res.* 5, pp. 279–290.

Taboada, Miguel (2003). *Soil Shrinkage Characteristics in Swelling Soils, Lecture given at the College on Soil Physics, Trieste.*

Tadza, Mohd Yuhyi Mohd (2011). "Soil-water characteristic curves and shrinkage behavious of highly plastic clays: An experimental investigation". PhD thesis. Geoenvironmental Research Centre, Cardiff School of Engineering, Cardiff University.

Tariq, A. and D. Durnford (1993a). "Soil Volumetric Shrinkage Measurements: A Simple Method". In: *Soil Science* 155, pp. 325–330.

Tariq, A. and D.S. Durnford (1993b). "Analytical volume change model for swelling clay soils." In: *Soil Science Society of America* Vol. 57, pp. 1183–1187.

Tessier, D. and J. Berrier (1979). "Utilisation de la microscopie électronique à balayage dans l'étude des sols". In: *Science du Sol* 17, pp. 67–82.

Trama, F et al. (2009). "Wetland Cover Types and Plant Community Changes in Response to Cattail-Control Activities in the Palo Verde Marsh, Costa Rica". In: *Ecological Restoration.*

Tunny, J. (1970). "Influence of saran resin coatings on swwelling of natural soil clods". In: *Soil Science* 109, pp. 254–256.

United States Environmental Protection Ageny (1998). *Estimation of Infiltration Rate in the Vadose Zone: Application of Selected Mathematical Models, Volume II.* Tech. rep. National Risk MAnagement Research Laboratory.

Van Schaik, N. Loes M.B., R.F.A. Hendriks, and J.C. van Dam (2009). "Parameterization of Macropore Flow Using Dye-Tracer Infiltration Patterns in the SWAP model". In: *Vadose Zone Journal* 9, pp. 1–12.

Walkley, A. and I.A. Black (1934). "An examination of the Degtjareff method for determining organic carbon in soils: Effect of variations in digestion conditions and of inorganic soil constituents." In: *Soil Science* 63, pp. 251–263.

Wilcox, Douglas A. et al. (2008). "The effects of water-level fluctuations on vegetation in Lake Huron Wetland". In: *Wetlands* Vol. 28, No.2, pp. 487–501.

Yule, D.F. and J.T. Ritchie (1980a). "Soil shrinkage relationaships in Texas vertisols. I: Small cores". In: *Soil Science Society of America* 44, pp. 1285–1291.

— (1980b). "Soil shrinkage relationaships in Texas vertisols. II: Large cores". In: *Soil Science Society of America* 44, pp. 1291–1295.

— (1980c). "Soil shrinkage relationships of Texas vertisols: II. Large cores." In: *Soil Science Society of America* Vol. 44, pp. 1285–1291.

A

Figures

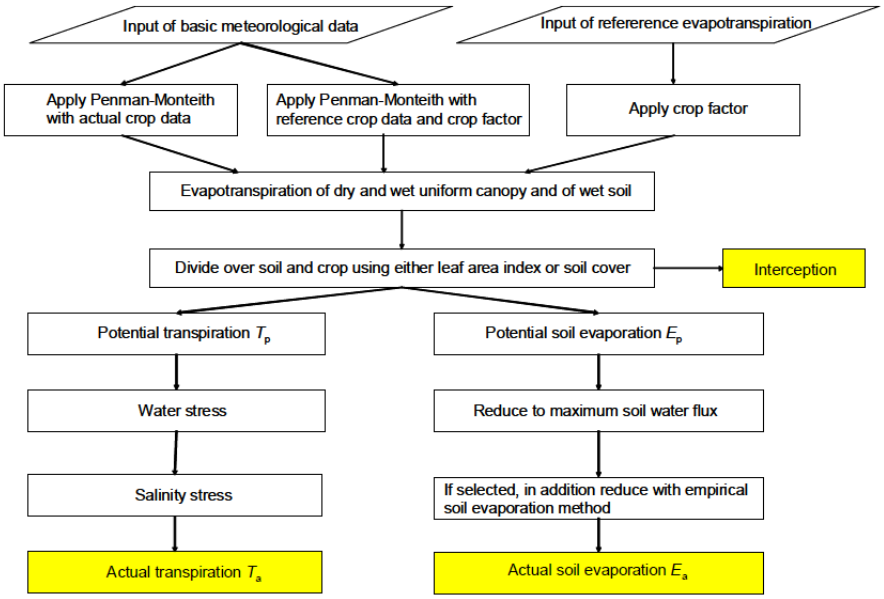

Figure A1: Method used in SWAP to derive actual transpiration and soil evaporation of partly covered soils from basic input data

Figure A2: Hydraulic digger used for digging the soil profiles (Posaverde site)

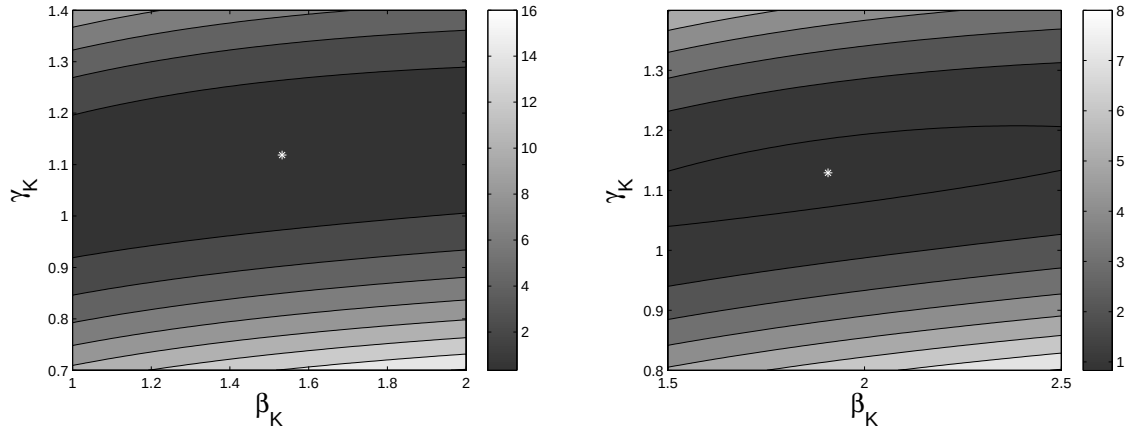

(a)

(b)

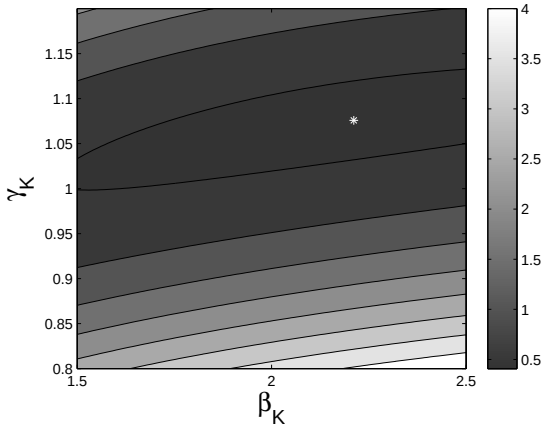

(c)

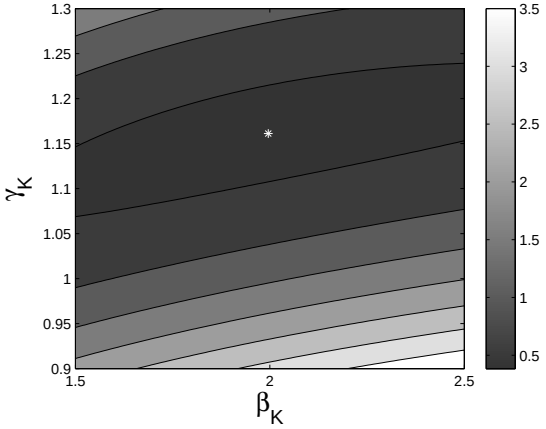

(d)

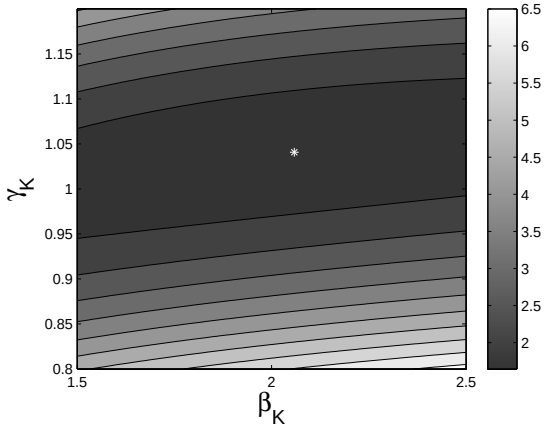

(e)

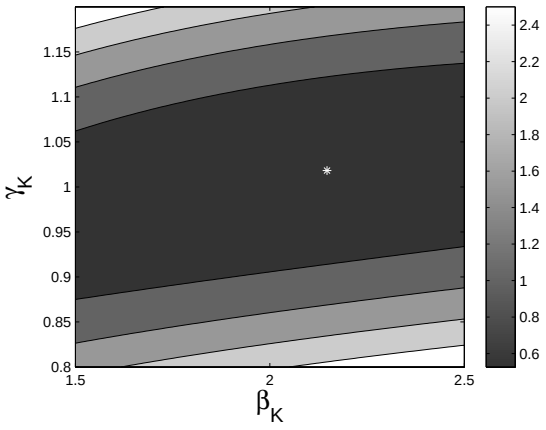

(f)

Figure A3: Shrinkage curves: (a) Laguna; (b) Chamorro; (c) Posaverde; (d) Varillal; (e) La Bocana; (f) Tempisque

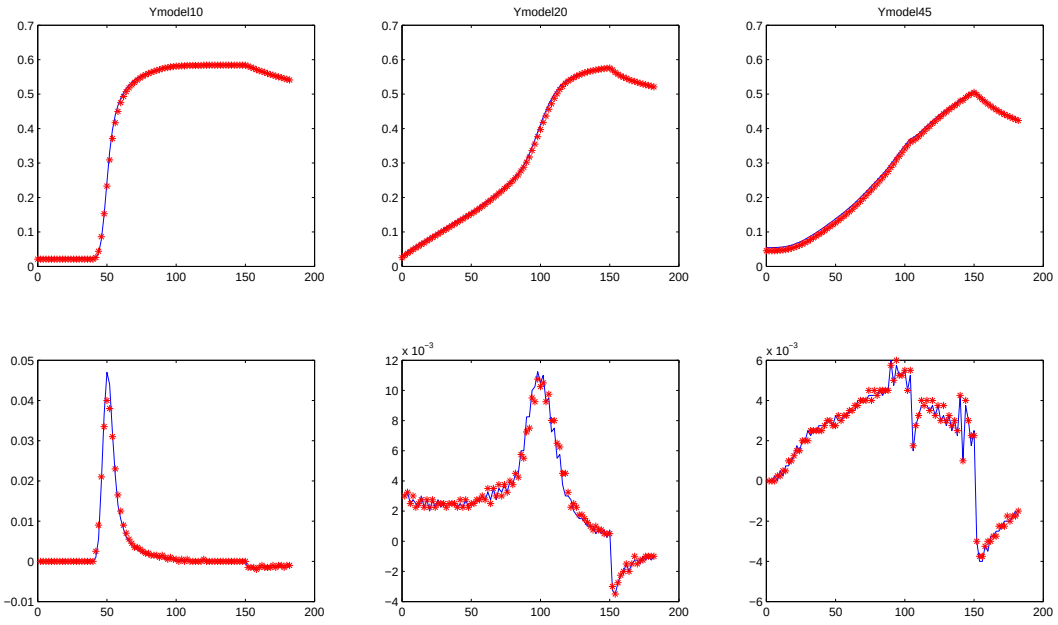

Figure A4: Graph of the results of model inversion or testing robustness with K_{sat} and α. The first line represents water content and the second line represents the variation of moisture content.

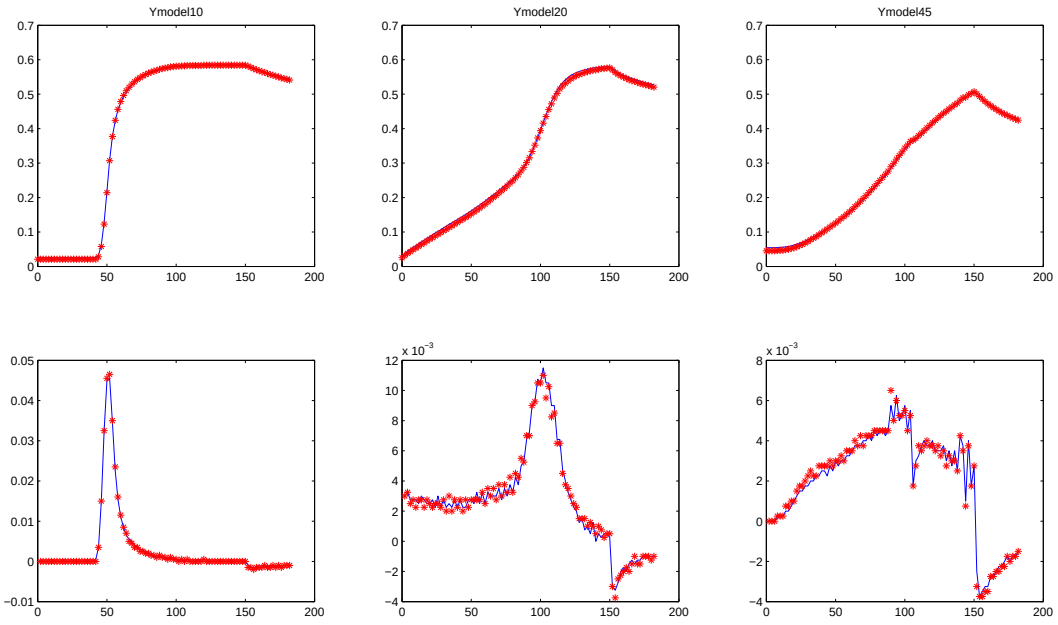

Figure A5: Graph of the results of model inversion or testing robustness with K_{sat}, α, Z_{IC}, m, and $P_{IC,0}$. The first line represents water content and the second line represents the variation of moisture content.

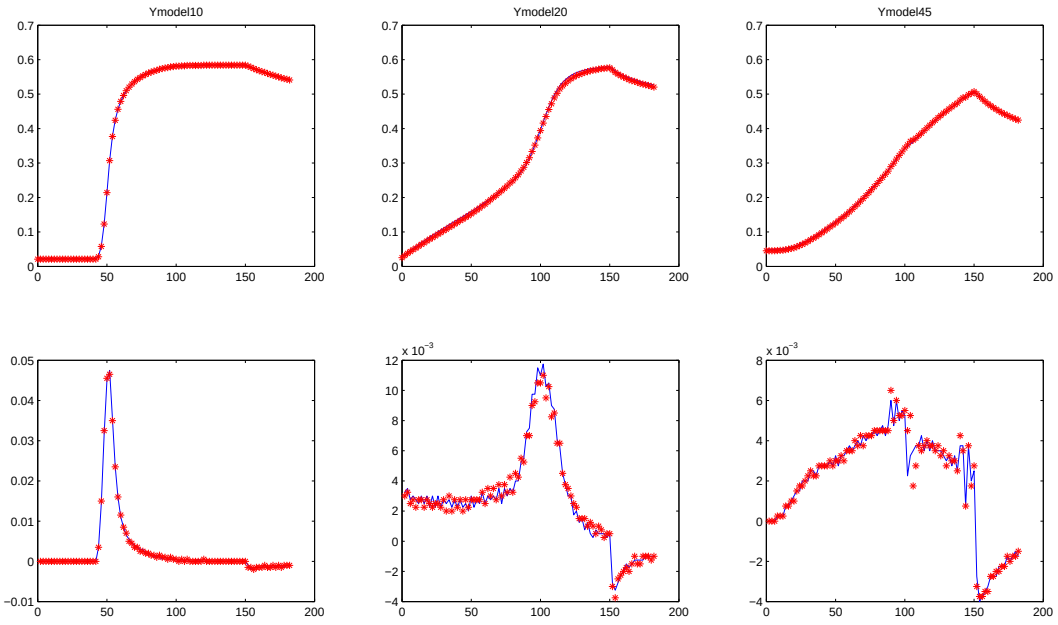

Figure A6: Graph of the results of model inversion or testing robustness with K_{sat}, α, Z_{IC}, m, $P_{IC,0}$ and $V_{st,0}$. The first line represents water content and the second line represents the variation of moisture content.

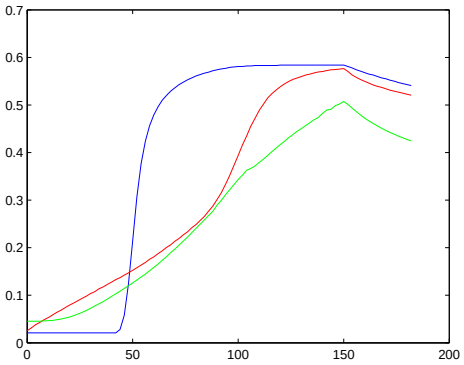

(a) Initial

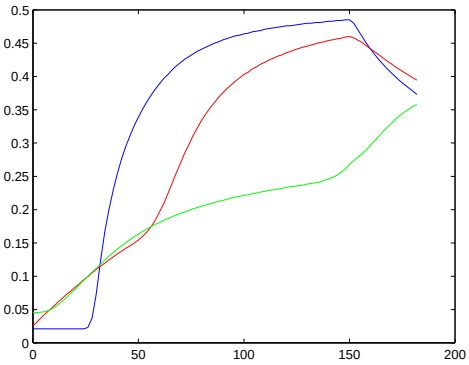

(b) K_{sat}

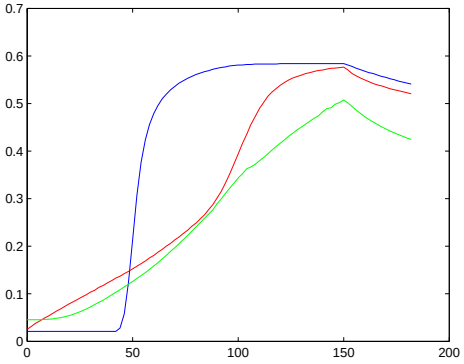

(c) Initial

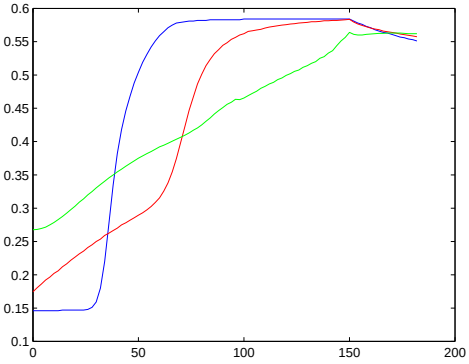

(d) α

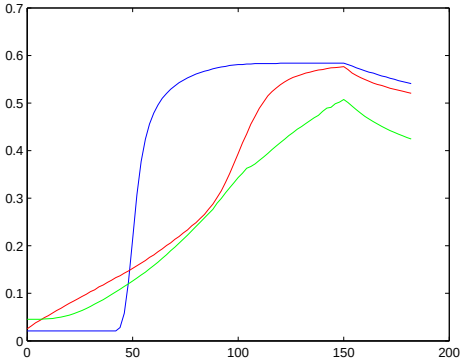

(e) Initial

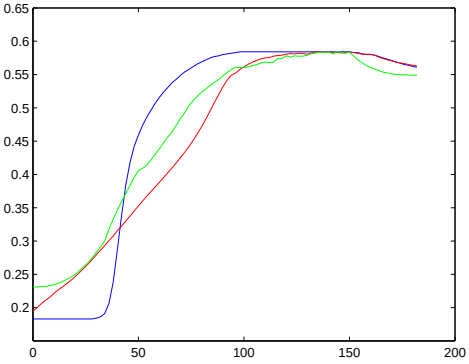

(f) n

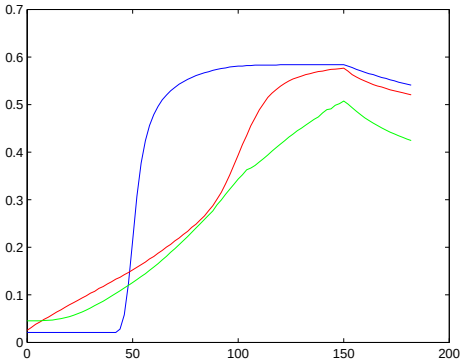

(g) Initial

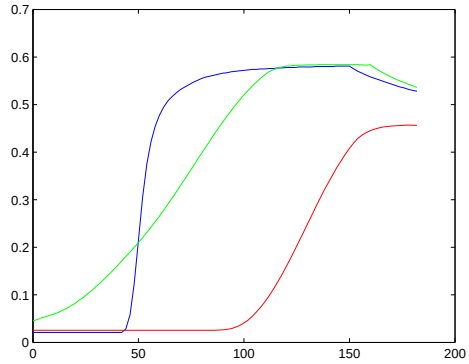

(h) Z_{IC}

Figure A7: Graphs of model response to parameter variation

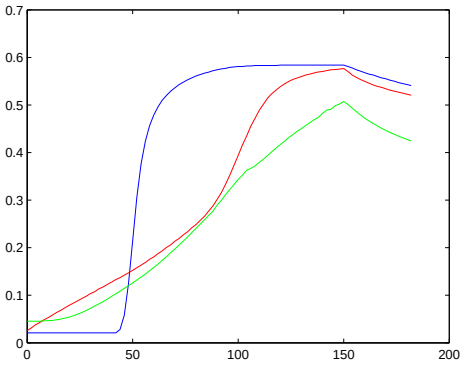

(a) Initial

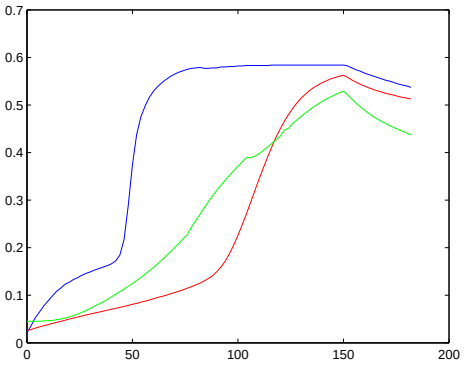

(b) m

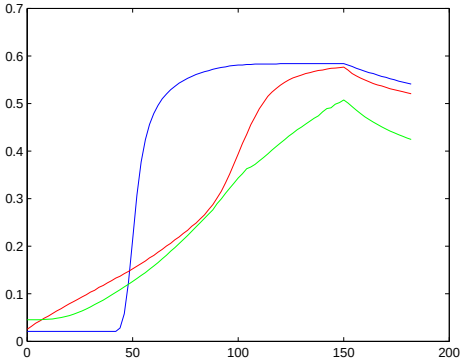

(c) Initial

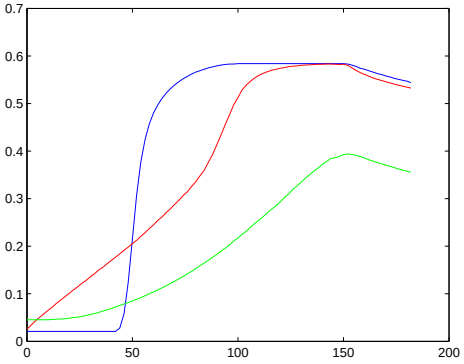

(d) $P_{IC,0}$

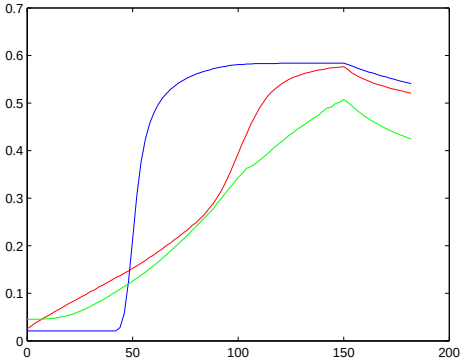

(e) Initial

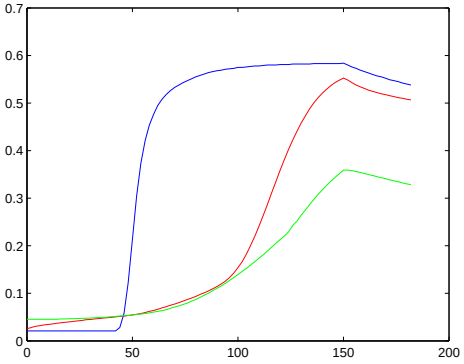

(f) $V_{st,0}$

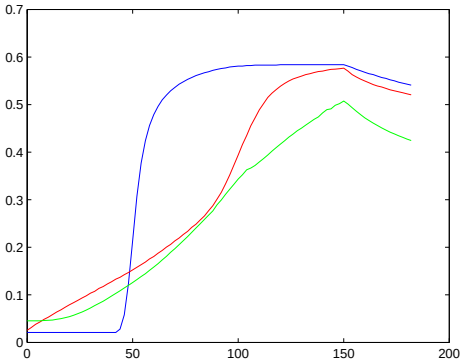

(g) Initial

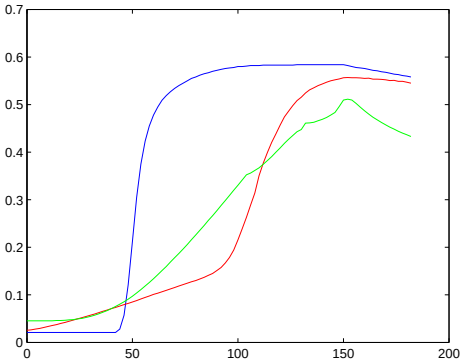

(h) $FacParl$

Figure A8: Graphs of model response to parameter variation

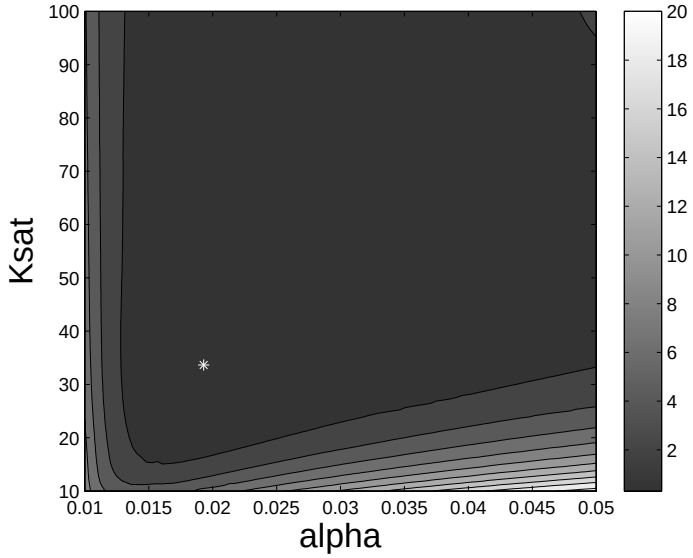

Figure A9: Response surface for parameters K_{sat} and α

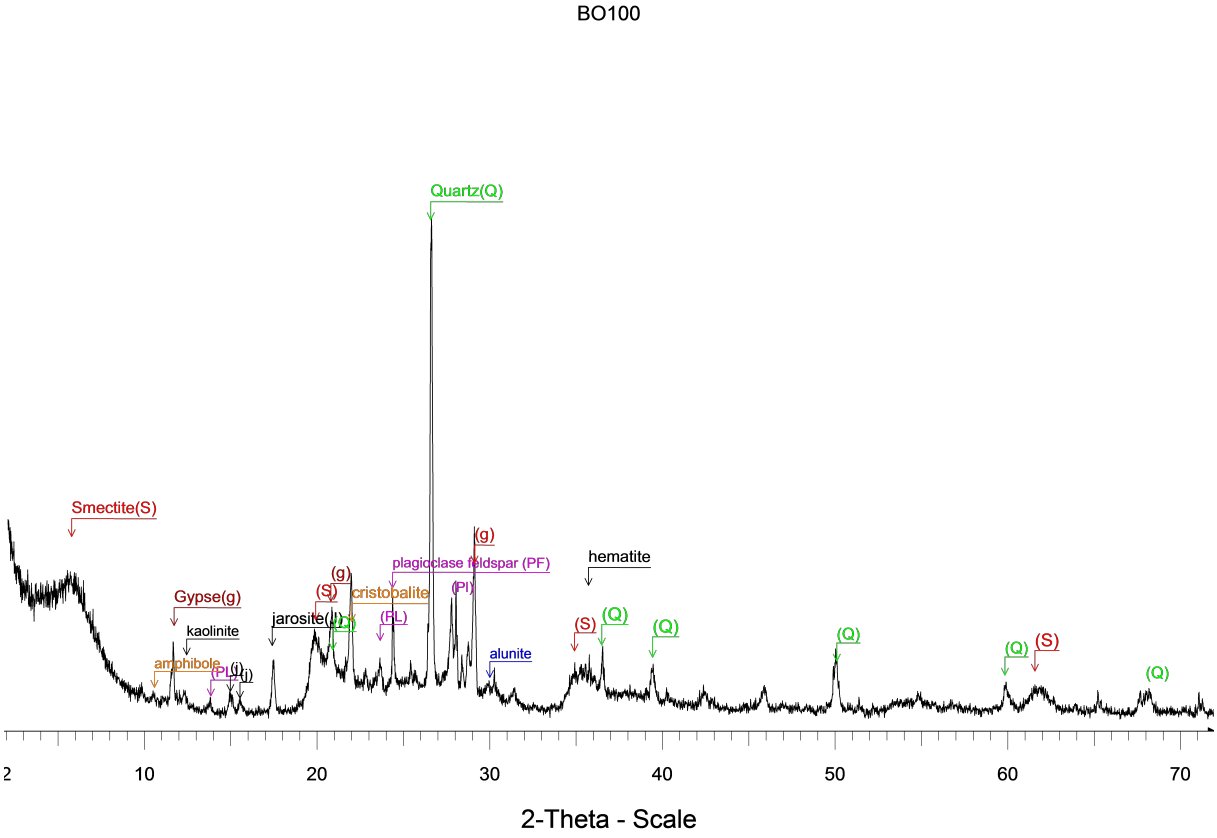

Figure A11: Graph of the results of the X-ray diffraction for La Bocana site at -100 cm

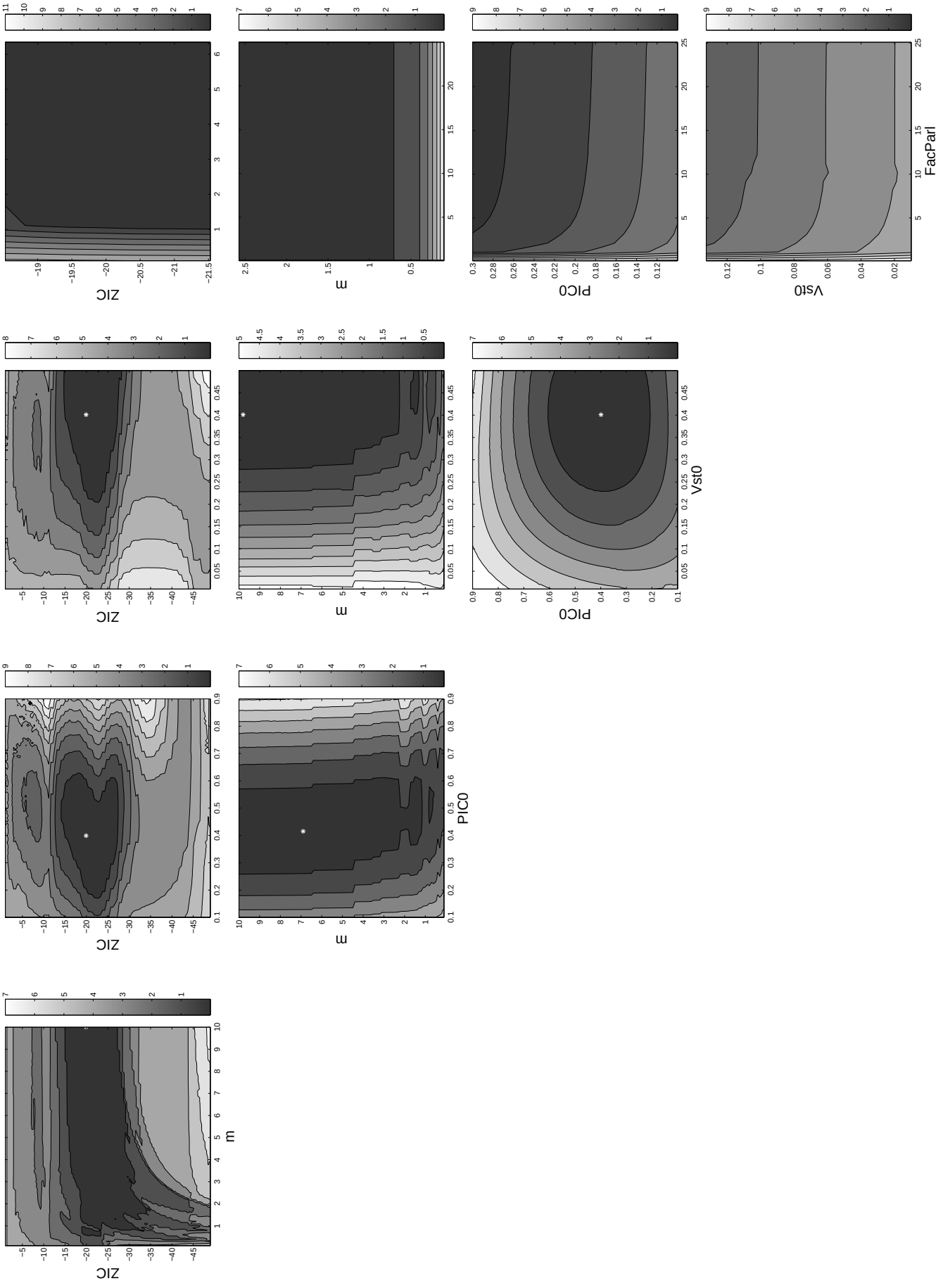

Figure A10: Response surfaces for macropore parameters, Z_{IC}, m, $P_{IC,0}$, $V_{st,0}$, and $FacParl$

B

Tables

Table B1: pH and exchangeable bases

Site	pH	Ca (meq/100g)	K (meq/100g)	Mg (meq/100g)	Na (meq/100g)
Laguna	8.24	49.569	1.133	17.057	3.100
	9.01	58.794	0.625	11.763	2.714
	8.6	40.521	1.786	16.895	5.840
Chamorro	6.3	18.584	0.736	18.997	1.761
	6.8	17.966	0.883	22.163	2.315
	7.76	17.159	1.414	23.777	4.588
Posaverde	7.18	54.422	0.227	10.402	0.334
	8.42	62.553	0.103	12.961	0.659
	8.71	50.936	0.083	21.191	2.350
Varillal	8.15	58.483	0.249	15.609	0.938
	8.83	51.715	0.276	20.212	4.668
	9.08	49.536	0.202	20.274	7.428
La Bocana	7.67	24.639	1.416	12.081	4.447
	6.44	41.644	1.559	16.018	11.537
	4.01	31.895	1.459	17.543	13.408
	3.82	26.513	0.585	8.554	8.773
Tempisque	7.37	13.694	2.006	21.340	9.613
	7.65	11.653	2.537	22.328	14.926
	7.8	10.072	2.855	21.026	22.359

Characterization and modeling of water infiltration in a swelling soil in the Palo Verde National Park
Présenté par Nicolas Stipo

Résumé

Keywords: Vertisol, SWAP, soil water flow, macropore flow

Situated in the Tempisque-Bebedero basin, the Palo Verde National Park is considered one of the most important nesting and feeding sites of the region. In the past few decades, this RAMSAR recognized natural reserve has been subject to a major ecological degradation in the form of cattail (*Typha spp.*) invasion. This invasion has greatly decreased avian nesting and feeding sites, resulting in a marked decrease in bird population and diversity.

This study proposes to aid in gaining more understanding of the hydrological dynamics of the basin by characterizing the infiltrometric properties of the soils in the Palo Verde National Park. The results of the study will inform a larger study, conducted by Alice Alonso at the University of Florida (CNIC 1132832 and 1132849, 2011-2013), that aims to model the hydrological dynamic of the wetland .

These soils are swelling clay soils, mostly vertisols. The parameters necessary for describing infiltration in this soil cannot be determined using traditional methods. The methods that will be used must take into account the shrinking-swelling nature of the vertisols.

The hydrological dynamics were modeled using the SWAP model. Soil shrinkage curves were established using a coated aggregate method with volume measurements by buoyancy. The coating used was Hansaplast plaster spray. Kim's shrinkage curve model was inverted using the shrinkage data in order to determine the parameters of the equation.

Hydraulic parameters (water retention characteristic and conductivity characteristic) were determined via model inversion using infiltration data, produced in the field using a rainfall simulator and capacitance probes. Model inversion proved to be very difficult with mitigated results. The causes of these poor results were studied via numerical experiments to establish the well-posedness of the inverse problem. The results, in addition to a review of the experimental protocol were discussed and recommendations for future characterizations were made.

Finally, using manually approximated parameters, four forward simulations were modeled in order to determine the effect of different components of the model on the model response. The results of the four forward simulations showed that the presence of macropore flow increases the depth of infiltration, increasing bottom drainage and decreasing soil evaporation. This effect is larger for soils which have relatively poorly conductive soils. However, it was observed that for a profile with free drainage, soil saturation was never achieved using actual rainfall data, even with relatively low conductivity values. This was attributed to overestimation of the hydraulic parameter values by the pedotransfer functions and to the importance of other inputs for creating ponding, such as runon and groundwater levels.

Année académique 2014-2015